



A.I. ALIKHANYAN NATIONAL SCIENCE LABORATORY

(YEREVAN PHYSICS INSTITUTE)

ARPINE G. KARAPETYAN

STUDY OF SUPERNOVAE AND  
THEIR HOST GALAXY DYNAMICAL  
FEATURES

Thesis

for acquiring the degree of candidate of physico-mathematical sciences

in division 01.03.02. “Astrophysics, radio astronomy”

SUPERVISOR: DR. ARTUR A. HAKOBYAN

YEREVAN – 2023

# Contents

<b>List of Figures</b>	<b>4</b>
<b>List of Tables</b>	<b>6</b>
<b>List of Publications</b>	<b>8</b>
<b>List of Abbreviations</b>	<b>9</b>
<b>Introduction</b>	<b>11</b>
<b>1 The impact of bars and bulges on the radial distribution of SNe</b>	<b>21</b>
1.1 Introduction . . . . .	21
1.2 Sample selection and reduction . . . . .	23
1.3 Results and discussion . . . . .	25
1.3.1 Galactocentric radius deprojection and normalization . . . . .	26
1.4 Influence of bars and bulges on the radial distribution of SNe . . . . .	30
1.4.1 The deprojected exponential surface density distribution . . . . .	39
1.5 Chapter Conclusions . . . . .	43
<b>2 Type Ia SNe in the star formation deserts of spiral host galaxies</b>	<b>46</b>
2.1 Introduction . . . . .	46
2.2 Sample selection and reduction . . . . .	47
2.3 Results and discussion . . . . .	51
2.3.1 SNe Ia in the SFDs and beyond . . . . .	51

<i>CONTENTS</i>	3
2.3.2 The radial distribution of SNe Ia . . . . .	55
2.4 Chapter Conclusions . . . . .	57
<b>3 The impact of spiral density waves on the distribution of SNe</b>	<b>58</b>
3.1 Introduction . . . . .	58
3.2 The sample . . . . .	60
3.2.1 Sample selection and reduction . . . . .	60
3.2.2 Determination of spiral arm classes . . . . .	61
3.3 Results . . . . .	65
3.3.1 The radial distribution and surface density . . . . .	65
3.4 Interpretation within the framework of density wave theory . . . . .	70
3.5 Chapter Conclusions . . . . .	78
<b>4 Constraining Type Ia SNe via their distances from spiral arms</b>	<b>81</b>
4.1 Introduction . . . . .	81
4.2 Sample selection and reduction . . . . .	82
4.3 Results and discussion . . . . .	87
4.3.1 SNe Ia in <i>arm</i> and <i>interarm</i> regions of spiral galaxies . . . . .	87
4.3.2 The distribution of SNe Ia relative to spiral arms . . . . .	89
4.4 Chapter Conclusions . . . . .	93
<b>General Conclusions</b>	<b>94</b>
<b>Acknowledgement</b>	<b>98</b>
<b>Bibliography</b>	<b>99</b>

# List of Figures

1	A simple scheme of SN classification . . . . .	13
2	Examples of light curves and spectra of different subtypes of CC SNe . . . . .	14
3	Spectral characteristics of SNe and their progenitor stars' pre-explosion structures	15
4	Examples of light curves and spectra for SNe Ia subclasses . . . . .	16
5	Diagram of various SN Ia explosion models (channels) . . . . .	17
6	Host galaxy morphological type versus SN Ia light curve decline rate . . . . .	19
1.1	Distributions of normalized galactocentric distances of Type Ia and CC SNe . . .	28
1.2	The radial distributions of Type Ia and CC SNe in barred and unbarred hosts . .	31
1.3	SNe fractions and surface density distributions versus radii in unbarred hosts . .	41
2.1	Optical and UV images of SN Ia hosts with different SF classes of their discs . .	49
2.2	Variation of normal SNe Ia $\Delta m_{15}$ as a function of galactocentric distance . . . .	52
3.1	SDSS image examples of unbarred Sa–Sc hosts with different arm classes . . . . .	62
3.2	Galactocentric radii and surface density of CC SNe in LGD, SGD and NGD hosts	68
3.3	The scheme of massive SF triggering by DWs in a model of a GD galaxy . . . . .	70
3.4	Galactocentric positions of normalized corotation radii for host galaxies . . . . .	74
3.5	Distributions of $R_C/R_{25}$ values of LGD and SGD galaxies . . . . .	74
3.6	Surface density profile of CC SNe in LGD host galaxies . . . . .	75
3.7	CC SNe differential distribution of the distances to nearest corotation radius . .	76
4.1	SDSS $g$ -band images and residual image of interarm and arm SNe examples . . .	84
4.2	A scheme of GD galaxy with logarithmic arms . . . . .	86

4.3	Cumulative $\Delta m_{15}$ distributions of all <i>arm</i> and <i>interarm</i> SNe Ia . . . . .	87
4.4	Distribution of the distances of SNe Ia relative to the peaks of spiral arms versus the deprojected and normalized galactocentric distance. . . . .	90
4.5	SNe Ia $\Delta m_{15}$ values versus $\tilde{D}$ distances from the shock fronts of spiral arms . . .	92

# List of Tables

1.1	Numbers of SNe within host disc galaxies as a function of morphological types . . . . .	24
1.2	Comparison of the 2D spatial distributions of SNe among different subsamples of hosts . . . . .	27
1.3	Comparison of the normalized, deprojected radial distributions of SNe among different pairs of subsamples possibly affected by selection effects . . . . .	32
1.4	Comparison of the normalized, deprojected radial distributions of SNe among different pairs of subsamples . . . . .	33
1.5	Fractions of inner SNe in barred and unbarred host galaxies . . . . .	35
1.6	Consistency of CC and Type Ia SN distributions with an exponential surface density model . . . . .	38
1.7	Consistency of Types Ibc and II SN distributions with an exponential surface density model . . . . .	40
2.1	Comparison of the projected and normalized distributions of the SN Ia subclasses	49
2.2	Numbers of the SN Ia subclasses according to their locations in the SFD hosts or beyond . . . . .	50
2.3	The database of 185 SNe Ia and their 180 host galaxies . . . . .	51
2.4	Comparison of the $B$ -band $\Delta m_{15}$ distributions between normal SNe Ia in different locations . . . . .	53
2.5	Spearman's rank correlation test for the $B$ -band $\Delta m_{15}$ values of the SN Ia subclasses versus their galactocentric distances . . . . .	56

3.1	Numbers of SNe in unbarred Sa–Sc hosts . . . . .	64
3.2	Comparison of the deprojected and normalized radial distributions of SNe . . . . .	66
3.3	Consistency of global ( $\tilde{r} \geq 0$ ) and inner-truncated ( $\tilde{r} \geq 0.2$ ) SN distributions . . . . .	67
3.4	Available corotation radii of our LGD and SGD host galaxies . . . . .	72
4.1	Morphological distribution of the sampled SNe Ia host galaxies . . . . .	83
4.2	Numbers of <i>arm</i> and <i>interarm</i> SNe Ia within Sab–Scd galaxies . . . . .	83
4.3	The database of 77 SNe Ia of the study . . . . .	85
4.4	Comparison of the LC decline rate distributions of <i>arm</i> and <i>interarm</i> SNe Ia . . . . .	88
4.5	Results of Spearman’s rank correlation tests for different continuous parameters of SNe Ia . . . . .	89

# List of Publications

This PhD thesis is based on the following *refereed publications*:

1. Hakobyan A. A., **Karapetyan A. G.**, Barkhudaryan L. V., Mamon G. A., Kunth D., Petrosian A. R., Adibekyan V., Aramyan L. S., Turatto M., “*Supernovae and their host galaxies - III. The impact of bars and bulges on the radial distribution of supernovae in disc galaxies*”, Monthly Notices of the Royal Astronomical Society, 2016, Volume 456, Issue 3, pp. 2848-2860.
2. **Karapetyan A. G.**, Hakobyan A. A., Barkhudaryan L. V., Mamon G. A., Kunth D., Adibekyan V., Turatto M., “*The impact of spiral density waves on the distribution of supernovae*”, Monthly Notices of the Royal Astronomical Society, 2018, Volume 481, Issue 1, pp. 566-577.
3. Hakobyan A. A., **Karapetyan A. G.**, Barkhudaryan L. V., Gevorgyan M. H., Adibekyan V., “*Type Ia supernovae in the star formation deserts of spiral host galaxies*”, Monthly Notices of the Royal Astronomical Society: Letters, 2021, Volume 505, Issue 1, pp. L52–L57.
4. **Karapetyan A. G.**, “*Constraining Type Ia supernovae via their distances from spiral arms*”, Monthly Notices of the Royal Astronomical Society: Letters, 2022, Volume 517, Issue 1, pp. L132-L137.

# List of Abbreviations

<b>AC</b>	arm class
<b>AD</b>	Anderson–Darling
<b>ASC</b>	Asiago Supernova Catalogue
<b>CC</b>	core–collapse
<b>CDF</b>	cumulative distribution function
<b>CO</b>	carbon–oxygen
<b>DD</b>	double–degenerate
<b>DR</b>	Data Release
<b>DTD</b>	delay time distribution
<b>DW</b>	density wave
<b>EFIGI</b>	Extraction de Formes Idéalisées de Galaxies en Imagerie
<b>GALEX</b>	Galaxy Evolution Explorer
<b>GD</b>	grand–design
<b>KS</b>	Kolmogorov–Smirnov
<b>LC</b>	light curve
<b>LGD</b>	long–armed GD
<b>LOSS</b>	Lick Observatory Supernova Search
<b>MC</b>	Monte Carlo
<b>MLE</b>	maximum likelihood estimation
<b>MS</b>	main–sequence
<b>MW</b>	Milky Way
<b>NGD</b>	non–GD
<b>PA</b>	position angle
<b>PDF</b>	probability density function

<b>PGC</b>	Principal Galaxy Catalogue
<b>SD</b>	single-degenerate
<b>SDSS</b>	Sloan Digital Sky Survey
<b>SF</b>	star formation
<b>SFD</b>	star formation desert
<b>SGD</b>	short-armed GD
<b>SN</b>	Supernova
<b>UV</b>	ultraviolet
<b>WD</b>	white dwarf

# Introduction

Supernova (SN) events have been witnessed over millennia. These fleeting phenomena occasionally attained a brilliance that made them visible to the unaided eye. The earliest documented SN, observed by ancient Chinese astronomers, dates back to the year 185. Employing modern nomenclature, it is designated as SN 185. Other significant SNe of historical importance encompass SN 1006, distinguished by its remarkable apparent brightness; SN 1054, the progenitor of the renowned Crab Nebula; SN 1572, observed by Tycho Brahe, which played a vital role in refuting archaic cosmological models centered around a static celestial realm; and SN 1604, the most recent supernova directly observed within our own Galaxy. The inaugural extragalactic SN was detected in 1885 within the Andromeda galaxy. Tycho Brahe and his contemporaries categorized SN 1572 as the emergence of a novel star, or *nova stella*, within the celestial expanse. This interpretation led to the widespread adoption of the term “nova” to describe such occurrences of transient star-like entities that endured for weeks or months before gradually diminishing. Subsequently, Walter Baade and Fritz Zwicky in 1934 made a distinction between novae and a more intrinsically luminous category of events termed “supernovae”. Novae were discerned as eruptions from white dwarf (WD) stars that accumulated matter, whereas the origins of the significantly more potent SNe were proposed to involve the metamorphosis of massive ordinary stars into extraordinarily dense neutron stars during their final stages, culminating in immensely energetic detonations. Subsequent observations of SNe validated this hypothesis. Further variants of SNe were also identified, stemming from diverse sources such as the terminal detonations of WDs in the class known as thermonuclear SNe. Taking all of this into account, astronomical research of the SNe progenitor stars was and is of

crucial importance. The progenitors can be studied in a variety of ways, from directly observing them before the explosion to other techniques that look into their environments statistically.

In 1938, Baade made a notable observation that SNe constitute a homogenous category of celestial objects. For 18 SNe, he determined that the average absolute magnitude at the peak is  $-14.3$  mag, exhibiting a dispersion of 1.1 mag. Subsequently, SNe have emerged as reliable etalons for measuring distances in the Cosmos [1]. Seven decades later, the Nobel Prize was bestowed upon Saul Perlmutter, Brian Schmidt, and Adam Riess for their groundbreaking contributions in unveiling the enigma of dark energy and the Universe’s accelerating expansion, made possible by scrutinizing SNe. Curiously, both teams led by Perlmutter and Schmidt initially anticipated a decelerating expansion of the Universe [2, 3].

In a broad context, SNe are star explosions that can culminate in the formation of a neutron star or a black hole, or in the complete destruction of the progenitor star. With advancements in our observational capabilities regarding SNe, the diverse nature of these events has become progressively evident. This trend underscores the growing significance of investigating the progenitors of SNe. In the initial stages, the categorization of SNe was established by Minkowski [4] through differentiation in their photospheric spectra: Type I SNe displayed spectra devoid of hydrogen characteristics, while Type II SNe exhibited such hydrogen features. These primary classifications underwent additional partitioning into a subtypes, meticulously explicated by Filippenko [5]. Fig. 1 shows a scheme of simplified classification of SNe.

In the modern view, SNe are generally divided into two categories according to their progenitors: core-collapse (CC) and Type Ia SNe. CC SNe result from massive young stars that undergo CC [6–8]. They are observationally classified in three major classes, according to the strength of lines in optical spectra [5]: Type II SNe show hydrogen lines in their spectra, including the II<sub>n</sub> (dominated by emission lines with narrow components) and II<sub>b</sub> (transitional objects with observed properties closer to SNe II at early times, then metamorphosing to SNe Ib) subclasses; Type Ib SNe show helium but not hydrogen, while Type Ic SNe show neither hydrogen nor helium. According to their light curves (LCs), Type II SN is divided into the II-P and II-L subclasses. Type II-P SN shows a “plateau” in its LC, whereas a Type II-L SN has a steady

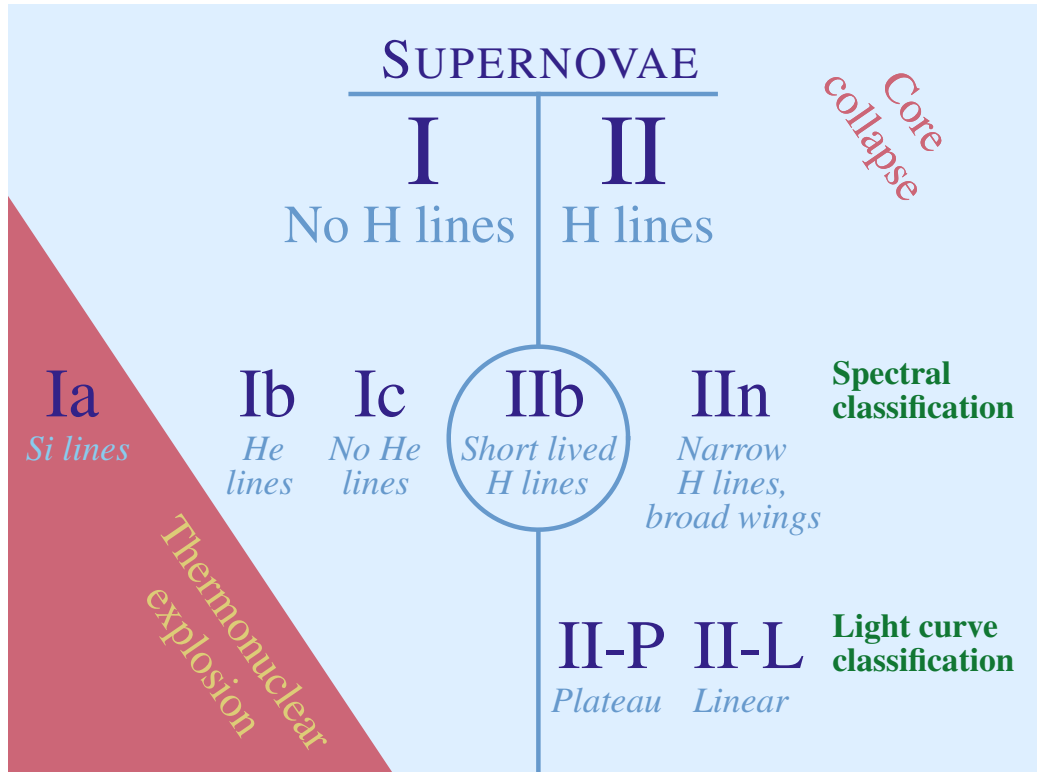


Figure 1: A simplified scheme of SN classification (is taken from [9]).

(linear) decline. All these CC SNe types arise from young massive progenitors with possible differences in their masses, metallicities, ages, etc [10]. Fig. 2 presents LCs and photospheric spectra of different CC SNe subtypes.

Two main channels have been suggested for the removal of the hydrogen and helium envelopes from SNe Ibc progenitors: (1) Wolf-Rayet massive stars ( $M \geq 30 M_{\odot}$ ), which have lost all its hydrogen and helium through winds, eruptions or mass transfer to a companion star [11]; (2) Binaries with lower masses due to interaction with a nearby companion may be stripped of outer envelopes. The progenitors of SN II may be less massive ( $8 - 16 M_{\odot}$  [8]) than those of SN Ib and SN Ic. Fig. 3 presents an optical spectra of SNe, as well as their progenitor stars' pre-explosion structures.

It is now evident that SNe Ia are not a homogeneous population of WD explosions, instead they exhibit photometric and spectroscopic diversities [12]. One of the characteristic parameters of SNe Ia is the difference in  $B$ -band magnitudes between the max and 15 day, or the so-called SN LC decline rate  $\Delta m_{15}$ , which is practically extinction-independent [13]. There is a

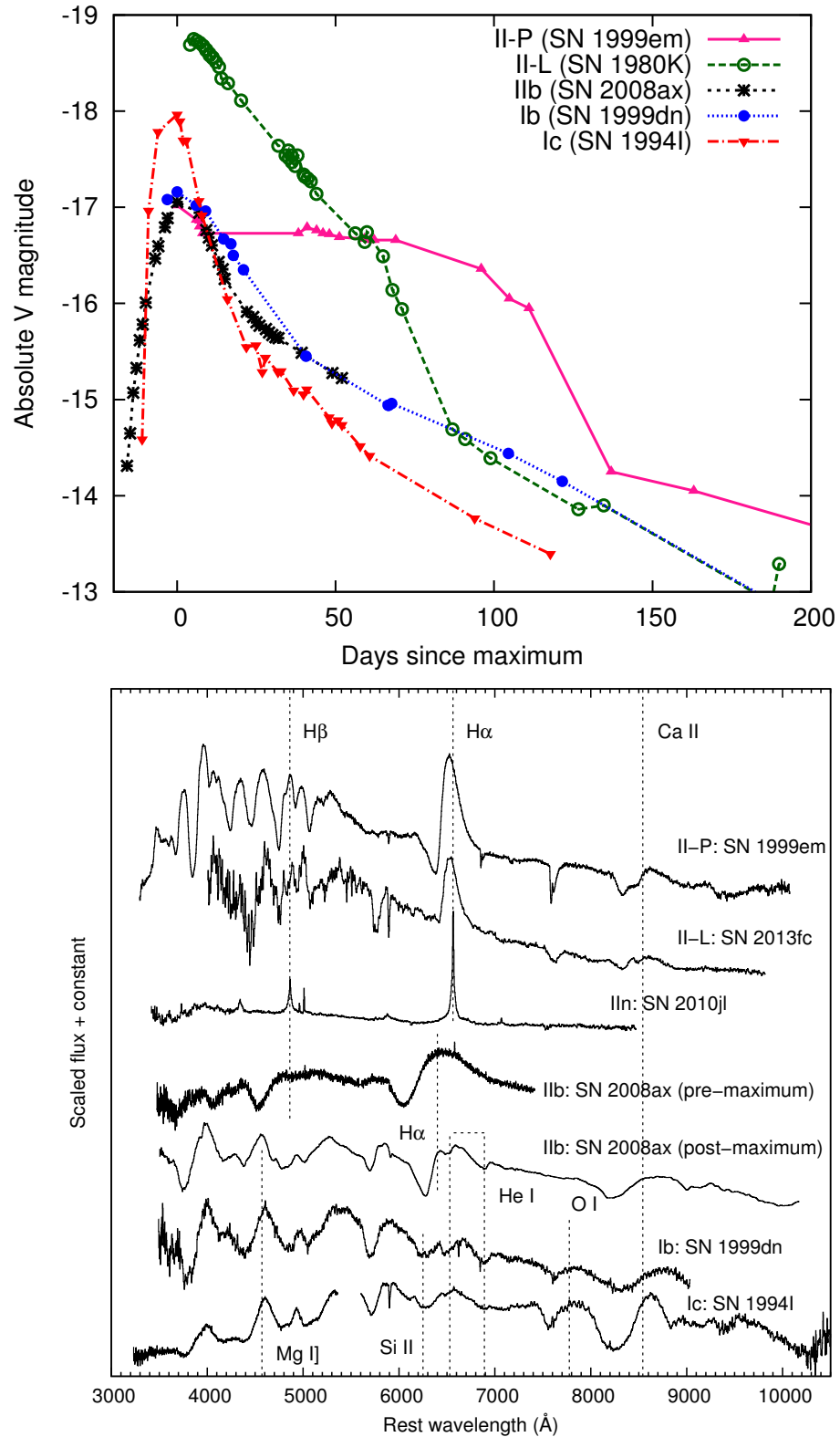


Figure 2: *Upper panel:* examples of LCs of different subtypes of CC SNe. Type IIIn is absent in this representation, as SNe of this subtype do not exhibit a consistent pattern in their LCs. *Bottom panel:* examples of photospheric spectra of the subtypes of CC SNe with some prominent spectral lines identified. Both panels are taken from [14].

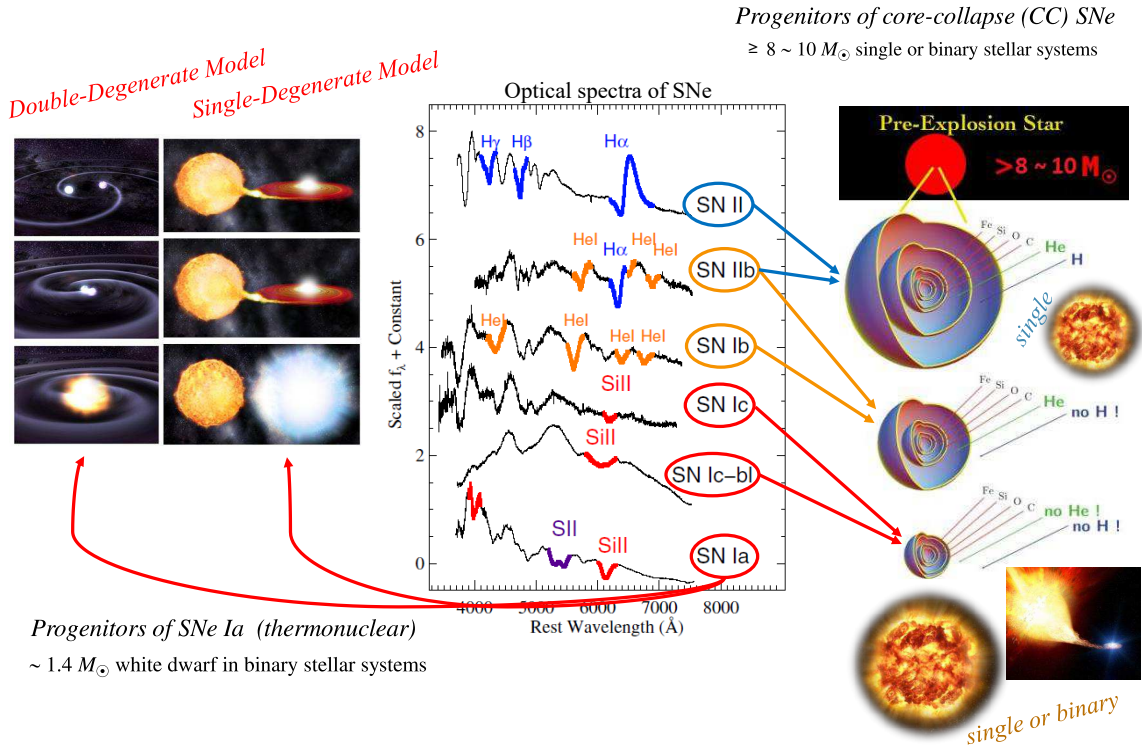


Figure 3: Spectral characteristics of SNe and their progenitor stars' pre-explosion structures (spectra and visuals are borrowed from [15] and modified).

correlation between this parameter and SN Ia luminosities at the maximum light: SNe Ia with larger  $\Delta m_{15}$  values, or faster declining LCs, are fainter [16]. There are two most prevalent subclasses of peculiar SNe Ia: (1) 91T-like events show strong Fe III lines at pre-maximum phases in their optical spectra. These events are  $\sim 0.6$  mag overluminous than normal ones and have slow-declining LCs [12]; (2) 91bg-like events show strong O I and Ti II lines at pre-maximum phases in their optical spectra. These events are  $\sim 2$  mag subluminous at the  $B$ -band maximum than normal SNe Ia and have fast-declining LCs. Fig. 4 presents examples of optical LCs and spectra for the SN Ia subclasses.

It is believed that the progenitor of SNe Ia is a carbon–oxygen (CO) WD in close binaries, whose properties and explosion channels are still under debate [17]. To encompass a range of progenitor scenarios for Type Ia SNe, several explosion models have been suggested [17, 18]. They are mainly grouped into the classes outlined below: the *single-degenerate* (SD) and *double-degenerate* (DD) channels (Fig. 3). In the SD channel [19], an older WD accretes material from

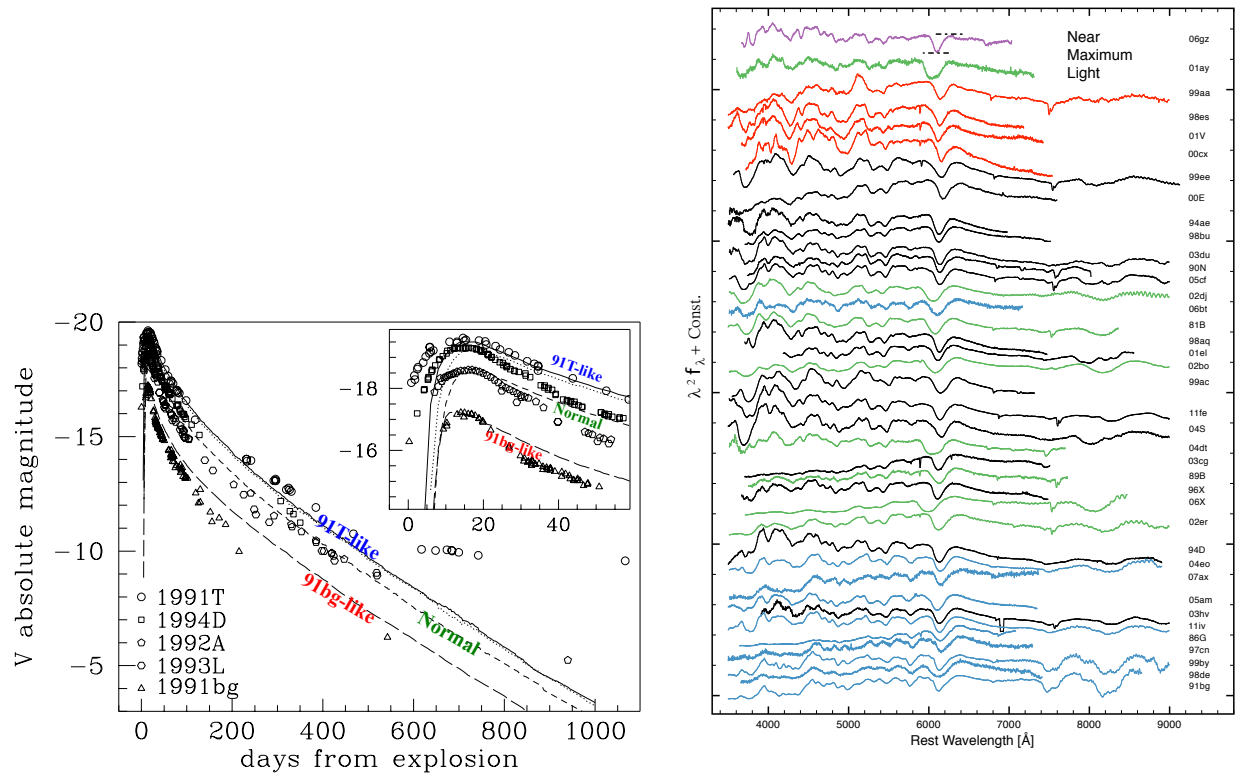


Figure 4: *Left panel*: examples of LCs for the SN Ia subclasses (are borrowed from [20]). *Right panel*: examples of optical spectra for subclasses of Type Ia SNe. Spectra of 91T-like, normal SNe Ia, and 91bg-like events are plotted in red, black, and blue, respectively. Spectra of other peculiar SNe Ia are plotted in different colours (are taken from [21]).

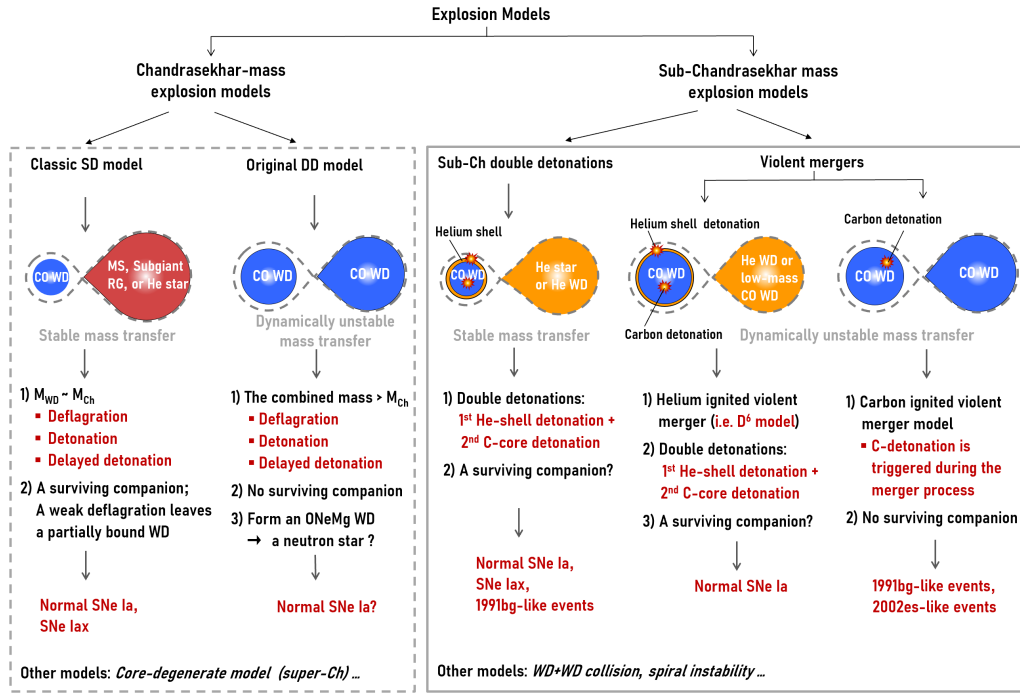


Figure 5: Various SN Ia explosion models in the framework of either Chandrasekhar-mass or sub-Chandrasekhar-mass explosions (is taken from [22]). The models that are shown here are not yet comprehensive.

its companion, causing the WD mass to exceed the Chandrasekhar limit ( $\approx 1.4M_{\odot}$ ), at that moment a thermonuclear explosion ensues. In the DD channel [23, 24], double WD system loses angular momentum due to gravitational wave emission, leading to coalescence and explosion (see [25], for a comprehensive review including the scenarios where the WD explodes at masses both above and below the Chandrasekhar limit.

Theoretically, in sub-Chandrasekhar-mass ( $\text{sub-}M_{Ch} < 1.4M_{\odot}$ ) explosion models, the luminosity of SN Ia is closely proportional to the exploding WD’s mass [26, 27]: WD in DD system, which has mass lower than  $M_{Ch}$  may, under appropriate circumstances, explodes as fainter SN Ia with faster declining LCs [28, 29]. Note that, in comparison to WD around the  $M_{Ch}$  mass, WD with a lower mass comes from a main-sequence progenitor star with a lower mass and consequently with a longer lifetime (older progenitors). Fig. 5 provides a diagrammatic representation illustrating different explosion models (channels) for Type Ia SNe, proposed within the context of either  $M_{Ch}$  or  $\text{sub-}M_{Ch}$  detonations.

It is observationally confirmed that CC SNe host galaxies are mostly spiral or irregular

galaxies with young stellar populations, while only SNe Ia can be produced by the aged stellar population residing within early-type galaxies [30, 31]. The spatial distribution of SNe within host galaxies offers a significant constraint on the characteristics of their progenitor stars. Instead of SNe Ia [32], CC SNe are strongly connected to the spiral arm structure [33–35] and all to the disc of their hosts [33]. Much work has been done to determine the nature of SNe progenitors by studying the relations between the properties of SNe and characteristics of galaxies in which they are discovered [36–45].

Interestingly, in addition to regular spiral arms and bars, the star formation desert (SFD) phenomenon has been observed in discs of some spiral galaxies [46–48], which is a region swept up by a strong bar with almost no recent star formation (SF) on both sides of the bar. There are increasing evidences in observations and simulations that SFD consists of old stars, and the quenching of SF in this region was due to the bar formation [49, 50], which dynamically removed gas from SFD over a timescale of  $\sim 2$  Gyr [49]. It can be considered that the SFD is practically not contaminated by the radial migration of young stars from the outer disc [51].

On the other hand, the distribution of Type Ia SNe traces the distribution of old stellar population via  $R$ -band continuum emission in host disc galaxies, while the distribution of CC SNe is strongly related to the distribution of young SF population traced by  $H\alpha$  emission (see [42], for the recent review). Therefore, it is expected that the bar effect (or SFD) in disc galaxies would leave its “fingerprints” on the radial distributions of Type Ia and CC SNe.

Importantly, SN Ia LC decline rate can be linked to the global age (or morphology, see Fig. 6) of host galaxy [28], which is usually considered as a rough proxy for the SN Ia delay time (i.e. time interval between the progenitor formation and its subsequent explosion). The correlation between the  $\Delta m_{15}$  of normal SNe Ia and hosts’ global age appears to be due to the superposition of at least two distinct populations of faster and slower declining SNe Ia from older and younger stellar populations, respectively [52]. For the most common peculiar SNe Ia, the 91bg-like (subluminous and fast declining) events probably come only from the old population, while 91T-like (overluminous and slow declining) SNe originate only from the young population of galaxies. Thus, the SN Ia LC properties, delay time distribution (DTD),

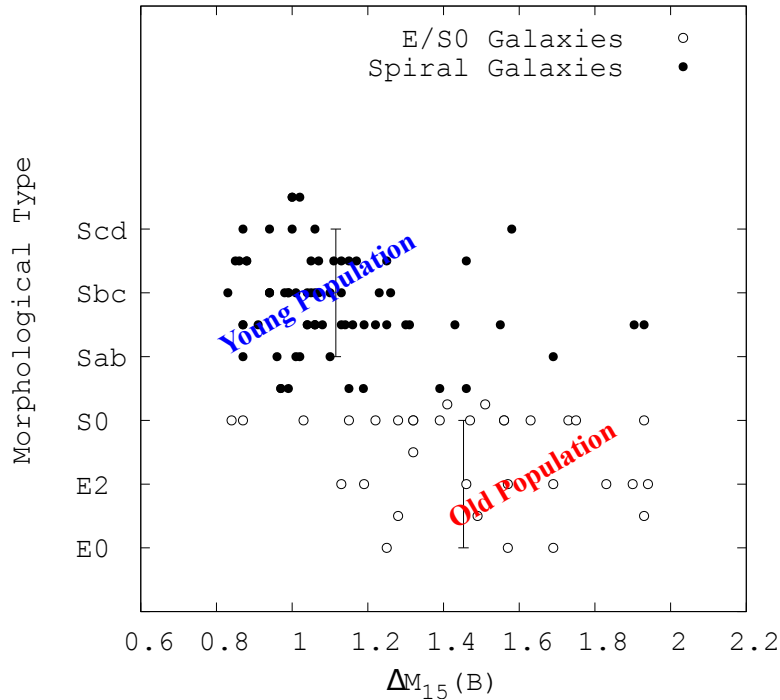


Figure 6: Host galaxy morphological type (a proxy of global age) versus SN Ia LC decline rate  $\Delta m_{15}$ . Figure is taken from [36] and modified.

and relations with other host characteristics allow to strongly constrain the SN Ia progenitor scenarios (see discussion in [52]). Given this, and if the progenitor age is the main driver of the decline rate, the SNe Ia discovered in the SFDs should have faster declining LCs.

Constraints on SN progenitors can also be approached from an alternative perspective, such as by studying the spiral structure of host galaxies. The spiral arm structure of star-forming disc galaxies was explained in the framework of density wave (DW) theory by the pioneering work of Lin & Shu [53]. According to this theory, semi-permanent spiral patterns especially in grand-design (GD) galaxies, i.e. spiral galaxies with prominent and well-defined spiral arms, are created by long-lived quasi-stationary DWs. The results of many studies are consistent with the picture where the DWs cause massive SF to occur by compressing gas clouds as they pass through the spiral arms of GD galaxies [54–58]. The first attempt to study the distribution of SNe within the framework of DW theory was performed by Moore [59]. The mentioned study suggested that stars in a spiral galaxy are formed in a shock front on the inner edge of a spiral arm, then drift across the arm as they age, predicting for SN progenitors (more likely for CC

SNe) a short lifetime (a few million years) and high masses (a few tens of solar masses). In the context of mentioned scenarios, it is important to study the possible impact of spiral DWs (SF triggering effect) on the distribution and surface density of SNe in discs of host galaxies, when viewing in the light of different nature of Type Ia and CC SNe progenitors [60, 61]. Thus, the distance from the spiral arm/from progenitor birthplace is a potential indicator of SN progenitor lifetime, offering a means to constrain SN progenitors. In addition, SN Ia LC decline rates can be examined based on their spatial location, whether on spiral arms or in the interarm regions. Moreover, the SN Ia LC decline rate  $\Delta m_{15}$  can be associated with the aforementioned distance from the host arms, functioning as a proxy for progenitor stellar age.

The central aim of this PhD thesis is to scrutinize the spectral and photometric properties of Type Ia and CC SNe and establish connections with the properties of their host stellar populations, specifically focusing on dynamical ages within galaxies. This exploration seeks to provide additional constraints on the nature of the SNe progenitors.

The thesis consists of four chapters. In Chapter 1 is analysed the impact of bars and bulges on the radial distributions of the different types of SNe in the stellar discs of host galaxies with various morphologies. Chapter 2 performs a comparative analysis of the locations and LC decline rates ( $\Delta m_{15}$ ) of normal and peculiar SNe Ia in the SFDs and beyond. Chapter 3 presents an analysis of the impact of spiral DWs on the radial and surface density distributions of CC SNe in host galaxies with different arm classes. Chapter 4 performs an analysis of the distribution of SNe Ia relative to spiral arms of their host galaxies and study their LC decline rates. The derived principal findings are succinctly recapped in the General Conclusions.

A substantial part of this research embodies *new exploration*, and the resultant findings are *mostly unprecedented*. These outcomes constitute the essence of the thesis defense.

# Chapter 1

## The impact of bars and bulges on the radial distribution of SF in disc galaxies

### 1.1 Introduction

In the realm of disc galaxies, bars are a common feature observed in approximately 40 per cent of nearby S0–Sm galaxies [62]. In the central regions of these disc galaxies, about one-third have strong barred structure, which generally affects both the motions of stars and interstellar gas and can affect spiral arms as well (for a comprehensive review see [63]). In addition, the relative sizes of bars and bulges seems to be correlated [64], thus indicating that the growth of bars and bulges are somehow connected.

In spiral galaxies, most of the massive SF occurs in the discs where bars, if present, have a strong impact on the radial distribution of SF, particularly in early Hubble types. [46] used H $\alpha$  and *R*-band imaging to determine the distributions of young and old stellar populations in several hundreds of nearby S0/a–Im field galaxies. They identified a clear effect of bars on the pattern of massive SF as a function of radius within discs. This effect results in a strongly enhanced H $\alpha$  emission, and moderately enhanced *R*-band emission in both the central regions and at the bar-end radius of galaxies (see also [47]). The authors noted that this effect seems to be stronger in galaxies classified as barred Sb or Sbc, where the overall distributions of SF

markedly different from that in their unbarred counterparts.

In this context, we are investigating the possible impact of stellar bars and bulges on the radial distributions of the different types of SNe in S0–Sm host galaxies.

[65] attempted to find differences in the radial distributions of SNe in barred and unbarred spiral host galaxies (see also [66–68]). No significant differences were found, most probably due to small number statistics, inhomogeneous data sets of SNe and their hosts, and unsatisfying considerations for the relations between the bar lengths, bulge sizes, and morphological types of SNe host galaxies. On the other hand, [69] attempted to estimate the contribution from bulge components of spiral host galaxies to the entire radial distribution of SNe Ia. They noted that the stellar bulges in spirals are not efficient producers of Type Ia SNe (see also [70]). But again, the above mentioned impact of bars on the radial distributions of young and old stellar populations in the discs was not considered.

The aim of this Chapter is to address these questions properly through a study of the radial distributions of Type Ia and CC (Ibc and II) SNe in a well-defined and homogeneous sample of 500 nearby SNe and their low-inclined and morphologically non-disturbed S0–Sm galaxies from the coverage of Sloan Digital Sky Survey-III (SDSS-III; [71]).

In [72] is created a large and well-defined database that combines extensive new measurements and a literature search of 3876 SNe and their 3679 host galaxies located within the sky area covered by the SDSS Data Release 8 (DR8). This database is much larger than previous ones, and provides a homogeneous set of global parameters of SN hosts, including morphological classifications and measures of activity classes of nuclei. Moreover, [72] is analysed and discussed many selection effects and biases, which usually affect the statistical studies of SNe. In [73] is presented an analysis of the relative frequencies of the different SN types in nearby spiral galaxies with various morphological types and with or without bars. We used a subsample of spiral host galaxies of 692 SNe in different stages of galaxy–galaxy interaction and activity classes of nucleus. We proposed that the underlying mechanisms shaping the number ratios of SNe types could be interpreted within the framework of interaction-induced SF, in addition to the known relations between morphologies and stellar populations. For more details, the reader

is referred to [72] and [73].

Throughout this Chapter, we adopt a cosmological model with  $\Omega_m = 0.27$ ,  $\Omega_\Lambda = 0.73$ , and a Hubble constant is taken as  $H_0 = 73 \text{ km s}^{-1} \text{ Mpc}^{-1}$  [74], both to conform to values used in the mentioned database.

## 1.2 Sample selection and reduction

For this Chapter, we compiled our sample by cross-matching the coordinates of classified Ia, Ibc<sup>1</sup>, and II SNe from the Asiago Supernova Catalogue<sup>2</sup> (ASC; [75]) with the coverage of SDSS DR10 [71]. All SNe are required to have coordinates and/or positions (offsets) with respect to the nuclei of their host galaxies. We use SDSS DR10 and the techniques presented in [72] to identify the SNe host galaxies and classify their morphological types. Since we are interested in studying the radial distribution of SNe in stellar discs of galaxies, the morphologies of hosts are restricted to S0–Sm types.

[72] showed that the sample of SNe is largely incomplete beyond 100 Mpc (see also [73]). Thus, to avoid biasing the current sample against or in favour of one of the SN types, we truncate the sample to distances  $\leq 100$  Mpc.

In addition, following the approach described in detail in [73], we classify the morphological disturbances of the host galaxies from the visible signs of galaxy–galaxy interactions in the SDSS DR10. We adopted the following categories for SN host disturbances: normal (hosts without any visible disturbance in their morphological structure), perturbed (hosts with visible morphological disturbance, but without long tidal arms, bridges, or destructed spiral patterns), interacting (hosts with obvious signs of galaxy–galaxy interaction), merging (hosts with ongoing merging process), and post-merging/remnant (single galaxies that exhibit signs of a past interaction, with a strong or relaxed disturbance). Here, we make use of this classification in order to exclude from the present analysis any host galaxy exhibiting strong disturbances

---

<sup>1</sup>By SN Ibc, we denote stripped-envelope SNe of Types Ib and Ic, as well as mixed Ib/c whose specific subclassification is uncertain.

<sup>2</sup>We use the updated version of the ASC to include all classified SNe exploded before 2014 January 1.

Table 1.1: Numbers of SNe at distances  $\leq 100$  Mpc and inclinations  $i \leq 60^\circ$  within host disc galaxies as a function of morphological types, split between barred and unbarred.

	Barred											
	S0	S0/a	Sa	Sab	Sb	Sbc	Sc	Scd	Sd	Sdm	Sm	All
Ia	1	9	5	8	13	13	13	6	12	3	0	83
Ib	0	0	0	0	1	5	3	0	1	2	1	13
Ib/c	0	0	0	0	0	2	0	0	0	0	0	2
Ic	0	0	0	0	1	3	5	4	4	0	0	17
II	0	0	0	2	15	17	19	8	25	8	2	96
IIb	0	0	1	0	0	3	2	0	2	0	0	8
All	1	9	6	10	30	43	42	18	44	13	3	219
	Unbarred											
	S0	S0/a	Sa	Sab	Sb	Sbc	Sc	Scd	Sd	Sdm	Sm	All
Ia	7	11	4	4	10	22	26	5	4	0	4	97
Ib	0	0	0	1	0	7	8	2	0	0	0	18
Ib/c	0	0	0	1	3	0	1	1	1	0	0	7
Ic	0	0	0	0	1	6	13	2	1	0	0	23
II	1	0	0	0	15	22	64	13	6	3	2	126
IIb	0	0	0	0	0	0	5	3	0	2	0	10
All	8	11	4	6	29	57	117	26	12	5	6	281

Among the SNe types, there are only 31 uncertain (‘.’ or ‘\*’) and 35 peculiar (‘pec’) classifications. All Type IIIn SNe are removed from the sample due to uncertainties in their progenitor nature, and often in their classification [7, 76].

(interacting, merging, and post-merging/remnant).

We measure the geometry of host galaxies using the Graphical Astronomy and Image Analysis<sup>3</sup> tool according to the approaches presented in [72].<sup>4</sup> First, we construct 25 mag arcsec<sup>-2</sup> isophotes in the SDSS DR10  $g$ -band, and then we visually fit on to each isophote an elliptical aperture centred at each galaxy centroid position. From the fitted elliptical apertures, we derive the major axes ( $D_{25}$ ), elongations ( $a/b$ ), and position angles (PA) of the major axes of galaxies. In further analysis, we use the  $D_{25}$  corrected for Galactic and host galaxy internal extinction. We then calculate the inclinations of host galaxies using elongations and morphological types following the classical Hubble formula. More details on these procedures are found in [72]. Finally, an additional restriction on the inclinations ( $i \leq 60^\circ$ ) of hosts is required to minimize

<sup>3</sup>Graphical Astronomy and Image Analysis tool is available for download as part of JAC Starlink Release at <http://starlink.jach.hawaii.edu>.

<sup>4</sup>The database of [72] is based on the SDSS DR8. Here, because we added new SNe in the sample, for homogeneity we re/measure the geometry of all host galaxies based only on DR10.

absorption and projection effects in the discs of galaxies.<sup>5</sup>

After these restrictions, we are left with a sample of 500 SNe within 419 host galaxies.<sup>6</sup> For these host galaxies, we do visual inspection of the combined SDSS  $g$ -,  $r$ -, and  $i$ -band images, as well as check the different bands separately to detect any sign of barred structure in the stellar discs. In [72], it is demonstrated that given their superior angular resolution and three-colour representations, the SDSS images, especially for low-inclined galaxies, offer a much more reliable and capacious source for bar detection than do the other images, e.g. plate-based images on which most of the HyperLeda/NED classifications were performed. To check the consistency of bar detection in our sample with that of the SDSS-based EFIGI<sup>7</sup> catalogue of nearby visually classified 4458 PGC galaxies [77], we select a subsample of 149 galaxies that are common to both EFIGI and to our sample of SNe hosts. Following [73], we compare the EFIGI `Bar Length` attribute<sup>8</sup> with our detection (bar or no bar). When the `Bar Length` is 0 or 2, our bar detection is different for only 6 per cent of cases. When the `Bar Length` is 3 or 4, our bar detection completely matches with that of the EFIGI. However, we do not detect bars in 30 per cent of the cases when `Bar Length` is 1. Hence, the EFIGI `Bar Length` = 1 mainly corresponds to the threshold of our bar detection, i.e., barely visible bar feature with a length about one-tenth of  $D_{25}$ .<sup>9</sup> Table 1.1 displays the distribution of all SNe types among the various considered morphological types for their barred and unbarred host galaxies.

### 1.3 Results and discussion

We now study the possible influence of bars and bulges on the SNe distributions through an analysis of the radial distributions of different types of SNe in discs of host galaxies with various

---

<sup>5</sup>The sample with  $i > 60^\circ$  is only used in Section 1.3.1 for ancillary purposes.

<sup>6</sup>The full database of 500 individual SNe (SN designation, type, and offset from host galaxy nucleus) and their 419 host galaxies (galaxy SDSS designation, distance, morphological type, bar, corrected  $g$ -band  $D_{25}$ ,  $a/b$ , PA, and inclination) is available online [78].

<sup>7</sup>Extraction de Formes Idéalisées de Galaxies en Imagerie.

<sup>8</sup>This attribute quantifies the presence of a central bar component in the galaxy, in terms of length relative to the galaxy major axis  $D_{25}$ . `Bar Length` = 0 (no visible bar); 1 (barely visible bar feature); 2 (short bar, with a length about one-third of  $D_{25}$ ); 3 (long bar, that extends over about half of  $D_{25}$ ); 4 (very long, prominent bar that extends over more than half of  $D_{25}$ ).

<sup>9</sup>Later in this Chapter, we will see that this very central region of galaxies with tiny bars is almost always restricted to the first bin of the radial distribution of SNe, and therefore cannot statistically bias our results.

morphological types. Here, we widely use our morphological classification, bar detection, and geometry for SNe host galaxies, while for bulge parameters (e.g. bulge-to-disc mass ratio: B/D) we only indirectly consider their statistical relations to the Hubble sequence [62]).

### 1.3.1 Galactocentric radius deprojection and normalization

We apply the inclination correction to the projected (observed) galactocentric radii of SNe as described in [65]. The reliability of the inclination correction is based on the fundamental assumption that SNe belong mostly to the disc, rather than the bulge component in S0–Sm galaxies [33, 79–87]. This assumption is natural for CC SNe, considering the requirement that massive young stars are progenitors [7, 8] located in the discs of host galaxies [65, 88]. The spatial distribution of SNe Ia, arising from older WD in binary systems [25], is more complicated and consists of two interpenetrating components [89]: disc and bulge SNe.

If SNe belong mostly to the bulge component, one would expect that the distributions of their projected galactocentric distances (normalized to the  $g$ -band 25<sup>th</sup> magnitude isophotal semimajor axis;  $R_{25} = D_{25}/2$ ) along major ( $U/R_{25}$ ) and minor ( $V/R_{25}$ ) axes would be the same both in face-on ( $i \leq 60^\circ$ ) and in edge-on ( $i > 60^\circ$ ) disc galaxies. The projected  $U$  and  $V$  galactocentric distances (in arcsec) of an SN are

$$\begin{aligned} U &= \Delta\alpha \sin \text{PA} + \Delta\delta \cos \text{PA} , \\ V &= \Delta\alpha \cos \text{PA} - \Delta\delta \sin \text{PA} , \end{aligned} \tag{1.1}$$

where  $\Delta\alpha$  and  $\Delta\delta$  are offsets of the SN in equatorial coordinate system, and PA is position angle of the major axis of the host galaxy. For more details of these formulae, the reader is referred to [65].

The  $R_{25}$  normalization is important because the distribution of linear distances (in kpc) is strongly biased by the greatly different intrinsic sizes of host galaxies (see fig. 2 in [65]). In linear scale, there would be a systematic overpopulation of SNe at small galactocentric distances as this region would be populated by SNe exploding in all host galaxies, including the smaller

Table 1.2: Comparison of the 2D spatial distributions of SNe among different subsamples of S0–Sm galaxies.

Subsamples		SN	$i \leq 60^\circ$					$i > 60^\circ$				
(1)	versus (2)		$N_{\text{SN}}$	$\sigma_1$	$\sigma_2$	$P_{\text{KS}}$	$P_{\text{AD}}$	$N_{\text{SN}}$	$\sigma_1$	$\sigma_2$	$P_{\text{KS}}$	$P_{\text{AD}}$
$U/R_{25}$	versus $V/R_{25}$	Ia	180	0.394	0.299	0.217	<b>0.026</b>	105	0.385	0.154	<b>0.001</b>	<b>0.000</b>
$U/R_{25}$	versus $V/R_{25}$	CC	320	0.382	0.299	<b>0.003</b>	<b>0.002</b>	181	0.349	0.132	<b>0.000</b>	<b>0.000</b>
$U/R_{25}$	versus $V/r_{25}$	Ia	180	0.394	0.387	0.561	0.646	105	0.385	0.390	0.174	0.321
$U/R_{25}$	versus $V/r_{25}$	CC	320	0.382	0.384	0.120	0.162	181	0.349	0.327	0.564	0.568

The  $P_{\text{KS}}$  and  $P_{\text{AD}}$  are the probabilities from two-sample KS and AD tests, respectively, that the two distributions being compared (with respective standard deviations  $\sigma_1$  and  $\sigma_2$ ) are drawn from the same parent distribution. The  $P_{\text{KS}}$  and  $P_{\text{AD}}$  are calculated using the calibrations by [90] and [91], respectively. The statistically significant differences between the distributions are highlighted in bold.

ones, while larger distances would only be populated by the SNe occurring in the larger hosts.

Fig. 1.1 shows (in red) the  $V/R_{25}$  versus  $U/R_{25}$  distributions in face-on and edge-on S0–Sm galaxies, as well as their histograms. The sample of SNe in face-on galaxies consists of 180 Ia and 320 CC SNe (see Table 1.1), while the ancillary sample of SNe in edge-on hosts (not shown in Table 1.1) includes 105 Ia and 181 CC SNe. In disc galaxies, all types of SNe preferentially appear along the major  $U$  axis (see the standard deviations in Table 1.2). This effect is stronger in edge-on galaxies. In fact, the two-sample Kolmogorov–Smirnov (KS) and Anderson–Darling (AD) tests,<sup>10</sup> shown in Table 1.2, indicate that the distributions of  $U/R_{25}$  and  $V/R_{25}$  are significantly different, both for Type Ia and CC SNe (except for Type Ia SNe in face-on hosts with the KS test).

It is worth mentioning that Sa–Sm galaxies contain stellar populations of different ages and host both Type Ia and CC SNe. While S0 and S0/a galaxies, which are mostly populated by old stars and have prominent bulges, host Type Ia SNe. A tiny fraction of CC SNe has also been detected in galaxies classified as S0. Nevertheless, in these rare cases, there is some evidence of residual SF in the SN hosts, due to merging/accretion or interaction with close neighbours in the past [72, 92]. The distribution of SNe types versus morphology of the host

<sup>10</sup>The two-sample AD test is more powerful than the KS test [93], being more sensitive to differences in the tails of distributions. Traditionally, we chose the threshold of 5 per cent for significance levels of the different tests.

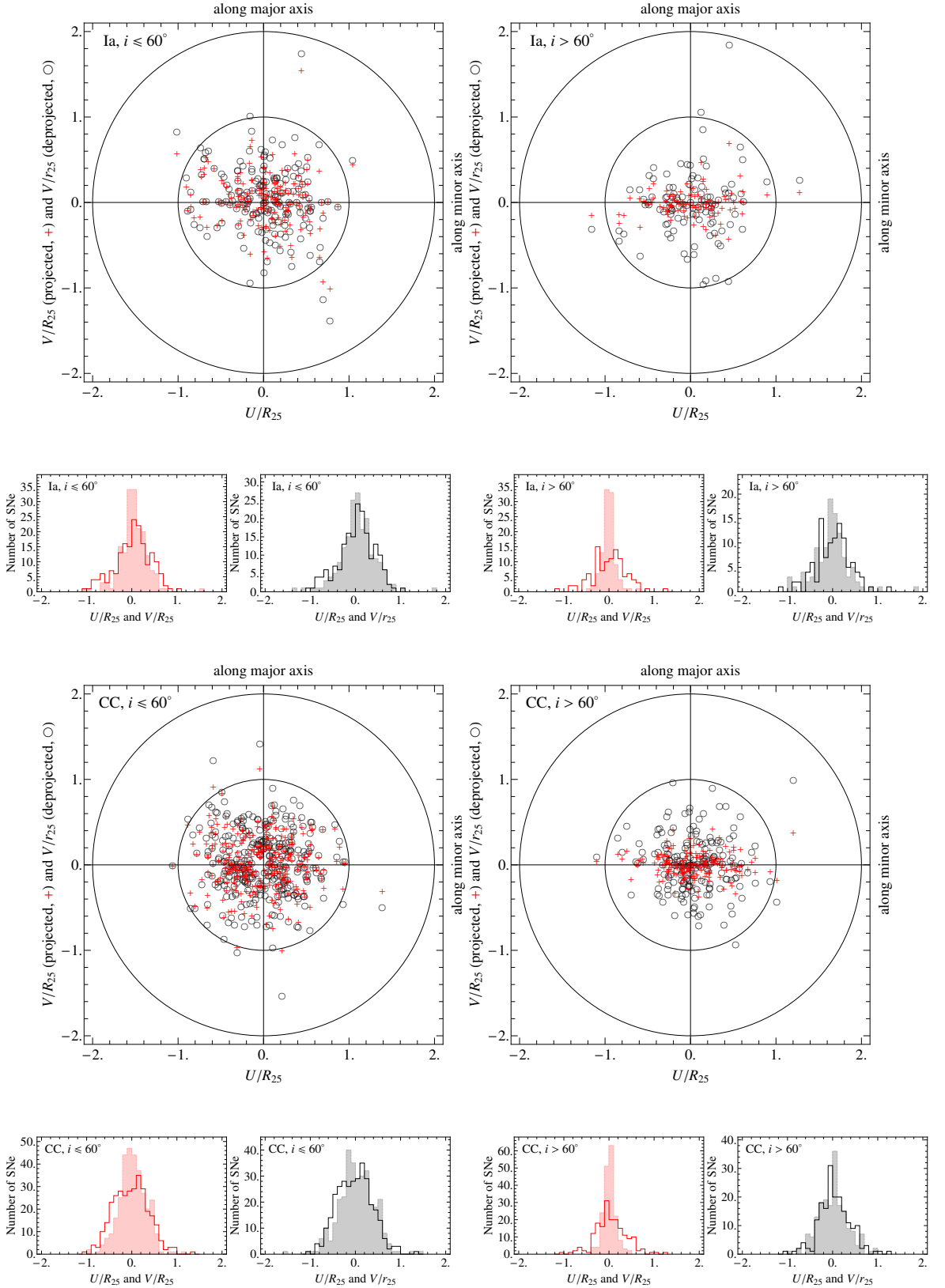


Figure 1.1: Distributions of normalized galactocentric distances of Type Ia and CC SNe along major ( $U/R_{25}$ ) and minor ( $V/R_{25}$  and  $V/r_{25}$ ) axes in face-on ( $i \leq 60^\circ$ ) and edge-on ( $i > 60^\circ$ ) disc (S0–Sm) galaxies, where  $r_{25} = R_{25} \cos i$  is the isophotal semiminor axis. The red crosses represent  $U/R_{25}$  and  $V/R_{25}$  pairs, while the black open circles show  $U/R_{25}$  and  $V/r_{25}$  pairs. The solid histograms are the distributions of  $U/R_{25}$ , while the shaded histograms are the distributions of  $V/R_{25}$  and  $V/r_{25}$ . The two concentric circles are the host galaxy  $R_{25}$  and  $2R_{25}$  sizes.

galaxies, shown in Table 1.1, is consistent with this picture. In this sense, when selecting only Sa–Sm hosts, the  $P_{\text{KS}}$  for Type Ia SNe in the face-on sample becomes significant (it is reduced to 0.045), suggestive of a possible contribution from bulge SNe Ia in S0–S0/a galaxies. For Sa–Sm galaxies, the probabilities of KS and AD tests for the other subsamples do not change the results of Table 1.2.

Performing simple calculations, we find that the ratio of the mean values of  $|V|$  and  $|U|$  is 0.71 for Type Ia and 0.75 for CC SNe in face-on, and, respectively, 0.35 and 0.36 in edge-on galaxies. These numbers are very close to the mean values of the cosines of the inclinations ( $\langle \cos i \rangle = 0.74 \pm 0.01$  in face-on galaxies and  $0.31 \pm 0.02$  in edge-on galaxies – where the uncertainties are the errors on the means), thus supporting the fact that the vast majority of SNe in S0–Sm galaxies are distributed within the stellar discs. Similar results are found when only considering Sa–Sm galaxies. This also suggests that the rate of SNe Ia in spiral galaxies is dominated by a relatively young/intermediate progenitor population [94–97].

For deprojected host discs, in Fig. 1.1 we also show (in black) the  $V/r_{25}$  versus  $U/R_{25}$  distributions and their histograms for different samples, where  $r_{25}$  is the  $g$ -band 25th magnitude isophotal semiminor axis ( $r_{25} = R_{25} \cos i$ ). In contrast to the previous normalization, the KS and AD tests show that the distributions of  $U/R_{25}$  and  $V/r_{25}$  both for Type Ia and CC SNe could be drawn from the same parent distribution (see Table 1.2). In addition, the ratios of the mean values of  $|V|/r_{25}$  and  $|U|/R_{25}$  in different samples are approximately equal to unity. Thus, after correcting the host galaxies for inclination effects, the distributions of SNe along major ( $U/R_{25}$ ) and minor ( $V/r_{25}$ ) axes turn to be equivalent (see also the standard deviations in Table 1.2). Hereafter, we restrict our analysis to the face-on sample to minimize absorption and projection effects in the discs of galaxies.

We now adopt the oversimplified model where all SNe are distributed on infinitely thin discs of the host galaxies. While this is a reasonable assumption for SNe within spiral hosts, we shall extend this assumption to S0–S0/a galaxies, for which many find a disc distribution of SNe [65, 88] for CC and [86, 98] for Type Ia SNe.

In this thin-disc approximation, the corrected galactocentric radius (in arcsec) of the SN in

the host disc satisfies

$$R_{\text{SN}}^2 = U^2 + \left( \frac{V}{\cos i} \right)^2. \quad (1.2)$$

We pay particular attention and discuss the cases when the contribution from the bulge SNe Ia becomes apparent, especially in S0–S0/a hosts.

## 1.4 Influence of bars and bulges on the radial distribution of SNe

The upper panel of Fig. 1.2 compares the distributions of deprojected, normalized galactocentric radii ( $\tilde{r} = R_{\text{SN}}/R_{25}$ ) of Type Ia and CC SNe in S0–S0/a and Sa–Sm galaxies. In this panel, we see an initial rise of SNe number as a function of  $\tilde{r}$  and a negative radial gradient outside the maximum, suggestive of the exponential surface brightness distribution of stellar discs, which we will study in more detail in Section 1.4.1. In previous studies, based on smaller samples, similar deprojected distributions of SNe were already obtained by normalizing them to the radii of hosts at some fixed surface brightness isophot [33, 65–68, 80–82, 86, 87, 99–107].

The observed numbers of SNe at  $\tilde{r} \lesssim 0.2$  indicate that different SN searches fail to discover objects at or near the centre of the surveyed galaxies [98, 108]. In an earlier study, [109] noted that this effect is stronger for distant host galaxies relative to nearer ones. Then it became apparent that this *Shaw effect* is important for deep photographic searches and negligible for visual and CCD searches [108, 110]. Presently, SN searches are conducted only with CCD cameras and SNe are discovered via image subtraction, so the discrimination against SNe occurring near the bright nuclei of galaxies is less strong. Nevertheless, an area with a radius of a few pixels centred on every galaxy nucleus is usually excluded during a search, because galactic nuclei often suffer imperfect image subtraction and introduce many false sources [111]. Another difficulty is that extinction by dust in host galaxy discs, depending on inclination, can affect the radial distributions of SNe, particularly in the nuclear region [69, 89, 112].

To check the possible influences of these selection effects on the radial distribution of SNe,

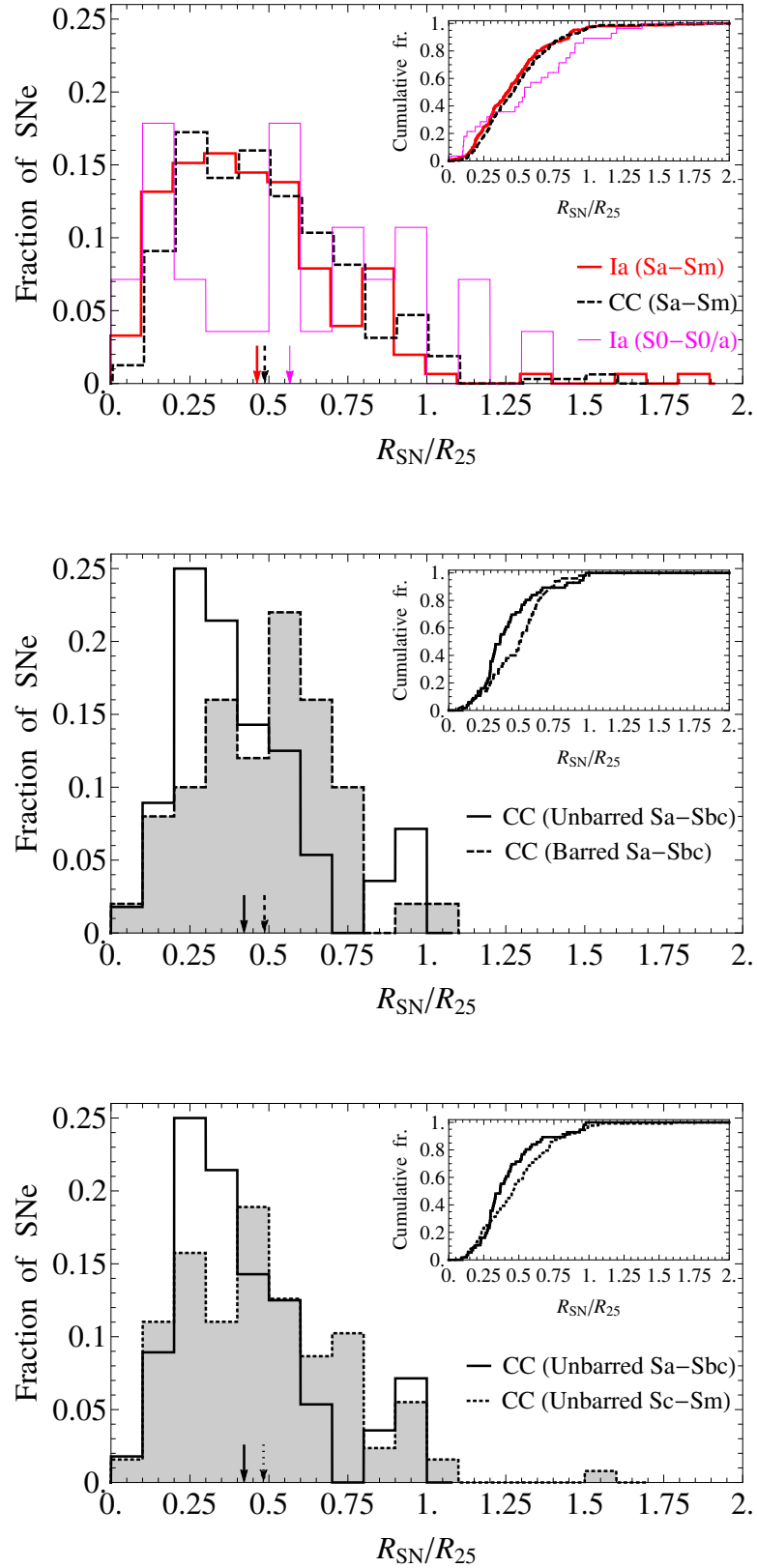


Figure 1.2: Upper panel: distributions of deprojected and normalized galactocentric radii ( $\tilde{r} = R_{\text{SN}}/R_{25}$ ) of Type Ia SNe in S0-S0/a and Sa-Sm hosts, as well as CC SNe in Sa-Sm galaxies. Middle panel: the distributions of CC SNe in barred and unbarred Sa-Sbc hosts. Bottom panel: the distributions of CC SNe in unbarred Sa-Sbc and Sc-Sm galaxies. The insets present the cumulative distributions of SNe. The mean values of the distributions are shown by arrows.

Table 1.3: Comparison of the normalized, deprojected radial distributions of SNe among different pairs of subsamples possibly affected by selection effects.

Subsample 1	Subsample 2	Ia				CC			
		$N_{\text{SN}}(1)$	$N_{\text{SN}}(2)$	$P_{\text{KS}}$	$P_{\text{AD}}$	$N_{\text{SN}}(1)$	$N_{\text{SN}}(2)$	$P_{\text{KS}}$	$P_{\text{AD}}$
$0 < D(\text{Mpc}) \leq 60$ (S0–S0/a)	versus $60 < D(\text{Mpc}) \leq 100$ (S0–S0/a)	10	18	0.566	0.416	0	1	–	–
$0 < D(\text{Mpc}) \leq 60$ (Sa–Sm)	versus $60 < D(\text{Mpc}) \leq 100$ (Sa–Sm)	69	83	0.692	0.620	168	151	0.683	0.465
$0^\circ \leq i \leq 40^\circ$ (S0–S0/a)	versus $40^\circ < i \leq 60^\circ$ (S0–S0/a)	11	17	0.973	0.883	0	1	–	–
$0^\circ \leq i \leq 40^\circ$ (Sa–Sm)	versus $40^\circ < i \leq 60^\circ$ (Sa–Sm)	64	88	0.190	0.412	134	185	0.938	0.821
$t \leq 2000$ yr (S0–S0/a)	versus $t > 2000$ yr (S0–S0/a)	6	22	0.348	0.560	0	1	–	–
$t \leq 2000$ yr (Sa–Sm)	versus $t > 2000$ yr (Sa–Sm)	58	94	0.997	0.857	108	211	0.517	0.635

Each pair of the subsamples is selected, if possible, to include comparable numbers of SNe in both subsamples.

we compare, in Table 1.3, the radial distributions of SNe in different pairs of subsamples where these selection effects may produce different radial SN distributions. For this, we performed two-sample KS and AD tests between the pairs of radial SN distributions. These tests show that the radial distributions of Type Ia and CC SNe in our sample are not affected by distance or inclination of the host galaxy, nor by the SN discovery epoch (photographic/CCD searches).

We now compare, in Table 1.4, the distributions of the normalized deprojected radii for pairs of subsamples that should not be affected by selection effects. We see no statistically significant differences between the radial distributions of Type Ia and CC SNe in all the subsamples of Sa–Sm galaxies. In contrast, the cumulative radial distributions of SNe Ia in S0–S0/a and Sa–Sm galaxies apparently deviate from one another (as seen in the AD statistic but only very marginally so in the KS statistic). Fig. 1.2, indeed shows signs of a bimodal radial distribution for SNe Ia in S0–S0/a galaxies.

Naturally, one expects that among disc galaxies, bulge SNe Ia should have highest contribution to the whole distribution of SNe Ia in S0–S0/a subsample, because among disc galaxies the ratio of bulge luminosity over disc luminosity (or B/D) is highest in the S0–S0/a subsample [62, 113–115]. In the case of Sa–Sm galaxies, both Type Ia and CC SNe dominate in the Sbc–Sc morphological bin (see Table 1.1), where the B/D ratio is significantly lower than that in S0–S0/a galaxies [62, 113]. Moreover, the radial distributions of Type Ia and CC SNe in all the Sa–Sm subsamples can be drawn from the same parent distribution (see the  $P$ -values in Table 1.4) supporting the fact that in these galaxies SNe Ia mostly exploded in the disc

Table 1.4: Comparison of the normalized, deprojected radial distributions of SNe among different pairs of subsamples.

Subsample 1			Subsample 2			$P_{KS}$	$P_{AD}$	
Host	SN	$N_{SN}$	Host	SN	$N_{SN}$			
S0–S0/a	Ia	28	versus	Sa–Sm	Ia	152	0.099	<b>0.020</b>
Sa–Sm	Ia	152	versus	Sa–Sm	CC	319	0.568	0.259
Sa–Sm (barred)	Ia	73	versus	Sa–Sm (barred)	CC	136	0.483	0.378
Sa–Sm (unbarred)	Ia	79	versus	Sa–Sm (unbarred)	CC	183	0.349	0.342
Sa–Sm (barred)	Ia	73	versus	Sa–Sm (unbarred)	Ia	79	0.192	0.313
Sa–Sm (barred)	CC	136	versus	Sa–Sm (unbarred)	CC	183	0.060	0.076
Sa–Sbc	Ia	79	versus	Sa–Sbc	CC	106	0.683	0.751
Sa–Sbc (barred)	Ia	39	versus	Sa–Sbc (barred)	CC	50	0.528	0.627
Sa–Sbc (unbarred)	Ia	40	versus	Sa–Sbc (unbarred)	CC	56	0.702	0.473
Sa–Sbc (barred)	Ia	39	versus	Sa–Sbc (unbarred)	Ia	40	0.242	0.617
Sa–Sbc (barred)	CC	50	versus	Sa–Sbc (unbarred)	CC	56	<b>0.008</b>	<b>0.028</b>
Sc–Sm	Ia	73	versus	Sc–Sm	CC	213	0.424	0.276
Sc–Sm (barred)	Ia	34	versus	Sc–Sm (barred)	CC	86	0.670	0.575
Sc–Sm (unbarred)	Ia	39	versus	Sc–Sm (unbarred)	CC	127	0.340	0.355
Sc–Sm (barred)	Ia	34	versus	Sc–Sm (unbarred)	Ia	39	0.503	0.615
Sc–Sm (barred)	CC	86	versus	Sc–Sm (unbarred)	CC	127	0.581	0.276
Sa–Sbc	Ia	79	versus	Sc–Sm	Ia	73	0.850	0.956
Sa–Sbc	CC	106	versus	Sc–Sm	CC	213	0.183	0.156
Sa–Sbc (barred)	Ia	39	versus	Sc–Sm (barred)	Ia	34	0.992	0.967
Sa–Sbc (barred)	CC	50	versus	Sc–Sm (barred)	CC	86	0.489	0.278
Sa–Sbc (unbarred)	Ia	40	versus	Sc–Sm (unbarred)	Ia	39	0.822	0.961
Sa–Sbc (unbarred)	CC	56	versus	Sc–Sm (unbarred)	CC	127	<b>0.033</b>	0.067

The statistically significant differences between the distributions are highlighted in bold.

component where all CC SNe also occur. Thus, the apparent deviation of the radial distribution of Type Ia SNe in S0–S0/a galaxies from that in Sa–Sm hosts (upper panel of Fig. 1.2) is attributed to the contribution by SNe Ia from the bulge component of S0–S0/a galaxies.

Another interesting results stands out in Table 1.4. The radial distributions of CC SNe in barred versus unbarred Sa–Sbc galaxies are inconsistent (middle panel of Fig. 1.2), while for Type Ia SNe the radial distributions between barred and unbarred Sa–Sbc galaxies are not significantly different. At the same time, the radial distributions of both Type Ia and CC SNe in Sc–Sm galaxies are not affected by bars.

Interestingly, [46] discovered that several early-type barred spiral galaxies that had strong dips in their radial H $\alpha$  line emission profiles, near  $0.25 R_{25}$ .<sup>11</sup> This region is roughly where their unbarred counterparts host the strongest SF. The H $\alpha$  emission from barred Sb–Sbc galaxies showed central components and concentrations of SF at or just outside the bar-end radius. Except for the central component, where we have difficulties to discover SNe, the picture of [46] is very similar to that we observe for CC SNe in barred and unbarred Sa–Sbc galaxies (see the middle panel of Fig. 1.2 and fig. 8 in [46]). The region between the central component and bar-end radius of H $\alpha$  emission profiles is termed the star formation desert (SFD) by [47]. In addition, they noted that the SFD had significant continuum emission in the  $R$ -band and even showed line emission not consistent with expectations from SF, but most probably from an old stellar population.

Taking into consideration that the distributions of Type Ia and CC SNe, respectively, trace the distributions of  $R$ -band continuum emission/stellar mass and H $\alpha$  emission/SF [107, 116], we compare the inner ( $\tilde{r} \leq 0.3$ ) fractions of different SNe ( $F_{\text{SN}}$ ) in barred and unbarred host galaxies (see Table 1.5). This inner region is selected because in Sa–Sbc subsample the SNe dominate in Sb–Sbc galaxies (see Table 1.1), where the mean SFD region has outer radius  $\sim 0.3$  of the optical radius (see fig. 5 in [46]).<sup>12</sup>

<sup>11</sup>The dip in H $\alpha$  occurs at one-quarter of the isophotal radius corresponding to a surface magnitude of  $\mu_R = 24 \text{ mag arcsec}^{-2}$ , which in turn is roughly equal to  $R_{25}$ .

<sup>12</sup>Ideally, instead of using the  $\tilde{r} \leq 0.3$  region, we could perform bar length measurements for each of barred galaxy in the sample to obtain the fractions of different SNe in the radial range swept by bars. However, this is beyond the scope of this Chapter.

Table 1.5: Fractions of inner SNe in barred and unbarred host galaxies

Fractions of inner ( $R_{\text{SN}} \leq 0.3 R_{25}$ ) SNe in barred and unbarred host galaxies.

Host	SN	Barred		Unbarred		$P_{\text{B}}$
		$N_{\text{SN}}$	$F_{\text{SN}}$	$N_{\text{SN}}$	$F_{\text{SN}}$	
Sa–Sbc	Ia	39	$0.26^{+0.05}_{-0.04}$	40	$0.38^{+0.05}_{-0.05}$	0.170
Sa–Sbc	CC	50	$0.20^{+0.04}_{-0.03}$	56	$0.36^{+0.04}_{-0.04}$	<b>0.044</b>
Sc–Sm	Ia	34	$0.26^{+0.05}_{-0.05}$	39	$0.36^{+0.05}_{-0.05}$	0.240
Sc–Sm	CC	86	$0.26^{+0.03}_{-0.03}$	127	$0.28^{+0.02}_{-0.02}$	0.741

The standard deviations of the fractions are calculated using the approach of [117]. The significance value  $P_{\text{B}}$  is calculated using Barnard’s exact test [118], which compares the pairs of numbers rather than the fractions. The statistically significant difference between the fractions is highlighted in bold.

Table 1.5 shows that the inner  $\tilde{r} \leq 0.3$  fractions of Type Ia SNe in Sa–Sbc and Sc–Sm hosts are not statistically different between barred and unbarred galaxies. The same situation holds true for CC SNe in Sc–Sm galaxies. However, the inner fraction of CC SNe is significantly lower in barred Sa–Sbc galaxies compared with their unbarred counterparts. It is important to note that the inner fractions of Type Ia and CC SNe are not statistically different one from another when the same morphological and barred/unbarred categories are selected.

The results of Table 1.5 agree quite well with the findings of [47] that barred galaxies of earlier Hubble types have substantially suppressed SF [46], hence the lack of CC SNe in the inner radial range swept by the strong bars of Sa–Sbc galaxies. On the other hand, this region is not ‘forbidden’ to Type Ia SNe, because these SNe originate from an older stellar population also located in the bulge. CC SNe in barred Sc–Sm galaxies can appear in the inner regions because the effect of SF suppressing by bars is not seen in late-type barred galaxies [46, 47]. Thus, we see that bars of host galaxies affect the radial distributions of SNe, at least the CC ones, in the stellar discs of early-type galaxies.

According to Table 1.4 and the bottom panel of Fig. 1.2, we also see that the radial distribution of CC SNe in unbarred Sa–Sbc galaxies is more centrally peaked and inconsistent with that in unbarred Sc–Sm hosts (as seen in the KS statistic but only marginally so in the AD statistic). In contrast, the radial distribution of Type Ia SNe in unbarred galaxies is unaffected by host morphology.

The different radial distributions of SNe in unbarred spirals can be explained by the strong dependence of massive SF distribution in the discs on the morphological type of galaxies. In particular, for S0/a–Im galaxies [46] studied the distribution of H $\alpha$  and  $R$ -band concentration indices (C30)<sup>13</sup> as a function of Hubble type. They found a strong correlation of H $\alpha$  C30 index with Hubble sequence, with the early-type having about two times higher H $\alpha$  C30 indices in comparison with the late-type galaxies. The same is true for  $R$ -band C30 indices, but with less difference between early- and late-type galaxies (see fig 1. in [46]). Moreover, the authors showed that the unbarred galaxies have more centrally concentrated H $\alpha$  emission than do their strongly barred counterparts. Note that, in some cases, the C30 indices may be biased by Active Galactic Nuclei emission from the very central region ( $< 0.2R_{25}$ ) of galaxies. However, fig. 8 in [46] shows that for unbarred early-type galaxies the trends above are virtually unaffected when the inner regions ( $< 0.2R_{25}$ ) are not considered. Since Type Ia SNe are less tightly connected to the H $\alpha$  emission of the explosion site [119, 120], the radial distribution of SNe Ia in Sa–Sm hosts is not strongly affected by the morphology.

It is important to note that, when selecting Sa–Sbc and Sc–Sm morphologies without splitting between barred and unbarred subsamples, all the significant differences in the radial distributions of SNe are washed out (see Table 1.4). Therefore, the lack of significant differences in the radial distributions of CC SNe as a function of the morphological type of host galaxies presented in the earlier studies [65–67, 104, 106, 121, 122]) is a consequence of these samples mixing barred and unbarred galaxies with different levels of mixing of the stellar populations.

To exclude the effects of (1) bars (two distinct types of bars: strong bars, which are more common in early-type discs, and weak bars, which are frequently found in late-type spirals; see fig. 5 of [73]) and (2) the morphological differences between Type Ia and CC SNe hosts (the mean morphological type of SNe Ia host galaxies is earlier than that of the CC SNe hosts, as can be deduced from the numbers in our Table 1.1; see also fig. 2 and table 11 of [73]), we repeat the analysis of the inner ( $\tilde{r} \leq 0.3$ ) fractions of SNe, restricting to unbarred morphological bins (Sbc and Sb–Sbc). We carry out this analysis because the bulge stars of Sb–Sbc galaxies

---

<sup>13</sup>The C30 index is the ratio of the flux within 0.3 times the optical radius and the total flux, which provides a simple measure of the observed radial distribution of the luminosity of a galaxy in a specified bandpass.

are typically located in our chosen inner region,<sup>14</sup> which enables a better estimation of the possible contribution of bulge SNe Ia on top of that of the inner disc population. We find that there is no significant difference in the inner fractions of Type Ia and CC SNe in the Sbc bin ( $F_{\text{Ia}} = 0.32_{-0.06}^{+0.07}$  and  $F_{\text{CC}} = 0.31_{-0.05}^{+0.05}$ ). Even selecting unbarred Sb–Sbc bins where the bulge should be (slightly) more prominent, we get  $F_{\text{Ia}} = 0.31_{-0.05}^{+0.06}$  and  $F_{\text{CC}} = 0.33_{-0.04}^{+0.04}$ . Here, we do not use the earlier morphological bins because they are rarely populated by CC SNe making it impossible to estimate the  $F_{\text{CC}}$  (see Table 1.1). On the other hand, the later morphological bins are not suitable because of the weaker bulge component [62, 113].

Interestingly,  $F_{\text{Ia}} = 0.32_{-0.05}^{+0.06}$  for 28 Type Ia SNe in all S0–S0/a galaxies, which is the same as  $F_{\text{Ia}} = 0.32_{-0.02}^{+0.02}$  for 152 SNe Ia in all Sa–Sm hosts and even the same as  $F_{\text{Ia}}$  for only unbarred Sbc galaxies. With the results in Section 1.3.1, this suggests that the deviation of the radial distribution of Type Ia SNe in S0–S0/a galaxies from that in Sa–Sm hosts (upper panel of Fig. 1.2 and Table 1.4) is mostly attributed to the contribution by the outer bulge SNe Ia in S0–S0/a galaxies (see also the corresponding mean values of  $\tilde{r}$  in Fig. 1.2).

These results confirm that the old bulges of Sa–Sm galaxies are not significant producers of Type Ia SNe, while the bulge populations are significant for SNe Ia only in S0–S0/a galaxies. In S0–S0/a hosts, the relative fraction of bulge to disc SNe Ia is probably changed in comparison with that in Sa–Sm hosts, because the progenitor population from the discs of S0–S0/a galaxies should be much lower due to the lower number of young/intermediate stellar populations.

Moreover, we do not detect the relative deficiency of Type Ia SNe in comparison with CC SNe in the inner regions of spiral hosts, contrary to [69, 123], and [70]. Instead, the radial distributions of both types of SNe are well matched between each other in all the subsamples of Sa–Sbc and Sc–Sm galaxies supporting the idea that the relative concentration of CC SNe in the centres of spirals found by these authors is most probably due to a contribution of the central excess of CC SNe in disturbed galaxies [73, 124], which are excluded from our sample (see Section 1.2).

---

<sup>14</sup>Fig. 23 of [125] indicates that the bulge half-light radius,  $R_{\text{bulge}}$ , is roughly one-quarter of the disc scale length, which for typical central disc surface brightness amounts to  $R_{\text{bulge}} < R_{25}/10$  (using the relation between disc scale length and  $R_{25}$  given in equation 3 of [65]).

Table 1.6: Consistency of CC and Type Ia SN distributions with an exponential surface density model.

Host (1)	SN (2)	$\tilde{r} \in [0; \infty)$				$\tilde{r} \in [0.2; \infty)$			
		$N_{\text{SN}}$ (3)	$\langle \tilde{r} \rangle \pm \sigma$ (4)	$P_{\text{KS}}$ (5)	$P_{\text{AD}}$ (6)	$N_{\text{SN}}$ (7)	$P_{\text{KS}}$ (8)	$P_{\text{AD}}$ (9)	$\tilde{h}_{\text{SN}}$ (10)
S0–S0/a	Ia	28	$0.57 \pm 0.38$	0.593	0.344	21	0.297	0.455	$0.32 \pm 0.04$
Sa–Sm	Ia	152	$0.46 \pm 0.28$	0.209	0.091	127	0.533	0.488	$0.21 \pm 0.02$
Sa–Sm (barred)	Ia	73	$0.47 \pm 0.23$	0.095	0.076	64	0.421	0.244	$0.21 \pm 0.03$
Sa–Sm (unbarred)	Ia	79	$0.46 \pm 0.32$	0.520	0.548	63	0.962	0.912	$0.22 \pm 0.02$
Sa–Sbc	Ia	79	$0.46 \pm 0.29$	0.441	0.295	69	0.968	0.980	$0.21 \pm 0.02$
Sa–Sbc (barred)	Ia	39	$0.46 \pm 0.23$	0.315	0.210	35	0.595	0.601	$0.20 \pm 0.03$
Sa–Sbc (unbarred)	Ia	40	$0.47 \pm 0.34$	0.864	0.874	34	0.683	0.917	$0.21 \pm 0.03$
Sc–Sm	Ia	73	$0.46 \pm 0.27$	0.443	0.265	58	0.432	0.408	$0.22 \pm 0.02$
Sc–Sm (barred)	Ia	34	$0.47 \pm 0.24$	0.279	0.359	29	0.424	0.477	$0.22 \pm 0.03$
Sc–Sm (unbarred)	Ia	39	$0.45 \pm 0.30$	0.666	0.628	29	0.932	0.792	$0.23 \pm 0.03$
Sa–Sm	CC	319	$0.49 \pm 0.26$	<b>0.001</b>	<b>0.000</b>	286	0.075	0.056	$0.21 \pm 0.01$
Sa–Sm (barred)	CC	136	$0.52 \pm 0.26$	<b>0.045</b>	<b>0.005</b>	125	0.062	0.116	$0.23 \pm 0.02$
Sa–Sm (unbarred)	CC	183	$0.46 \pm 0.25$	<b>0.028</b>	<b>0.008</b>	161	0.454	0.359	$0.20 \pm 0.01$
Sa–Sbc	CC	106	$0.45 \pm 0.21$	<b>0.004</b>	<b>0.008</b>	95	0.102	0.118	$0.19 \pm 0.02$
Sa–Sbc (barred)	CC	50	$0.49 \pm 0.21$	<b>0.050</b>	<b>0.029</b>	45	<b>0.030</b>	<b>0.046</b>	$0.21 \pm 0.04$
Sa–Sbc (unbarred)	CC	56	$0.42 \pm 0.22$	<b>0.035</b>	0.052	50	0.384	0.432	$0.17 \pm 0.03$
Sc–Sm	CC	213	$0.50 \pm 0.27$	<b>0.036</b>	<b>0.004</b>	191	0.125	0.190	$0.23 \pm 0.02$
Sc–Sm (barred)	CC	86	$0.54 \pm 0.29$	0.118	0.066	80	0.715	0.785	$0.24 \pm 0.03$
Sc–Sm (unbarred)	CC	127	$0.48 \pm 0.26$	0.146	<b>0.041</b>	111	0.164	0.226	$0.22 \pm 0.02$

Columns 1 and 2 give the subsample; Col. 3 is the number of SNe in the subsample for the full radial range  $\tilde{r} \in [0; \infty)$ ; Col. 4 is the mean of  $\tilde{r}$  with standard deviation; Cols. 5 and 6 are the  $P_{\text{KS}}$  and  $P_{\text{AD}}$  probabilities from one-sample KS and AD tests, respectively, that the distribution of SNe is drawn from the best-fitting exponential surface density profile; Cols. 7, 8, and 9 are, respectively, the same as Cols. 3, 5, and 6, but for  $\tilde{r} \in [0.2; \infty)$ ; Col. 10 is the maximum likelihood value of  $\tilde{h}_{\text{SN}} = h_{\text{SN}}/R_{25}$  with bootstrapped error (repeated  $10^4$  times) for the inner-truncated disc. The  $P_{\text{KS}}$  and  $P_{\text{AD}}$  are calculated using the calibrations by [90] and [126], respectively. The statistically significant deviations from an exponential law are highlighted in bold.

[69] discussed the possibilities that the relative deficiency of Type Ia SNe that they found (and which we do not confirm) in the inner regions of spiral galaxies may be due to a stronger dust extinction for Type Ia events than for CC SNe. They suggested that massive progenitors of CC SNe within associations might create large cavities in the discs through their own stellar winds or earlier SN explosions, therefore making the discovery of CC SNe easier. Despite the higher luminosity of Type Ia SNe at maximum, their lower mass progenitors make such cavities less likely [127]. However, our results discussed above show that dust extinction in the discs of nearby non-disturbed spirals should not be different for Type Ia and CC SNe. Moreover, in [61], it is shown that although CC SNe are more concentrated to the brightness peaks of spiral arms than are Type Ia events, both SN types occur mostly in spiral arms [34, 128] where large cavities, if present, should be shared, on average, between the progenitors of both SN types.

The differences between our results and those of previous studies is that we deproject and normalize the galactocentric radii of SNe, while the other studies used projected and normalized [123], or projected linear [69], or normalized to flux [70] galactocentric radii. Another important difference is that, contrary to this study, [69] and [70] included highly inclined galaxies in their studies.

### 1.4.1 The deprojected exponential surface density distribution

It is widely accepted that the surface density distribution of SNe in discs follows an exponential law [65, 68, 80, 82, 106, 121, 123]. However, a comprehensive analysis of the surface density distribution in different samples of barred and unbarred galaxies has not been performed and this is one of the main goals of the present study.

Following [65], we fit an exponential surface density profile,  $\Sigma(R)$ , to the distribution of deprojected normalized radii, using maximum likelihood estimation (MLE). Here,  $\Sigma^{\text{SN}}(\tilde{r}) = \Sigma_0^{\text{SN}} \exp(-\tilde{r}/\tilde{h}_{\text{SN}})$ , where  $\tilde{h}_{\text{SN}}$  is the scale length of the distribution and  $\Sigma_0^{\text{SN}}$  is the central surface density of SNe. To check whether the distribution of SN radii follows the best-fitting exponential surface density profile, we perform one-sample KS and AD tests on the normalized cumulative distributions of SNe, where the exponential model has a cumulative normalized

Table 1.7: Consistency of Types Ibc and II SN distributions with an exponential surface density model.

Host (1)	SN (2)	$\tilde{r} \in [0; \infty)$				$\tilde{r} \in [0.2; \infty)$			
		$N_{\text{SN}}$ (3)	$\langle \tilde{r} \rangle \pm \sigma$ (4)	$P_{\text{KS}}$ (5)	$P_{\text{AD}}$ (6)	$N_{\text{SN}}$ (7)	$P_{\text{KS}}$ (8)	$P_{\text{AD}}$ (9)	$\tilde{h}_{\text{SN}}$ (10)
Sa–Sm	Ibc	80	$0.40 \pm 0.20$	0.063	<b>0.043</b>	67	0.240	0.396	$0.17 \pm 0.02$
Sa–Sm (barred)	Ibc	32	$0.42 \pm 0.22$	0.485	0.383	27	0.698	0.649	$0.18 \pm 0.02$
Sa–Sm (unbarred)	Ibc	48	$0.38 \pm 0.19$	0.121	0.105	40	0.430	0.713	$0.16 \pm 0.02$
Sa–Sbc	Ibc	31	$0.35 \pm 0.15$	0.112	0.093	25	0.127	0.160	$0.14 \pm 0.02$
Sa–Sbc (barred)	Ibc	12	$0.37 \pm 0.18$	0.308	0.536	9	0.204	0.251	$0.17 \pm 0.03$
Sa–Sbc (unbarred)	Ibc	19	$0.34 \pm 0.12$	0.170	0.114	16	0.419	0.482	$0.13 \pm 0.02$
Sc–Sm	Ibc	49	$0.43 \pm 0.23$	0.267	0.277	42	0.477	0.855	$0.18 \pm 0.03$
Sc–Sm (barred)	Ibc	20	$0.45 \pm 0.24$	0.670	0.591	18	0.792	0.984	$0.19 \pm 0.03$
Sc–Sm (unbarred)	Ibc	29	$0.41 \pm 0.23$	0.589	0.616	24	0.881	0.911	$0.18 \pm 0.03$
Sa–Sm	II	239	$0.52 \pm 0.27$	<b>0.005</b>	<b>0.000</b>	219	0.063	0.052	$0.23 \pm 0.01$
Sa–Sm (barred)	II	104	$0.55 \pm 0.27$	0.074	<b>0.007</b>	98	0.113	0.131	$0.24 \pm 0.02$
Sa–Sm (unbarred)	II	135	$0.49 \pm 0.26$	0.093	<b>0.024</b>	121	0.393	0.323	$0.22 \pm 0.02$
Sa–Sbc	II	75	$0.49 \pm 0.23$	<b>0.012</b>	<b>0.022</b>	70	0.323	0.220	$0.21 \pm 0.02$
Sa–Sbc (barred)	II	38	$0.52 \pm 0.20$	<b>0.029</b>	<b>0.029</b>	36	<b>0.022</b>	<b>0.050</b>	$0.22 \pm 0.03$
Sa–Sbc (unbarred)	II	37	$0.46 \pm 0.25$	0.097	0.229	34	0.588	0.668	$0.19 \pm 0.03$
Sc–Sm	II	164	$0.53 \pm 0.28$	0.079	<b>0.008</b>	149	0.189	0.155	$0.24 \pm 0.01$
Sc–Sm (barred)	II	66	$0.56 \pm 0.30$	0.176	0.107	62	0.571	0.711	$0.25 \pm 0.03$
Sc–Sm (unbarred)	II	98	$0.50 \pm 0.27$	0.140	0.051	87	0.186	0.197	$0.23 \pm 0.02$

The explanation for the columns is the same as for Table 1.6. In the SNe II subsample, there are 18 Type IIb SNe (see Table 1.1) with  $\langle \tilde{r} \rangle \pm \sigma = 0.61 \pm 0.25$ , suggesting that in terms of the radial distribution they likely belong to SNe II rather than to SNe Ibc group. The statistically significant deviations from an exponential law are highlighted in bold.

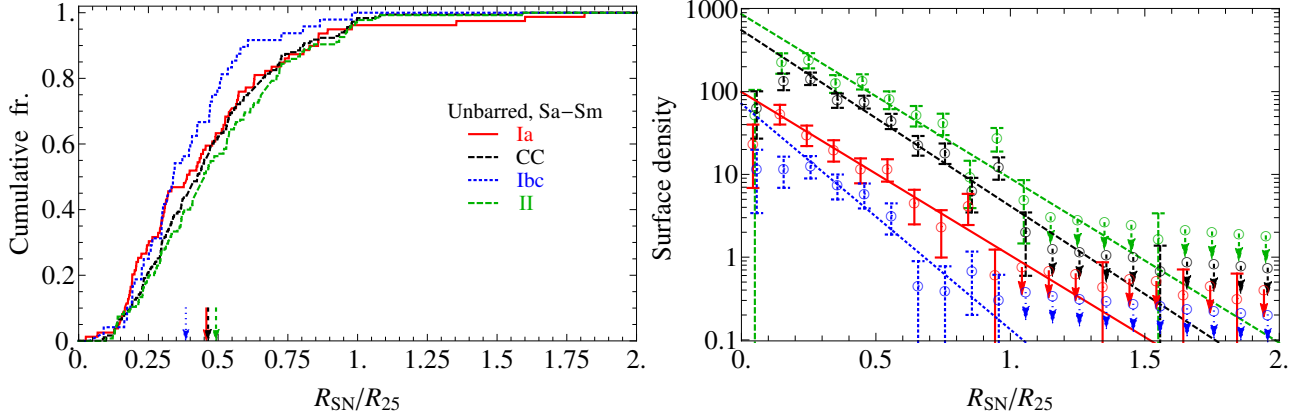


Figure 1.3: Left: cumulative fractions of the different types of SNe versus deprojected and normalized galactocentric radius ( $\tilde{r} = R_{\text{SN}}/R_{25}$ ) in unbarred Sa–Sm host galaxies. The mean  $\tilde{r}$  values of each SNe type are shown by arrows. Right: surface density distributions (with arbitrary normalization) of the different types of SNe in the same subsample of hosts. The different lines show the maximum likelihood exponential surface density profiles estimated for the inner-truncated disc. The error bars assume a Poisson distribution. Down arrows represent the upper-limits of surface density (with  $\pm 1$  SN if none is found). For better visibility, the distributions are shifted vertically sorted by increasing the mean  $\tilde{r}$  as one moves upwards.

distribution  $E(\tilde{r}) = 1 - (1 + \tilde{r}/\tilde{h}_{\text{SN}}) \exp(-\tilde{r}/\tilde{h}_{\text{SN}})$ .

In columns 3–6 of Table 1.6, the total number of SNe in the full radial range, their mean radius with standard deviation, the KS and AD test  $P$ -values,  $P_{\text{KS}}$  and  $P_{\text{AD}}$  are, respectively, presented for the different subsamples. In Table 1.7, despite the small number statistics of Type Ibc SNe (see Table 1.1), we consider Types Ibc and II SNe separately.

From columns 5 and 6 of Tables 1.6 and 1.7, we see that in many subsamples of CC SNe, in contrast to Type Ia SNe, the surface density distribution is not consistent with an exponential profile. Fig. 1.2 hints that the observed inconsistency is probably due to the central  $\tilde{r} \lesssim 0.2$  deficit of SNe (farther, see also in the right-hand panel of Fig. 1.3). For this reason, we repeat the above described tests for  $\tilde{r} \in [0.2; \infty)$  range and find that the inconsistency vanishes in most of the subsamples (see columns 8 and 9 in Tables 1.6 and 1.7). The corresponding scale lengths for the inner-truncated disc are listed in column 10 of Tables 1.6 and 1.7. As expected, only the distribution of CC SNe in early-type barred spirals is inconsistent with an exponential distribution due to the impact of bars on the radial distribution of CC SNe as discussed in Section 1.4. The effect is not seen for Type Ibc SNe probably due to the small

number statistics of these SNe in early-type barred spirals (see column 7 in Tables 1.7).

Finally, to eliminate the effects induced by bars, we compare the radial distributions of Types Ibc and II SNe in unbarred spiral galaxies only. The two-sample KS and AD tests show that the radial distribution of Type Ibc SNe is highly inconsistent with that of Type II ( $P_{\text{KS}} = 0.026$  and  $P_{\text{AD}} = 0.014$ ), because the former are more centrally concentrated (see the mean of  $\tilde{r}$  and  $\tilde{h}_{\text{SN}}$  values in Table 1.7).

The radial position within host galaxies can be used as a proxy for the local metallicity since the short lifetime of CC SN progenitor (tens of Myr) is not enough to allow far migration from its birthplace. Therefore, the physical explanation for the more concentrated distribution of SNe Ibc with respect to SNe II in non-disturbed and unbarred spiral galaxies is that SNe Ibc arise from more metal-rich environments,<sup>15</sup> as has been widely discussed [7, 65–67, 107, 123, 129, 130]). Here, we do not go into deeper considerations, instead we refer the reader to the mentioned references for more complete discussions.

Despite the smaller numbers statistics, we analyse the radial distributions of Types Ib and Ic SNe in unbarred galaxies (18 SNe Ib and 23 SNe Ic; see Table 1.1). Compared with the SNe Ibc versus SNe II test, the radial distributions of SNe Ib and SNe Ic are sufficiently similar that the two-sample KS and AD tests fail to distinguish them with statistical significance ( $P_{\text{KS}} = 0.119$  and  $P_{\text{AD}} = 0.202$ ). In the inner-truncated disc, the scale length of Type Ib SNe ( $0.14 \pm 0.03$ ) is not significantly lower from that of Type Ic SNe ( $0.17 \pm 0.03$ ), while the scale length of all the Ibc family is between these values (see Table 1.7).

Fig. 1.3 presents the cumulative and surface density distributions of the different types of SNe in unbarred Sa–Sm host galaxies. According to the scale lengths in Tables 1.6 and 1.7, the fit lines in Fig. 1.3 show the exponential surface density profiles of SNe in the same subsample. A central ( $\tilde{r} \lesssim 0.2$ ) drop from an exponential distribution is observed for all the SNe types, less prominent for SNe Ia.

It is important to note that the scale lengths of SNe ( $\tilde{h}_{\text{SN}} = h_{\text{SN}}/R_{25}$ ) in Tables 1.6 and

---

<sup>15</sup>The top-heavy initial mass function and/or enhanced close binary fraction in the central regions of strongly disturbed/interacting galaxies might play an important role in explaining the inner excess of SNe Ibc compared to SNe II [42, 124, 131]. However, the roles of these factors are difficult to estimate, since our analysis is restricted to non-disturbed host galaxies.

1.7 are calculated using the  $\mu_g = 25 \text{ mag arcsec}^{-2}$  isophotal level in the SDSS  $g$ -band (see Section 1.2), while the previous papers used the same magnitude isophotal level in  $B$ -band [65, 106, 122, 131, 132]. In [72], we showed that galaxies have sizes systematically larger in the  $g$ -band than in the  $B$ -band (see fig. 11 and table 4 in [72]) due to the fact that our  $g$ -band measurements are performed at the equivalent of the  $\langle \mu_B \rangle \simeq 25.48$  isophote, hence at typically lower surface brightness threshold. Therefore, considering that our radii of host galaxies are greater than those in the HyperLeda on average by a factor of  $1.32 \pm 0.01$  [72], we get generally about 25 per cent smaller scale lengths of SNe in  $g$ -band compared with the earlier estimations in  $B$ -band (see [65] for CC SNe).

## 1.5 Chapter Conclusions

In this Chapter, using a well-defined and homogeneous sample of SNe and their host galaxies from the coverage of SDSS DR10, we analyse the impact of bars and bulges on the radial distributions of the different types of SNe in the stellar discs of host galaxies with various morphologies. Our sample consists of 419 nearby ( $\leq 100$  Mpc), low-inclination ( $i \leq 60^\circ$ ), and morphologically non-disturbed S0–Sm galaxies, hosting 500 SNe in total.

All the results that we summarize below concerning the radial distributions of SNe in barred galaxies can be explained considering the strong impact of the bars on the distribution of massive SF in stellar discs of galaxies, particularly in early-type spirals. On the other hand, the bulge component of Type Ia SNe distribution shows a negligible impact on the radial distribution of SNe Ia, except in S0-S0/a galaxies.

We also check that there are no strong selection effects and biases within our SNe and host galaxies samples, which could drive the observed behaviours of the radial distributions of Type Ia and CC SNe in the disc galaxies presented in this study.

The results obtained in this Chapter are summarized below, along with their interpretations.

1. In Sa–Sm galaxies, all CC and the vast majority of Type Ia SNe belong to the disc, rather than the bulge component (Fig. 1.1 and Table 1.2). The result suggests that

the rate of SNe Ia in spiral galaxies is dominated by a relatively young/intermediate progenitor population. This observational fact makes the deprojection of galactocentric radii of both types of SNe a key point in the statistical studies of their distributions.

2. The radial distribution of Type Ia SNe in S0–S0/a galaxies is inconsistent with that in Sa–Sm hosts (as seen in Fig. 1.2 and Table 1.4 for the AD statistic but only very marginally so in the KS statistic). This inconsistency is mostly attributed to the contribution by SNe Ia in the outer bulges of S0–S0/a galaxies. In these hosts, the relative fraction of bulge to disc SNe Ia is probably changed in comparison with that in Sa–Sm hosts, because the progenitor population from the discs of S0–S0/a galaxies should be much lower due to the lower number of young/intermediate stellar populations.
3. The radial distribution of CC SNe in barred Sa–Sbc galaxies is not consistent with that of unbarred Sa–Sbc hosts (Fig. 1.2 and Table 1.4), while for Type Ia SNe the distributions are not significantly different (Table 1.4). At the same time, the radial distributions of both Type Ia and CC SNe in Sc–Sm galaxies are not affected by bars (Table 1.4). These results are explained by a substantial suppression of massive SF in the radial range swept by strong bars of early-type barred galaxies.
4. The radial distribution of CC SNe in unbarred Sa–Sbc galaxies is more centrally peaked and inconsistent with that in unbarred Sc–Sm hosts (as seen in Fig. 1.2 and Table 1.4 for the KS statistic but only marginally so in the AD statistic). On the other hand, the radial distribution of Type Ia SNe in unbarred galaxies is not affected by host morphology (Table 1.4). These results can be well explained by the distinct distributions of massive stars in the discs of early- and late-type spirals. In unbarred Sa–Sbc galaxies, SF is more concentrated to the inner regions ( $H\alpha$  emission outside the nucleus) and should thus be responsible for the observed radial distribution of CC SNe.
5. The radial distribution of CC SNe, in contrast to Type Ia SNe, is inconsistent with the exponential surface density profile (Tables 1.6 and 1.7), because of the central ( $\tilde{r} \lesssim 0.2$ ) deficit of SNe. However, in the  $\tilde{r} \in [0.2; \infty)$  range, the inconsistency vanishes for CC SNe

in most of the subsamples of spiral galaxies. In the inner-truncated disc, only the radial distribution of CC SNe in barred early-type spirals is inconsistent with an exponential surface density profile, which appears to be caused by the impact of bars on the radial distribution of CC SNe.

6. In the inner regions of non-disturbed spiral hosts, we do not detect a relative deficiency of Type Ia SNe with respect to CC (Table 1.5), contrary to what was found by other authors, who had explained this by possibly stronger dust extinction for Type Ia than for CC SNe. Instead, the radial distributions of both types of SNe are similar in all the subsamples of Sa–Sbc and Sc–Sm galaxies (Table 1.4), which supports the idea that the relative increase of CC SNe in the inner regions of spirals found by the other authors is most probably due to the central excess of CC SNe in disturbed galaxies.
7. As was found in earlier studies, the physical explanation for the more concentrated distribution of SNe Ibc with respect to SNe II in non-disturbed and unbarred spiral galaxies (Fig. 1.3) is that SNe Ibc arise from more metal-rich environments. The radial distributions of Types Ib and Ic SNe are sufficiently similar that the KS and AD tests fail to distinguish them with statistical significance.

# Chapter 2

## Type Ia SNe in the star formation deserts of spiral host galaxies

### 2.1 Introduction

Recently, [52] showed that the correlation between the  $\Delta m_{15}$  of normal SNe Ia and hosts' global age appears to be due to the superposition of at least two distinct populations of faster and slower declining SNe Ia from older and younger stellar populations, respectively. For the most common peculiar SNe Ia, [52] showed that 91bg-like (subluminous and fast declining) events probably come only from the old population, while 91T-like (overluminous and slow declining) SNe originate only from the young population of galaxies. Such results have been obtained also from more accurate age estimations of SNe Ia host populations, using the local properties for SN sites [40, 133, 134]. Eventually, the SN LC properties, DTD, and relations with other host characteristics allow to constrain the SN Ia progenitor scenarios (see discussion in [52]).

In this Chapter, for the first time, we link the  $\Delta m_{15}$  of SN Ia with the progenitor age from the perspective of SFD phenomenon. In short, the SFD, observed in some spiral galaxies [47, 48], is a region swept up by a strong bar with almost no recent SF on both sides of the bar. There are increasing evidences in observations and simulations that SFD consists of old stars, and the

quenching of SF in this region was due to the bar formation [49, 50], which dynamically removed gas from SFD over a timescale of  $\sim 2$  Gyr [49]. The bar can show SF through its length, or SF can be found only at the bar ends, or the entire bar might not show SF [135]. Some bars might even dissolve during the evolution [136], leaving the central SFD in galactic disc. On the other hand, it can be considered that the SFD is practically not contaminated by the radial migration of young stars from the outer disc [51]. Therefore, from the dynamical age-constrain of SFD ( $\gtrsim 2$  Gyr), we consider that the DTD of its SNe Ia is truncated on the younger side, starting from a few Gyr, in comparison with those outside the SFD, where mostly young/prompt SNe Ia occur (delay time of  $\sim 500$  Myr, [137]). Given this, and if the progenitor's age is the main driver of the decline rate, the SNe Ia discovered in the SFDs should have faster declining LCs. In this Chapter, we simply demonstrate the validity of this assumption according to the picture briefly described above, which provides an excellent new opportunity to constrain the nature of SN Ia progenitors.

## 2.2 Sample selection and reduction

We selected the sample for this Chapter from a well-defined sample of [52], which includes data on the spectroscopic subclasses of nearby ( $\leq 150$  Mpc) SNe Ia (normal, 91T-, 91bg-like, etc.) and their  $B$ -band LC decline rates ( $\Delta m_{15}$ ), as well as homogeneous data on the host galaxies (distance, corrected  $ugriz$  magnitudes, morphological type, bar detection, etc). The SFDs are observed in some barred Sa–Scd galaxies [47, 48], therefore we restricted the morphologies of SNe hosts to the mentioned types, with barred and unbarred counterparts. We also ignored hosts with strong morphological disturbances, which may add undesirable projection effects and complicate the assignment of an SN Ia to the SFD.

As seen in [69, 70, 138], the vast majority of SNe Ia in spiral galaxies belong to the disc, rather than the bulge (spherical) component. Here, we checked this observational fact for the most common SN Ia subclasses separately. If SNe Ia belong mostly to the disc component, where SFD can be located, one would expect that the distributions of projected and  $R_{25}$ -normalized

galactocentric distances<sup>1</sup> of SNe Ia along major ( $|U|/R_{25}$ ) and minor ( $|V|/R_{25}$ ) axes would be different, being distributed closer to the major axis (i.e. smaller  $\langle|V|/R_{25}\rangle$  in comparison with  $\langle|U|/R_{25}\rangle$ , for more details see [138]). Table 2.1 shows the results of the two-sample KS and AD tests on the comparison of the major versus minor axes distributions of 238 SNe Ia (based on a subsample from [52]). The  $P$ -values of the tests suggest that the SNe Ia distribution along the major axis is inconsistent with that along the minor axis in Sa–Scd host galaxies with different inclinations, showing that the SN Ia subclasses in these hosts originate mostly from the disc population.

It should be noted that, because of the absorption and projection effects in the discs, the SFDs are observed in some spiral galaxies only with low/moderate inclinations [47, 48]. Therefore, we also limited our host galaxy sample to inclinations  $i < 70^\circ$ . In total, there are 185 normal, 91T- and 91bg-like SNe Ia meeting the above criteria, of which 79 and 106 events have barred and unbarred hosts, respectively. These SNe Ia are discovered in 180 host galaxies, five of which host two events in each.

For these host galaxies, we used archival Galaxy Evolution Explorer (GALEX) far- and near-UV [139], *Swift* UV [140], and available H $\alpha$  images [141] to visually classify the morphology of their ionized discs into four SF classes: *i*) SF is distributed along the entire length of unbarred disc, from the center to the edge (97 SNe Ia hosts); *ii*) like in the first case, but for barred disc, SF along the bar, without SFD (36 objects); *iii*) SF along the bar, or SF might occur only at the bar ends, with SFD (43 objects); *iv*) SF is distributed along the unbarred disc, except the central SFD (9 objects). In all the cases, the circumnuclear SF is also possible. The  $r$ -band and UV images representing the classes<sup>2</sup> of galaxies can be found in Fig. 2.1. Note that the cosmic surface brightness dimming is insignificant for our galaxy sample, since hosts'  $z \lesssim 0.036$  ( $\langle z \rangle = 0.017 \pm 0.009$ ).

Based on the optical  $g$ -band images, we measured bar radii of host galaxies using ellipse fitting to the bar isophotes with maximum ellipticity [142] and references therein, for more details on the bar radius measurement method). Then we deprojected each bar radius for host

<sup>1</sup>Normalized to the  $g$ -band 25<sup>th</sup> magnitude isophotal semimajor axis of host galaxy ( $R_{25} = D_{25}/2$ ).

<sup>2</sup>With some differences, a similar visual classification is also proposed by [135].

Table 2.1: Comparison of the projected and normalized distributions of the SN Ia subclasses along major ( $U$ ) and minor ( $V$ ) axes of Sa–Scd hosts.

SN	$N_{\text{SN}}$	Subsample 1 $\langle  U /R_{25} \rangle$	vs	Subsample 2 $\langle  V /R_{25} \rangle$	$P_{\text{KS}}^{\text{MC}}$	$P_{\text{AD}}^{\text{MC}}$
Normal	196	$0.32 \pm 0.02$	vs	$0.20 \pm 0.02$	<b>&lt;0.001</b>	<b>&lt;0.001</b>
91T	27	$0.38 \pm 0.06$	vs	$0.20 \pm 0.03$	<b>0.018</b>	<b>0.021</b>
91bg	15	$0.34 \pm 0.06$	vs	$0.18 \pm 0.06$	<b>0.020</b>	<b>0.037</b>

Notes: The  $P_{\text{KS}}^{\text{MC}}$  ( $P_{\text{AD}}^{\text{MC}}$ ) is the two-sample KS (AD) test probability that the distributions are drawn from the same parent sample, using a Monte Carlo (MC) simulation with  $10^5$  iterations as explained in [52]. The respective mean values and standard errors are listed. The statistically significant differences ( $P \leq 0.05$ ) between the distributions are highlighted in bold.

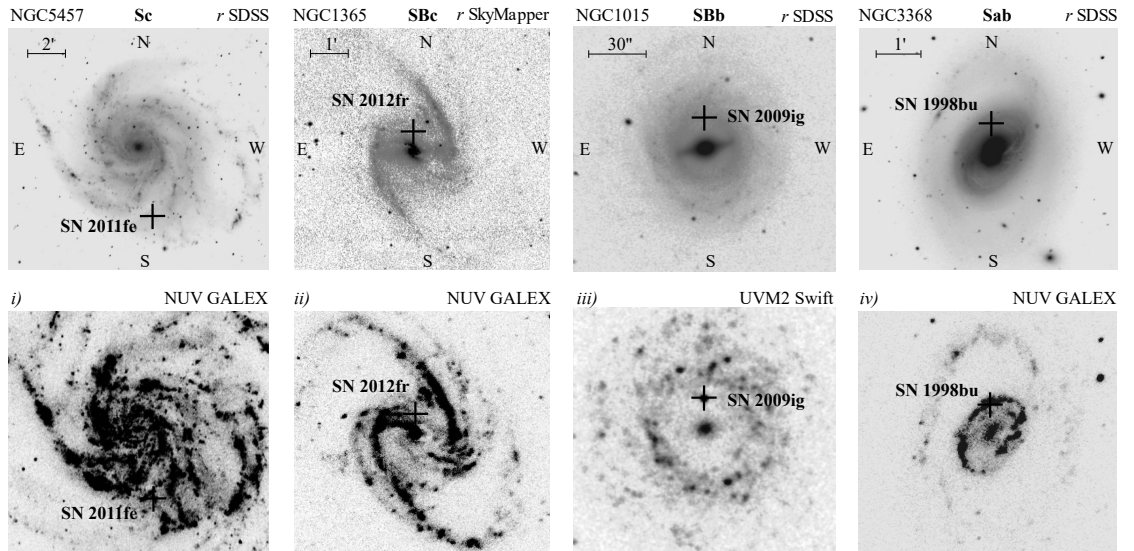


Figure 2.1: Optical (top) and UV images (bottom) representing examples of SN Ia hosts with different SF classes of their discs. Galaxies' identifiers, morphologies, and discs' classes are listed at the top. Classes *i* and *ii* do not have SFD, while classes *iii* and *iv* have SFD. SN Ia names/positions are also shown.

Table 2.2: Numbers of the SN Ia subclasses according to their locations in the SFD of Sa–Scd hosts or beyond.

SNe Ia in $\tilde{r}_{\text{SN}}$	class $i$ disc $>0$	outer disc $\geq \tilde{r}_{\text{dem}}$	bar/SF $< \tilde{r}_{\text{dem}}$	SFD $< \tilde{r}_{\text{dem}}$	All
Normal	75	52	12	12	151
91T	19	4	1	0	24
91bg	3	5	0	2	10
All	97	61	13	14	185

inclination and normalized it to the disc radius, i.e.  $\tilde{r}_{\text{bar}} = R_{\text{bar}}/R_{25}$ . For unbarred hosts with the central SFD (class *iv* in Fig. 2.1), we used the UV images to roughly estimate the radii of SFDs ( $\tilde{r}_{\text{SFD}} = R_{\text{SFD}}/R_{25}$ ), where almost no UV fluxes are detected. Note that for our sample  $\langle \tilde{r}_{\text{SFD}} \rangle \approx \langle \tilde{r}_{\text{bar}} \rangle = 0.30$ . For further simplicity, we define a demarcation radius as:

$$\tilde{r}_{\text{dem}} = \begin{cases} \tilde{r}_{\text{bar}}, & \text{for } ii \text{ and } iii \text{ disc classes,} \\ \tilde{r}_{\text{SFD}}, & \text{for } iv \text{ class.} \end{cases}$$

For SNe Ia, we deprojected and normalized their galactocentric distances as well, i.e.  $\tilde{r}_{\text{SN}} = R_{\text{SN}}/R_{25}$  [138].

Based on the host disc classification and the definition of demarcation radius, we grouped SNe according to their locations as follows: 97 SNe Ia are found in the disc of galaxies without a bar or SFD; 61 SNe are in the outer disc of hosts, which have either a bar or SFD; 13 SNe are found in bar or star-forming regions inside  $\tilde{r}_{\text{dem}}$ ; and 14 SNe Ia are in SFD. Table 2.2 displays the distribution of the SN Ia subclasses according to their locations in the SFD<sup>3</sup> or beyond.

The first 10 rows of the database of 185 SNe Ia (SN name, location, deprojected and  $R_{25}$ -normalized galactocentric distance) and their 180 hosts (galaxy name, morphological type, bar detection, disc’s class, and demarcation radius) are shown in Table 2.3. The full table is available online [143]. Recall that more data on these SNe Ia and their host galaxies are available in [52] (e.g. SN spectroscopic subclass,  $\Delta m_{15}$ , galaxy distance).

<sup>3</sup>Although detailed measurements of the underlying fluxes at SNe locations are beyond the scope of this *study*, nevertheless, for our confidence, we checked the vicinity of 14 SNe Ia in the SFDs simply using different apertures on the fits images, and found no detectable underlying UV/H $\alpha$  fluxes.

Table 2.3: The database (first 10 rows) of 185 SNe Ia and their 180 host galaxies. The full table is available online [143].

SN	Host	Morph.	Bar	Disc's class	Location	$\tilde{r}_{\text{SN}}$	$\tilde{r}_{\text{dem}}$
1974G	NGC4414	Sc		<i>i</i>	disc	0.425	–
1981B	NGC4536	Sbc		<i>i</i>	disc	0.697	–
1982B	NGC2268	Sc	B	<i>iii?</i>	outer disc	0.267	0.150
1989A	NGC3687	Sc	B	<i>iii:</i>	outer disc	0.524	0.175
1989B	NGC3627	Sb	B	<i>ii</i>	bar/SF	0.171	0.200
1990N	NGC4639	Sbc	B	<i>iii</i>	outer disc	0.859	0.253
1990O	MCG+03-44-003	Sbc	B	<i>iii?</i>	outer disc	0.764	0.333
1991T	NGC4527	Sbc		<i>i</i>	disc	0.518	–
1992bc	ESO300-009	Scd:		<i>i</i>	disc	0.897	–
1992bg	PGC343503	Sb:		<i>i</i>	disc	0.546	–

## 2.3 Results and discussion

With the aim of linking the  $\Delta m_{15}$  of SN Ia with the progenitor age, we study the SN decline rates that exploded in SFDs and other regions of hosts. In addition, we compare the SN galactocentric distances between the spectroscopic subclasses, and check the possible correlations between the  $\Delta m_{15}$  and galactocentric distances.

### 2.3.1 SNe Ia in the SFDs and beyond

To link the LC properties of SN Ia with the progenitor age from the perspective of the dynamical age-constrain of SFD, in Table 2.4, we compare the  $\Delta m_{15}$  distribution of normal SNe Ia in the SFD with that in the bar/SF (see also the upper panel of Fig. 2.2). The KS and AD tests show that these distributions are significantly different. Normal SNe Ia that are in the SFD, dominated by the old population ( $\gtrsim 2$  Gyr; [49]), have, on average, faster declining LCs compared to those located in the bar/SF, where UV/H $\alpha$  fluxes are observed (i.e. age  $\lesssim$  a few 100 Myr; [144]).

Table 2.4 also shows that the  $\Delta m_{15}$  distribution of normal SNe Ia that are in the outer disc population is consistent with that in the bar/SF and inconsistent with that in the SFD (see also Fig. 2.2). Interestingly, any inconsistency vanishes when we combine the bar/SF and SFD subsamples and compare the LC decline rates with those in the outer disc population

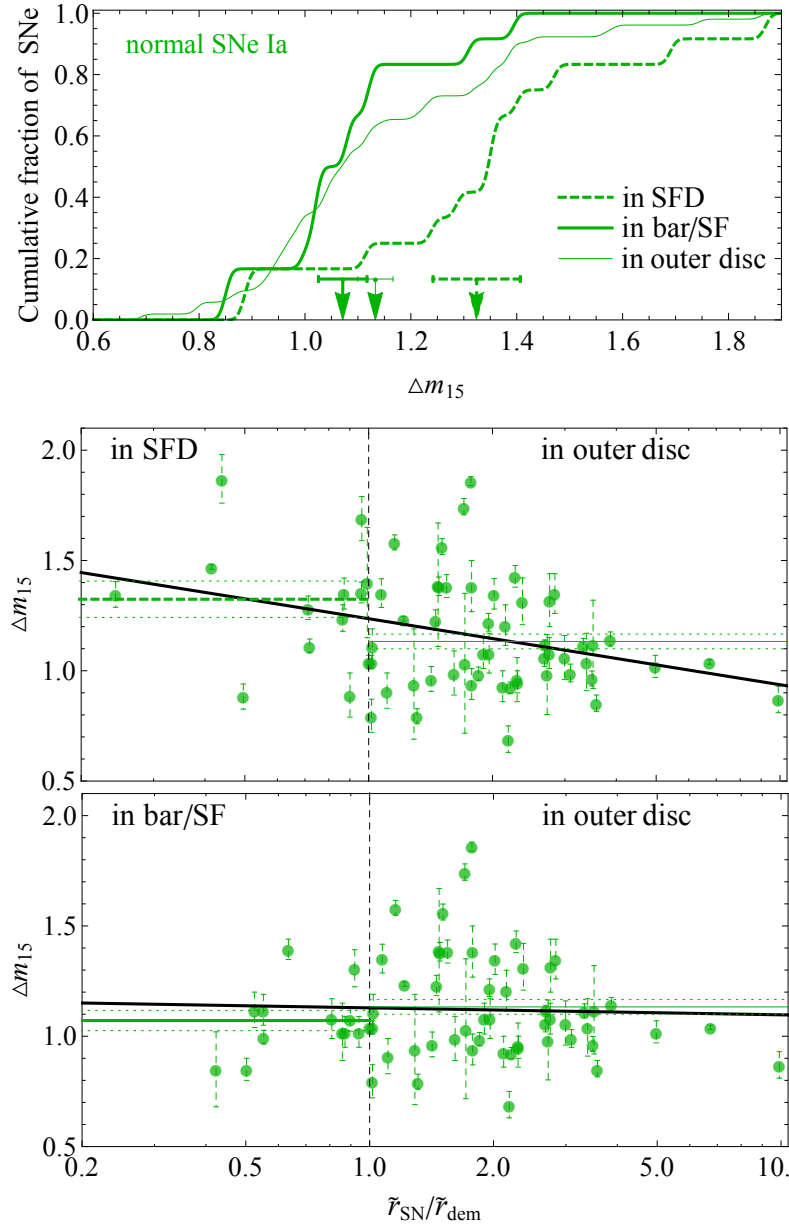


Figure 2.2: Upper panel: cumulative  $\Delta m_{15}$  distributions for normal SNe Ia inside (in SFD and bar/SF) and outside the demarcation radius (in outer disc). Bottom panel: variation of the  $\Delta m_{15}$  as a function of  $\tilde{r}_{\text{dem}}$ -normalized galactocentric distance, split between different SN locations. The best-fits are shown by thick (black) solid lines. The vertical dashed line indicates the location of radial demarcation (see the text for details). The mean values (with standard errors) of the distributions are shown by arrows (with error bars) in the upper panel, and by horizontal lines in the bottom panel.

Table 2.4: Comparison of the  $B$ -band  $\Delta m_{15}$  distributions between normal SNe Ia in different locations (as described in Table 2.2).

Subsample 1			vs	Subsample 2			$P_{\text{KS}}^{\text{MC}}$	$P_{\text{AD}}^{\text{MC}}$
SN in	$N_{\text{SN}}$	$\langle \Delta m_{15} \rangle$		SN in	$N_{\text{SN}}$	$\langle \Delta m_{15} \rangle$		
SFD	12	$1.32 \pm 0.08$	vs	bar/SF	12	$1.07 \pm 0.05$	<b>0.005</b>	<b>0.020</b>
SFD	12	$1.32 \pm 0.08$	vs	outer disc	52	$1.13 \pm 0.03$	<b>0.009</b>	<b>0.029</b>
bar/SF	12	$1.07 \pm 0.05$	vs	outer disc	52	$1.13 \pm 0.03$	0.660	0.682
SFD+bar/SF	24	$1.20 \pm 0.05$	vs	outer disc	52	$1.13 \pm 0.03$	0.445	0.477
inner class $i$ disc	17	$1.19 \pm 0.05$	vs	outer class $i$ disc	58	$1.11 \pm 0.02$	0.517	0.253

*Notes:* Since, the  $\langle \tilde{r}_{\text{dem}} \rangle = 0.30$  for class  $ii-iv$  discs, we define inner and outer class  $i$  discs when  $\tilde{r}_{\text{SN}} < 0.30$  and  $\geq 0.30$ , respectively. The explanations for  $P$ -values are the same as in Table 2.1.

(Table 2.4). This suggests that the discs of Sa–Scd hosts are indeed outnumbered by normal SNe Ia with slower declining LCs (e.g.  $\Delta m_{15} < 1.25$ , outside the  $\tilde{r}_{\text{dem}}$  in Fig. 2.2) whose progenitor ages peak below 1 Gyr, corresponding to the young/prompt SNe Ia [145].

In addition, even for discs of class  $i$  (without demarcation radius), the KS and AD tests, in Table 2.4, show that the  $\Delta m_{15}$  distributions are consistent for normal SNe Ia in the inner and outer discs, excluding a radial dependency of  $\Delta m_{15}$  (see also Section 2.3.2). For class  $i$  discs, the  $\langle \Delta m_{15} \rangle$  values are sufficiently consistent with the same values in the corresponding radial intervals for hosts having a demarcation radius (see Table 2.4). Thus, the SFD phenomenon gives an excellent possibility to separate a subpopulation of normal SNe Ia with old progenitors from a general population of host galactic disc, which contains both young and old progenitors. On average, the LCs of this SN Ia subpopulation decline faster, whose DTD is most likely truncated on the younger side, starting from a several Gyr ( $\gtrsim 2$  Gyr).

These results are qualitatively agree with the theoretical predictions. In particular, for sub-Chandrasekhar mass ( $M_{\text{Ch}} \approx 1.4M_{\odot}$ ) explosion models in double WD systems, the luminosity of SN Ia is directly related to the exploding WD’s mass, which decreases with age [26–29]. This is because WD’s mass is directly linked to the main-sequence (MS) mass of the progenitor star, which is in turn related to the MS lifetime. Therefore, older stellar populations would host less luminous SNe Ia, i.e. faster declining events [28]. Note that, we prefer sub- $M_{\text{Ch}}$  explosion models, because different mechanisms of the  $M_{\text{Ch}}$  explosions do not reproduce the observed

distribution in the luminosity–decline rate relation for various SN Ia subclasses (e.g. [17] and references therein).

Despite the small number statistics of peculiar 91T- and 91bg-like SNe, Table 2.2 shows that the old SFDs of Sa–Scd galaxies host along with faster declining normal SNe Ia also two 91bg-like (fast declining) events. While the bar/SF hosts along with slower declining normal events also one 91T-like (slow declining) SNe. Outer disc population hosts all the SN Ia subclasses (see Table 2.2). The latter is also correct for the entire class  $i$  disc. These results can be explained from the perspective of the SFD’s properties in addition to the previously known relations between the SNe Ia and the global (or SN local) properties of their hosts.

In particular, the discovery of 91bg-like events (progenitor age is greater than several Gyr [52, 133, 146, 147]) and a population of faster declining normal SNe Ia in the SFDs can be explained within the scenario of SF suppression by bar, where the SFDs of galaxies show a sharp truncation in SF histories and contain mostly old stellar population of several Gyr ( $\gtrsim 2$  Gyr; [49]). On the other hand, the discovery of 91T-like SNe (progenitor age is less than a Gyr, e.g. [148–150]) and a population of slower declining normal events in the bar/SF (Tables 2.2–2.4), can be explained in the context of SF suppression scenario, where the recently formed bar, within the  $\sim 1.5$  Gyr timescale, has not yet completely removed the gas and quenched ongoing SF inside the demarcation radius [49]. Recall that in the bar/SF regions, the UV fluxes are observed that trace the SF up to a few 100 Myr [144].

The outer disc of Sa–Scd galaxies (or entire class  $i$  disc), contains stellar populations of all ages [151]. Therefore, the appearance of all the SN Ia subclasses in this region is not unexpected (Table 2.2). Note that the results in Table 2.4 remain statistically unchanged when we combine (following [28]) normal, 91T-, and 91bg-like SNe together.

To test different galaxy properties that could affect the results in Tables 2.2–2.4, we compare the distributions of morphologies, masses, colours, and ages (available in [52]) of classes  $ii$ – $iv$  hosts with and without SFD. The KS and AD tests show that the global parameters of hosts are not statistically different ( $P > 0.1$ ), thus could not be the main drivers behind our results. On the other hand, the bar/SF regions have higher surface brightness and dust content in

comparison with the SFDs, and therefore the discovery of intrinsically faint (faster declining) SNe in the bar/SF can be complicated, biasing the statistical results in Table 2.4. However, this does not affect the result that the SFD’s SNe Ia are mostly faster declining (fainter) events.

Let us now briefly address the possible effects of the progenitor metallicity, which theoretically might cause a variation in the SN Ia LC properties. The mean radial metallicity profile of Sa–Scd galaxies declines from solar to  $\sim 0.3$  dex below solar from the galactic centre up to the disc end, respectively [151]. On the other hand, the simulation by [152] shows that the metallicity on both sides of the bar, i.e. in SFD, is only  $\sim 0.15$  dex below solar. For any progenitor model, such metallicity variations can account for less than 0.2 mag in SN Ia maximum brightness and about 0.1 mag in  $\Delta m_{15}$  [153, 154], which is not enough to be the main reason for the observed differences in  $\Delta m_{15}$  values in SFD and beyond (Fig. 2.2 and Table 2.4). Thus, our results support earlier suggestions that the progenitor age is most probably the decisive factor shaping the observed distribution of SN Ia decline rates [36]. Nevertheless, we would like to stress that the discussed effect of metallicity is heavily based on a very limited number of models. Therefore, further modelling of the impact of metallicity on the LC properties of SNe Ia would help to place our findings in context.

### 2.3.2 The radial distribution of SNe Ia

In spiral discs, a radial gradient of physical properties of stellar population (e.g. age gradient [151]) might be a useful tool and has been used in the past to probe the possible dependencies of SNe Ia decline rates on their galactocentric distance [36, 43, 155]. However, in these studies, the authors were unable to find a significant correlation between the decline rate and  $\tilde{r}_{\text{SN}}$ , which is correct also for our sample (Table 2.5). Moreover, the radial distributions of peculiar (extreme decliners) and normal SNe Ia in Sa–Scd galaxies are consistent with one another ( $P > 0.2$ ) [156]. Note that these results remain statistically insignificant ( $P > 0.1$ ) when we perform the same tests after separating the hosts into barred/unbarred, and early/late-types. The  $\Delta m_{15}$  is not correlated with  $\tilde{r}_{\text{SN}}$  ( $P > 0.4$ ) also for the class *i* disc only, where no bar/SFD phenomena are observed.

Table 2.5: Spearman’s rank correlation test for the  $B$ -band  $\Delta m_{15}$  values of the SN Ia subclasses versus their galactocentric distances.

SN	Galactocen. dist.	$N_{\text{SN}}$	$r_s$	$P_s^{\text{MC}}$
Normal	$\tilde{r}_{\text{SN}}$	151	−0.070	0.394
91T	$\tilde{r}_{\text{SN}}$	24	0.087	0.686
91bg	$\tilde{r}_{\text{SN}}$	10	0.503	0.138
Normal (SFD+outer disc)	$\tilde{r}_{\text{SN}}/\tilde{r}_{\text{dem}}$	64	−0.280	<b>0.025</b>
Normal (bar/SF+outer disc)	$\tilde{r}_{\text{SN}}/\tilde{r}_{\text{dem}}$	64	0.019	0.879
Normal (SFD+bar/SF+outer disc)	$\tilde{r}_{\text{SN}}/\tilde{r}_{\text{dem}}$	76	−0.147	0.206

*Notes:* Coefficient  $r_s$  ( $\in [-1; 1]$ ) is a measure of rank correlation. The variables are not independent when  $P \leq 0.05$ . The  $P_s^{\text{MC}}$  values are obtained using permutations with  $10^5$  MC iterations.

In this context, it should be taken into account that a significant correlations between SNe Ia decline rates (stretch parameters) and the global ages of hosts have been observed when the ages range from about 1 to  $\sim 10$  Gyr [39, 52, 157, 158]. In the stacked discs of Sa–Scd galaxies, however, the azimuthally averaged age of the stellar population ranges roughly from 8.5 to 10 Gyr from the disc edge to the center, respectively [151]. Most likely, this narrow average age distribution across the mean (stacked) host disc does not allow to see a significant correlation between the  $\Delta m_{15}$  and  $\tilde{r}_{\text{SN}}$  in Table 2.5.

It is clear that such a mean disc contains an overlaid components of old and young stars at any radius. On the other hand, as shown in [61, 159], a considerable fraction of SNe Ia in spiral galaxies is (observationally) linked to the young/star-forming disc population, rather than to the population of old disc or bulge. These SNe Ia exhibit an average delay time of 200–500 Myr (prompt events, e.g. [137]) and should have slower declining LCs (smaller  $\Delta m_{15}$  values, e.g. [28]). For this reason, the SNe Ia host disc is outnumbered by slower declining events outside the SFD (Fig. 2.2).

Given these results, we check the  $\Delta m_{15} - \tilde{r}_{\text{SN}}/\tilde{r}_{\text{dem}}$  correlation for normal SNe Ia in the SFD+outer disc, bar/SF+outer disc, and combined samples. Table 2.5 shows that the mentioned correlation is statistically significant for the first sample, while it is not significant for the second and combined samples. Thus, the old SFD population ( $\gtrsim 2$  Gyr), which contains mostly faster declining SNe Ia (larger  $\Delta m_{15}$ ), in combination with the younger outer disc, which

is outnumbered by SNe Ia with slower declining LCs (smaller  $\Delta m_{15}$ ), cause the observed trend in the SFD+outer disc (Fig. 2.2 and Table 2.5).

## 2.4 Chapter Conclusions

In this *Chapter*, using a sample of nearby Sa–Scd galaxies hosting 185 SNe Ia and our visual classification of the ionized (UV and/or H $\alpha$ ) discs of the galaxies, we perform an analysis of the locations and LC decline rates ( $\Delta m_{15}$ ) of normal and peculiar SNe Ia in the SFDs and beyond.

As in earlier studies, we confirm that in the stacked spiral disc, the  $\Delta m_{15}$  of SNe Ia do not correlate with their galactocentric radii, and such disc is outnumbered by slower declining/prompt events.

For the first time, we demonstrate that from the perspective of the dynamical timescale of the SFD, its old stellar population ( $\gtrsim 2$  Gyr) hosts mostly faster declining SNe Ia ( $\Delta m_{15} > 1.25$ ).

By linking the LC decline rate and progenitor age, we show that the SFD phenomenon gives an excellent possibility to constrain the nature of SNe Ia.

# Chapter 3

## The impact of spiral density waves on the distribution of SNe

### 3.1 Introduction

Despite an excellent progress of the DW theory (for recent comprehensive reviews, see [160, 161]), there are many disputes on the lifetime of spiral patterns, and the ability of DWs to generate large-scale shocks and trigger SF, as originally proposed by [162]. For example, the simulations by [163] manifest short-lived patterns. In another example, using a multiband analysis for some GD galaxies, [164] found that there is no shock trigger, and that the spiral arms just reorganize the material from the disc out of which stars form (see also [165]).

Nevertheless, the results of many other studies are consistent with the picture where the DWs cause massive SF to occur by compressing gas clouds as they pass through the spiral arms of GD galaxies [54–58]. For example, using H $\alpha$  direct imaging accompanied with broad-band images in  $R$  and  $I$  bands, [166] studied the distribution of H II regions of spiral arms and found clear evidence for the triggering of SF in the sense of a high density of H II regions at the fixed radial ranges in some GD galaxies. Recently, [167] showed that pitch angle of galaxies is statistically more tightly wound, i.e. smaller, when viewed in the light from the evolved/older stellar populations. Both the results, complementing each other, are in excellent agreement

with the prediction of theory that stars are not only born in the DW but also move out of it as they age (see also most recent results by [168]).

An alternative to the DW theory is the idea of reorganization of the distribution of H II regions in multiple arms of differentially rotating disc with SF processes generated by the stochastic self-propagating method developed by [169] and [170]. This mechanism is supposed to work in non-GD (NGD) galaxies, producing flocculent spiral arms.

In the context of above-mentioned scenarios, the main goal of this study is to study the possible impact of spiral DWs (triggering effect) on the distribution of SNe in discs of host galaxies, when viewing in the light of different nature of Type Ia and CC SNe progenitors. Recall that Type Ia SNe result from stars with masses lower than  $\sim 7.5 M_{\odot}$  (ages from  $\sim 0.5$  Gyr up to  $\sim 10$  Gyr [171]) in close binary systems, while the progenitors of Types Ibc and II SNe,<sup>1</sup> collectively called CC SNe, are massive ( $M \gtrsim 7.5 M_{\odot}$  [172]) young short-lived stars (from a few up to  $\sim 100$  Myr [42, 173, 174]).

The first attempt to study the distribution of SNe within the framework of DW theory was performed by [59]. Using the locations of 19 SNe, he suggested that stars in a spiral galaxy are formed in a shock front on the inner edge of a spiral arm, then drift across the arm as they age, predicting for SN progenitors (more likely for SNe II) a short lifetime (a few million years) and high masses (a few tens of solar masses). However, using the fractions of GD and flocculent galaxies in a sample of 111 hosts with 144 SNe, [175] suggested that DWs do not greatly enhance the massive SF rate per unit luminosity of a galaxy, mentioning that SF in most galaxies may be dominated by stochastic processes. Results similar to those in [59] were obtained also by [128] and [60] for Types II and Ibc SNe, respectively. In other studies, different authors [34, 66, 176] investigated the distribution of SNe relative to spiral arms of galaxies. Such studies did not interpret their results within the DW theory nor did they distinguish among various spiral arm classes (ACs; [177]) of SNe host galaxies.

Indeed, in [61], we already studied the distribution of SNe relative to the spiral arms of their

---

<sup>1</sup>Traditionally, SNe of Types Ib and Ic, including uncertain spectroscopic Type Ib/c, are denoted as SNe Ibc. All these and other subtypes of CC SNe, i.e. Ibc, II, IIb (transitional objects with observed properties close to SNe II and Ib), and IIIn (dominated by emission lines with narrow components) SNe, arise from young massive stars with possible differences in their masses, metallicities, and ages (see e.g. for more details [10]).

GD and NGD host galaxies, using the SDSS images from the  $g$ ,  $r$ , and  $i$  bands. We found that the distribution of CC SNe (i.e. tracers of recent SF) is affected by the spiral DWs in their host GD galaxies, being distributed closer to the corresponding edges of spiral arms where large-scale shocks, thus SF triggering, are expected (see also farther in the text of Section 3.4). Such an effect was not observed for Type Ia SNe (less-massive and longer-lived progenitors) in GD galaxies, as well as for both types of SNe in NGD hosts. In this study, we expand our previous work, and for the first time study the differences between the radial distributions of SNe in unbarred Sa–Sc host galaxies with various spiral ACs. In parallel, to check the triggering effect at different galactocentric radii, we study the consistency of the surface density distribution of SNe (normalized to the optical radii, and for a smaller sample also to corotation radii of hosts) with an exponential profile in GD and NGD galaxies.

## 3.2 The sample

In order to obtain a homogeneous dataset of structural features of SNe host galaxies, including morphology, identification of bars and spiral ACs, we compile the sample of this Chapter in the same way as in [72], being restricted to relatively nearby SNe with distances  $\leq 150$  Mpc. The whole compilation, reduction, and classification procedures are given below.

### 3.2.1 Sample selection and reduction

In this Chapter, we used the updated version of the ASC [75], which includes SNe detected before 1 July 2017. To identify SNe host galaxies, we cross-matched the coordinates of all classified Type Ia and CC (Ibc and II) SNe from the ASC with the footprint of the SDSS DR13 [178]. We then classified the identified host galaxies according to [72] and selected only Sa–Sc types,<sup>2</sup> since it is known that both GD and NGD shapes are well represented in Sa–Sc spirals [179, 180].

---

<sup>2</sup>Many of the identified host galaxies are already listed in database of [72], which is based on the SDSS DR8. Here, because we added new SNe, for homogeneity we redid the entire reduction for this restricted sample based only on DR13.

We excluded all barred galaxies from our sample to eliminate the effect of substantial suppression of massive SF in the radial range swept by strong bars [46, 48], i.e. the observed suppression of CC SN numbers inside the bar radius [138], and study only the expected impact of the DWs on the distribution of SNe.<sup>3</sup> In addition, we removed host galaxies with strong morphological disturbances according to [73], i.e. interacting, merging and post-merging/remnant cases, which may add significant distortion into the SN distribution in discs of galaxies.

For the remaining SNe host galaxies, the next step is the measurement of their photometry and geometry. Following [72], we constructed 25 mag arcsec<sup>-2</sup> isophotes in the SDSS DR13 *g*-band, and then visually fit onto each isophote an elliptical aperture. We then measured the major axes ( $D_{25}$ ), elongations ( $a/b$ ), and PA of galaxies. In our analysis, we used the  $D_{25}$  corrected for Galactic [181] and host galaxy internal extinction [182]. Finally, we calculated the inclinations of host galaxies using elongations and morphological types, following the method presented in [183]. These procedures are explained in detail in [72].

We also removed highly inclined galaxies ( $i > 60^\circ$ ), because at these inclinations strong absorption and projection effects play a destructive role in discovering SNe [184] and correcting their radial distribution for inclination of host disc [138]. Moreover, it is difficult to classify highly inclined galaxies and determine their barred structure (see review by [185]).

After these operations, we obtained 353 SNe within 285 host galaxies with the aforementioned restrictions.

### 3.2.2 Determination of spiral arm classes

Following our recent study [61], we determined ACs of 285 host galaxies (unbarred Sa–Sc types) with  $i \leq 60^\circ$  according to the classification scheme by [177]. To accomplish this, we used the background subtracted and photometrically calibrated *g*-band<sup>4</sup> SDSS images, as well as the RGB colour images from the *g*, *r*, and *i* SDSS data channels. We assigned ACs according

<sup>3</sup>It is important to note that in some SN host galaxies we may not detect tiny bars with lengths shorter than a tenth of the optical disc [73]. However, by the inner truncation of host discs (see Subsection 3.3.1) we exclude any possible impact of these bars on the distribution of SNe.

<sup>4</sup>Among the SDSS *g*, *r*, and *i* bands with good signal-to-noise ratio, the arm-interarm contrast is the highest in the *g*-band, as it traces the young stellar populations in the spiral arms (see [61]).

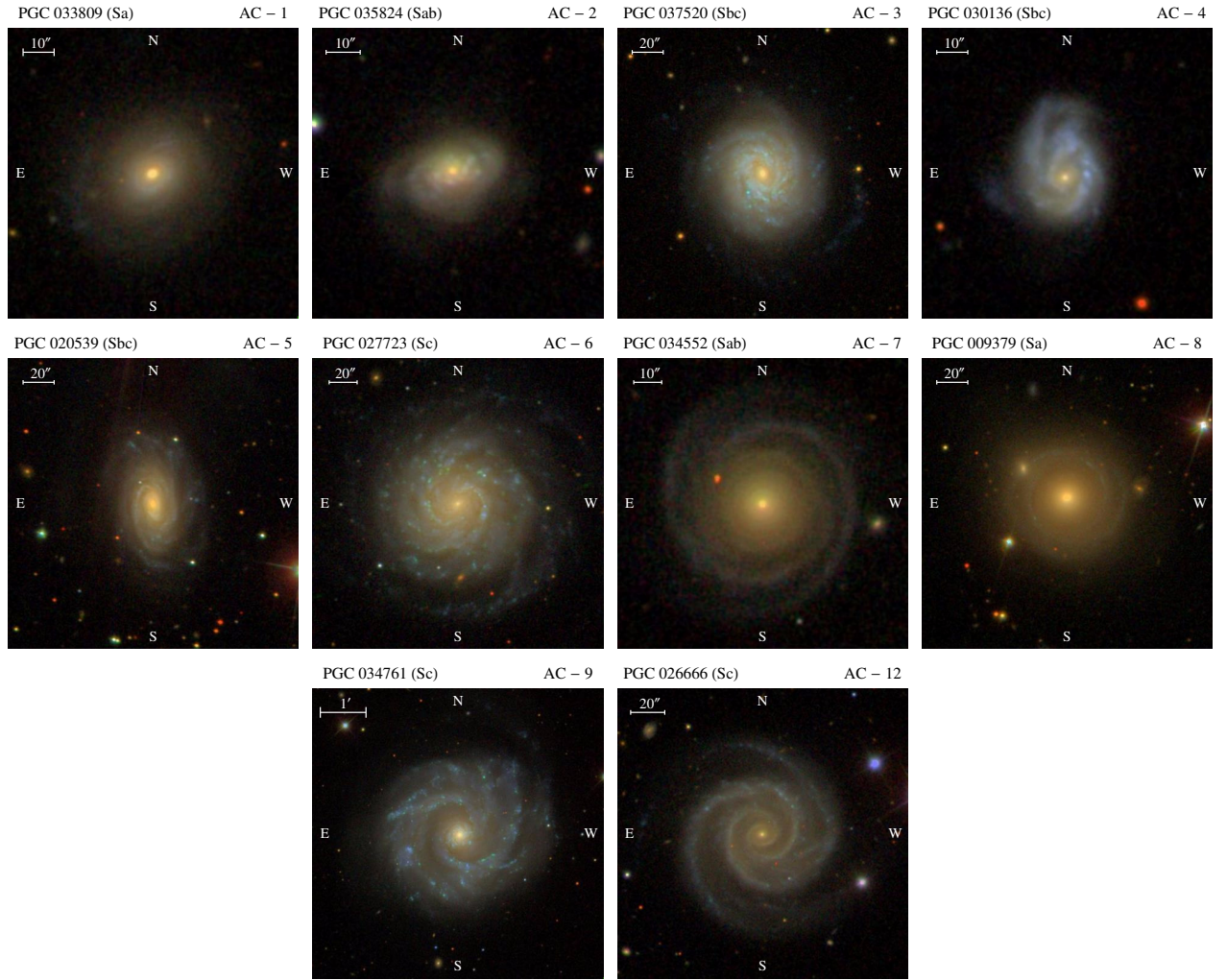


Figure 3.1: SDSS images representing examples of unbarred Sa–Sc host galaxies with different arm classes (ACs) according to [177]. The Principal Galaxy Catalogue (PGC) objects’ identifiers, morphological types (in parentheses), and ACs are listed at the top. In all images, north is up and east is to the left.

to the flocculence, regularity, and shapes of the spiral arms. The SDSS three-colour images representing examples of SN host galaxies with different ACs can be found in Fig. 3.1. Below, we describe these classes in detail according to [177].

Galaxies with AC 12 contain two long symmetric arms, and the ones with AC 9 have two symmetric inner arms, multiple long and continuous outer arms. The underlying mechanism that explains the lengths of arms and their global symmetry in these galaxies is most probably a DW, dominating the entire optical disc [186]. We denote galaxies with ACs 9 and 12 as long-armed GD (LGD) galaxies.

Galaxies with AC 5 have two symmetric short arms in the inner region and irregular outer arms. The AC 6 is like AC 5 in the inner disc region, however with feathery ringlike outer structure. The short inner symmetric arms in these galaxies might be explained by the DW mechanism, dominating only in the inner part of the optical disc [186]. We denote galaxies with ACs 5 and 6 as short-armed GD (SGD) galaxies.

Galaxies with AC 1 are described by chaotic, fragmented and unsymmetric arms, AC 2 is fragmented spirals arm pieces with no regular pattern, AC 3 is fragmented arms uniformly distributed around the galactic centre. Galaxies with AC 4 have only one permanent arm, otherwise fragmented arms. All these flocculent galaxies (ACs 1-4) appear to lack global DWs, instead their spirals may be sheared self-propagating SF regions (see review by [185] and references therein). We denote galaxies with ACs 1-4 as NGD galaxies.

Galaxies with AC 7 have two symmetric long outer arms, feathery or irregular inner arms. In these galaxies, the DWs play a role, most probably, only in the outer part of the optical disc (see review by [185] and references therein). In our study, due to the small number statistics (especially for CC SNe), these galaxies are not denoted to a separate class. We have only 11 Type Ia and 6 CC SNe in these hosts. On the other hand, because of the different placement of DWs, it is inadvisable to mix them with other classes. Therefore, we simply omit them from the sample.

Galaxies with AC 8 have tightly wrapped ringlike arms. These ringlike arms (rings and pseudorings) are thought to be related to the gathering of material near dynamical resonances in the disc (see review by [185]). Because of the different structural feature and small number statistics (only 3 Type Ia SNe), we omit these galaxies from the sample as well.

Finally, according to [177], ACs 10 and 11 were previously reported to be barred galaxies and objects with close neighbors, respectively, and are no longer used.

In the present study, we mainly used these broad classes: LGD (AC 9, 12), SGD (AC 5, 6), and NGD (AC 1-4). Table 3.1 presents the distributions of 333 SN types among various morphological types of the broad ACs of host galaxies. The number of individual host galaxies is 269. The mean distance of the galaxies is 82 Mpc (standard deviation is 39 Mpc). The mean

Table 3.1: Numbers of SNe at distances  $\leq 150$  Mpc in unbarred Sa–Sc hosts with inclinations  $i \leq 60^\circ$ , split between LGD, SGD, and NGD galaxies.

	Sa	Sab	Sb	Sbc	Sc	All
LGD (9, 12)						
Ia	2	4	7	21	27	61
Ibc	1	0	2	14	19	36
II	0	1	13	22	61	97
All	3	5	22	57	107	194
SGD (5, 6)						
Ia	0	0	2	8	8	18
Ibc	0	0	2	1	6	9
II	0	0	3	7	22	32
All	0	0	7	16	36	59
NGD (1-4)						
Ia	3	3	5	10	11	32
Ibc	0	5	1	4	4	14
II	1	1	4	9	19	34
All	4	9	10	23	34	80

*Notes.* Among these 333 SNe, there are only 23 uncertain (20 peculiar) classifications. SNe of Type II include only 10 SNe IIb. All Type II<sub>n</sub> SNe are removed from the sample due to uncertainties in their progenitor nature [76], and often in their classification [187, 188].

$D_{25}$  of the hosts is 120 arcsec with the minimum value of 23 arcsec. In Table 3.1, we present the numbers of Types Ibc and II SNe separately. However, to increase statistical significance of our results (especially in Section 3.4), we combined SNe Ibc and II into a single CC SNe class.

In order to test our visual classification of spiral arms, the entire sample of SNe host galaxies was independently classified. By comparing these classifications, we determined that our ACs are 97 per cent reliable. Following [61], it is important to note that the most common mis-classifications of ACs are from 2 or 3 to 4 (or vice versa), from 5 to 6 (or vice versa), and from 9 to 12 (or vice versa). Because we separated SNe host galaxies by their ACs into three broad classes: LGD, SGD, and NGD, the possible mis-classification between them is negligible.

Of the sample galaxies, 56 are in common with galaxies for which ACs were determined

by [177] on the blue images of the Palomar Observatory Sky Survey.<sup>5</sup> A comparison of the ACs shows that about 65 per cent of the galaxies have the same broad classes. On the other hand, about 25 per cent of objects change from NGD to SGD or from SGD to LGD (or vice versa). The ACs change from NGD to LGD (or vice versa) only in about 10 per cent of the cases (6 individual galaxies). In all the cases, the SDSS images have deeper exposure and better resolution than the blue photographic plates of the Palomar Observatory Sky Survey (in some cases, they are even overexposed due to high surface brightness of the object). Therefore, the SDSS based arm-classification seems to be more reliable and more structure is revealed.

The full database of 333 individual SNe (SN designation, type, and offset from host galaxy nucleus) and their 269 hosts (galaxy SDSS designation<sup>6</sup>, distance, morphological type,  $a/b$ , PA, corrected  $g$ -band  $D_{25}$ , and AC) is available online [189].

### 3.3 Results

To reveal the possible influence of DWs in discs of Sa–Sc galaxies on the distribution and surface density of SNe, we now study the deprojected and normalized galactocentric radii of Type Ia and CC SNe in discs of host galaxies with various ACs.

#### 3.3.1 The radial distribution and surface density

In [138, 190], it is already shown that in spiral galaxies all CC SNe and the overwhelming majority of Type Ia SNe belong to the disc, rather than the bulge component. Considering this observational fact, we adopt a simplified model where all SNe are located on infinitely thin host discs and, following [65], we deproject the galactocentric radii of SNe ( $R_{\text{SN}}$ ) for the inclinations of these discs. For each SN, we then normalize  $R_{\text{SN}}$  to the corresponding host galaxy optical radius, i.e.  $R_{25} = D_{25}/2$ , to neutralize the greatly different linear (in kpc) sizes of various hosts

---

<sup>5</sup>For comparison of ACs, another arm-classification by [191] might be used. However, it is based on middle-infrared images (while we use the SDSS/optical images) and another definition of broad ACs (flocculent: grouping 1-4 ACs, multi-arm: grouping 5-9 ACs, and GD: only AC 12), which complicate the comparison.

<sup>6</sup>For the host galaxies included in Table 3.4, the PGC names are also available in the database.

Table 3.2: Comparison of the deprojected and normalized radial distributions of SNe ( $\tilde{r} = R_{\text{SN}}/R_{25}$ ) among different pairs of NGD, SGD, and LGD subsamples. The corresponding values for the inner-truncated disc ( $\tilde{r} \geq 0.2$ ) are listed in parentheses.

Subsample 1			Subsample 2			$P_{\text{KS}}$	$P_{\text{AD}}$	
Host	SN	$N_{\text{SN}}$	Host	SN	$N_{\text{SN}}$			
LGD	Ia	61 (50)	versus	NGD	Ia	32 (24)	0.521 (0.497)	0.690 (0.708)
LGD	Ia	61 (50)	versus	SGD	Ia	18 (16)	0.761 (0.800)	0.505 (0.821)
NGD	Ia	32 (24)	versus	SGD	Ia	18 (16)	0.557 (0.641)	0.216 (0.671)
LGD	CC	133 (111)	versus	NGD	CC	48 (40)	0.087 ( <b>0.048</b> )	0.106 ( <b>0.022</b> )
LGD	CC	133 (111)	versus	SGD	CC	41 (39)	0.410 (0.096)	0.430 (0.125)
NGD	CC	48 (40)	versus	SGD	CC	41 (39)	0.080 (0.356)	0.108 (0.312)
LGD	Ia	61 (50)	versus	LGD	CC	133 (111)	0.720 (0.702)	0.719 (0.706)
SGD	Ia	18 (16)	versus	SGD	CC	41 (39)	0.834 (0.697)	0.862 (0.590)
NGD	Ia	32 (24)	versus	NGD	CC	48 (40)	0.545 (0.384)	0.284 (0.169)

*Notes.* The probabilities from two-sample KS and AD tests ( $P_{\text{KS}}$  and  $P_{\text{AD}}$ ) are calculated using the calibrations by [90] and [91], respectively. The statistically significant differences between the distributions are highlighted in bold.

(as was shown in [65]).<sup>7</sup>

In Table 3.2, using the two-sample KS and AD tests, we compare the deprojected and normalized ( $\tilde{r} = R_{\text{SN}}/R_{25}$ ) radial distributions of Type Ia and CC SNe in different pairs of NGD, SGD, and LGD subsamples. From the  $P$ -values in Table 3.2, we see no statistically significant differences between the radial distributions of SNe in various subsamples. However, when we compare the inner truncated radial distributions ( $\tilde{r} \geq 0.2$ ; shown in brackets), a significant difference appears for CC SNe in LGD versus NGD hosts. The upper panel of Fig. 3.2 presents the histograms of radii of CC SNe. From these histograms, we see that the radial distribution of CC SNe in NGD subsample is concentrated to the centre of galaxies with a relatively narrow peak and fast decline in the outer disc. In contrast, the distribution of CC SNe in LGD galaxies has a broader peak, shifted to the outer region of the discs, with a somewhat slower decline. The radial distribution of SNe in SGD hosts appears to be intermediate between

<sup>7</sup>For the normalization, one can suggest to use the SDSS scale lengths (exponential model fits) of galaxies. However, our sample includes a large number of host galaxies with large angular sizes ( $> 100$  arcsec) for which the SDSS fails in estimation of the model scale lengths due to the blending/defragmenting of galaxies with large angular sizes (the scales are not reliable, this is well-known problem). In [72], we already commented about the SDSS model failure. Thus, reliable scale lengths are not available for many galaxies of our sample.

Table 3.3: Consistency of global ( $\tilde{r} \geq 0$ ) and inner-truncated ( $\tilde{r} \geq 0.2$ ) SN distributions with exponential surface density models in different subsamples of host galaxies.

Host (1)	SN (2)	$\tilde{r} \geq 0$				$\tilde{r} \geq 0.2$			
		$N_{\text{SN}}$ (3)	$P_{\text{KS}}$ (4)	$P_{\text{AD}}$ (5)	$\tilde{h}_{\text{SN}}$ (6)	$N_{\text{SN}}$ (7)	$P_{\text{KS}}$ (8)	$P_{\text{AD}}$ (9)	$\tilde{h}_{\text{SN}}$ (10)
All	Ia	111	0.141	0.148	$0.21 \pm 0.01$	90	0.272	0.333	$0.20 \pm 0.01$
LGD	Ia	61	0.730	0.514	$0.22 \pm 0.02$	50	0.886	0.791	$0.20 \pm 0.02$
SGD	Ia	18	0.318	0.290	$0.24 \pm 0.03$	16	0.737	0.506	$0.21 \pm 0.03$
NGD	Ia	32	0.557	0.489	$0.19 \pm 0.02$	24	0.449	0.379	$0.18 \pm 0.02$
All	CC	222	<b>0.005</b>	<b>0.002</b>	$0.22 \pm 0.01$	190	0.117	0.172	$0.19 \pm 0.01$
LGD	CC	133	<b>0.017</b>	<b>0.018</b>	$0.22 \pm 0.01$	111	0.070	<b>0.043</b>	$0.20 \pm 0.01$
SGD	CC	41	<b>0.023</b>	<b>0.035</b>	$0.21 \pm 0.01$	39	0.349	0.440	$0.17 \pm 0.02$
NGD	CC	48	0.191	0.180	$0.20 \pm 0.02$	40	0.579	0.407	$0.18 \pm 0.02$

*Notes.* Columns 1 and 2 give the subsample; Col. 3 is the number of SNe in the subsample; Cols. 4 and 5 are the  $P_{\text{KS}}$  and  $P_{\text{AD}}$  probabilities from one-sample KS and AD tests, respectively, that the global ( $\tilde{r} \geq 0$ ) distribution of SNe is drawn from the best-fitting exponential surface density profile; Col. 6 is the maximum likelihood value of  $\tilde{h}_{\text{SN}} = h_{\text{SN}}/R_{25}$  with bootstrapped error (repeated  $10^3$  times); Cols. 7–10 are respectively the same as Cols. 3–6, but for the inner-truncated ( $\tilde{r} \geq 0.2$ ) distribution. The  $P_{\text{KS}}$  and  $P_{\text{AD}}$  are calculated using the calibrations by [90] and [126], respectively. The statistically significant deviations from an exponential law are highlighted in bold.

those in NGD and LGD galaxies.

The inner truncation of the radial distribution of SNe, especially for CC ones, is crucial because of several important effects. The observed numbers of SNe at  $\tilde{r} \lesssim 0.2$  indicate that because of high surface brightness of galactic nuclei and imperfect reduction of astronomical images it is difficult to discover objects at or near the centre of galaxies, even for nearby ones [111]. On the other hand, dust extinction in host galaxy disc, particularly in the nuclear region [112], can affect the radial distributions of SNe [69, 89]. Since CC SNe have peak luminosities that are  $\sim 2$  magnitudes lower than do SNe Ia [192], CC SNe are more strongly affected by these effects than are Type Ia SNe.

In [138], we already demonstrated that in the central regions of unbarred spiral galaxies the surface densities of SNe show a drop, significantly for CC SNe (see also in the middle panel of Fig. 3.2), in comparison with the exponential surface density profiles of the parent populations (see also [106, 123]). We list, in columns 4 and 5 of Table 3.3, for different subsamples of the

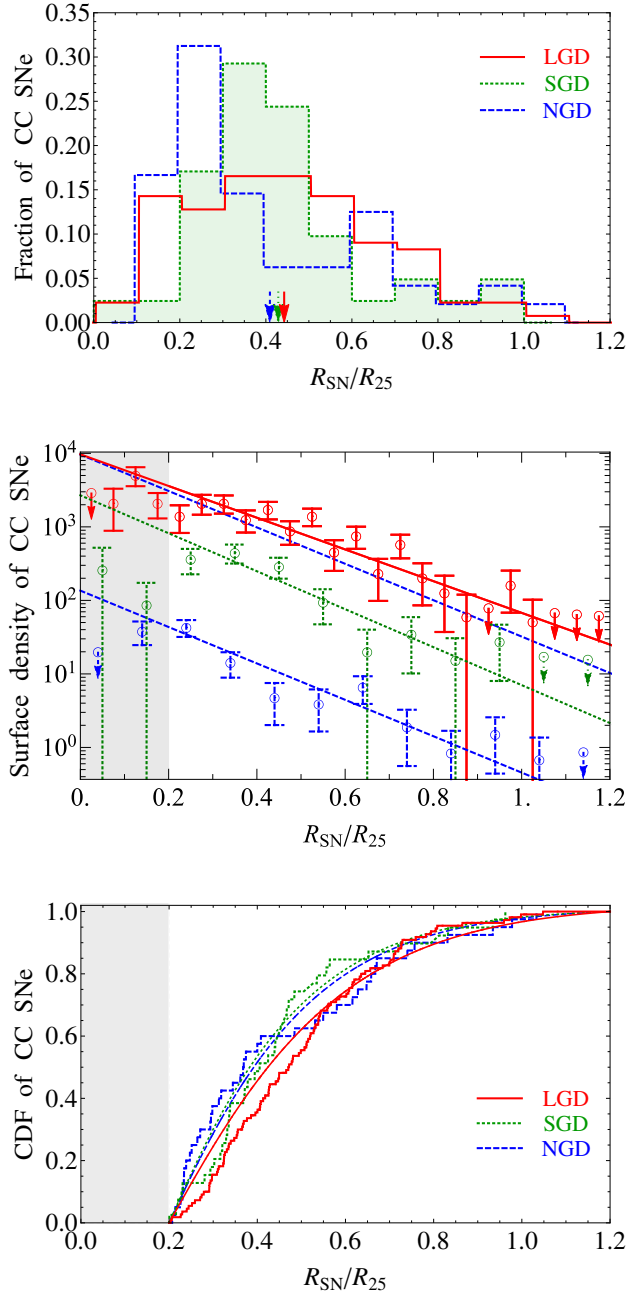


Figure 3.2: *Upper panel:* distributions of deprojected and normalized galactocentric radii ( $\tilde{r} = R_{\text{SN}}/R_{25}$ ) of CC SNe in LGD (red solid), SGD (green dotted), and NGD (blue dashed) host galaxies. The mean values of the distributions are shown by arrows. *Middle panel:* surface density distributions (with arbitrary normalization) of CC SNe in the mentioned hosts. For better visualization, thanks to more data points, the bin size of distribution in LGD galaxies is 0.05, in units of  $R_{25}$ , while for the other subsamples the bin size is 0.1. The error bars assume a Poisson distribution. The upper-limits of surface density (with +1 SN if none is found) are represented by down arrows. The fitted exponential surface density profiles are estimated for the inner-truncated discs (outside the shaded area). For better visibility, the distributions and profiles are shifted vertically sorted by increasing the mean  $\tilde{r}$  as one moves upwards, and also slightly shifted horizontally. To visually compare the distribution of CC SNe in LGD hosts with the fitted profile in NGD galaxies, the latter is also positioned with the central surface density matched with that in LGD hosts. *Bottom panel:* inner-truncated cumulative distributions of SN radii and their best-fitting exponential CDFs.

present study, the  $P_{\text{KS}}$  and  $P_{\text{AD}}$  probabilities from one-sample KS and AD tests, respectively, that the distributions of SNe are drawn from the best-fitting exponential surface density profiles. We obtain  $\Sigma^{\text{SN}}(\tilde{r}) = \Sigma_0^{\text{SN}} \exp(-\tilde{r}/\tilde{h}_{\text{SN}})$  profiles using the MLE method, where  $\tilde{h}_{\text{SN}}$  is the scale length of the distribution (column 6 of Table 3.3) and  $\Sigma_0^{\text{SN}}$  is the central surface density of SNe. The  $P$ -values in Table 3.3 show that the global ( $\tilde{r} \geq 0$ ) distributions of Type Ia SNe in different subsamples are consistent with the exponential profiles. However, the surface density distributions of CC SNe are not consistent with the exponential profiles in all subsamples of host galaxies, except the NGD hosts.

To exclude the selection effects at the centres of host galaxies, we repeat our procedure for  $\tilde{r} \geq 0.2$  range (see columns 7–10 in Table 3.3). Now, with only one exception, the surface density distributions of Type Ia and CC SNe in different subsamples are consistent with the exponential profiles. The inner-truncated scale lengths are in agreement with those in [138]: using nearby low-inclined early-type spiral galaxies (unbarred Sa–Sbc, without splitting the sample according to ACs) we found  $\tilde{h}_{\text{SN}}^{\text{Ia}} = 0.21 \pm 0.03$  and  $\tilde{h}_{\text{SN}}^{\text{CC}} = 0.17 \pm 0.03$  in the SDSS  $g$ -band.

Only the surface density distribution of CC SNe in LGD galaxies is inconsistent with an inner-truncated exponential profile (as seen in Table 3.3 for the AD statistic but only very marginally so in the KS statistic). From the middle panel of Fig. 3.2, we see that the surface density is marginally higher than the best-fitting exponential profile at  $0.4 \lesssim \tilde{r} \lesssim 0.7$ . The inconsistency becomes more evident if we compare the distribution of CC SNe in LGD galaxies with the inner-truncated exponential profile with the scale length of CC SNe in NGD galaxies ( $P_{\text{KS}} = 0.005$  and  $P_{\text{AD}} = 0.001$ ). For the visualization, the latter (upper blue dashed line in the middle panel of Fig. 3.2) is also scaled according to the central surface density of the profile in LGD hosts. The bottom panel of Fig. 3.2 shows the cumulative distributions of CC SN radii with their best-fitting exponential CDFs.

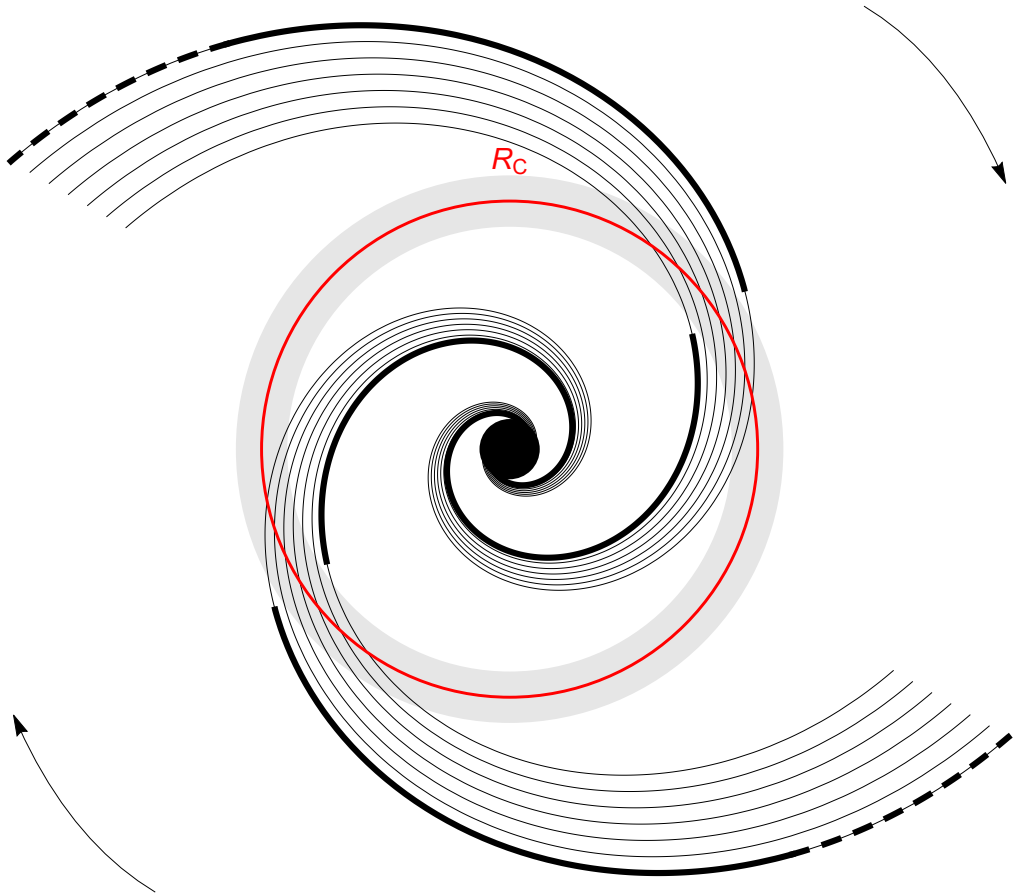


Figure 3.3: The scheme of massive SF triggering by DWs in a model of a GD galaxy with two logarithmic spiral arms. The direction of galaxy rotation is illustrated by arrows. The shock fronts of spiral arms are displayed with thick black curves. The corotation region and radius  $R_C$  are represented by a thick gray ring and red solid circle, respectively. At large radii ( $\gtrsim R_{25}$ ), the impact of DWs is expected to be weak (shock fronts are presented by thick dashed curves).

### 3.4 Interpretation within the framework of density wave theory

In this section, we interpret the results above in the context of triggered massive SF by the DWs in GD galaxies, especially in LGD hosts [54, 56, 166].

In a simple model of GD host galaxies (Fig. 3.3), we assume that the spiral pattern rotates with a constant angular velocity, while the gas and stars have differential rotation, and a corotation radius/region ( $R_C$ ) exists where these two angular velocities are equal. Inside the corotation radius, the disc rotates faster than the spiral arm pattern, and therefore massive SF

triggering is expected in a shock front around the inner edges of arms (thick black curves inside red solid circle in Fig. 3.3, see also fig. 9 of [61]), as originally proposed by [162]. On the contrary, outside the corotation radius, the arm pattern rotates faster than the disc. Therefore, gas and stars are caught up by the spiral arms. In this case, SF is expected to be triggered in a shock front around the outer edges of arms (thick black curves outside red solid circle in Fig. 3.3). Indeed, in [61] is already shown that the distribution of CC SNe (explosions of young short-lived massive stars) relative to the SDSS  $g$ -band peaks of spiral arms depends on the galactocentric radial range. In particular, the locations of CC SNe are shifted to the inner and outer edges of the spiral arms inside and outside the mean corotation radius ( $\langle R_C/R_{25} \rangle \approx 0.45$ ) of LGD galaxies, respectively. For Type Ia SNe (explosions of less-massive and longer-lived stars), the distribution relative to spiral arms showed no significant dependence on galactocentric radii.

In the corotation region (thick gray ring in Fig. 3.3) where the stars and gas rotate at the same velocity as the spiral pattern, the triggering of SF is not expected, given the absence of spiral shocks. Mainly, the gravitation instability is responsible for the SF in this region (as in the entire disc of a NGD galaxy). Due to absence of SF triggering spiral shocks in the corotation region [166], the surface density of CC SNe should show a drop around  $R_C$  in GD galaxies. At the same time, at large radii ( $\gtrsim R_{25}$ ) the DWs are expected to fade [186]. Therefore, at large radii, SF triggered by shock fronts at the outer edges of arms should be not significant (thick black dashed curves in Fig. 3.3).

To study the distribution of SNe relative to  $R_C$  of hosts, we carried out an extensive literature search for corotation radii of our SGD and LGD galaxies. Only 30 nearby host galaxies ( $\lesssim 80$  Mpc) with 8 Type Ia and 48 CC SNe have available corotation radii (Table 3.4). These radii were estimated using different methods. For example, [186] found clear evidences for the corotation radii in gas-rich galaxies, in the form of sharp endpoints to SF ridges and dust lanes in GD spirals. [193] used Fourier analysis and focused on the modes of the spiral arms, computing the torques between the gas and newly formed stars ( $H\alpha$  emission), and the bulk of the optical matter ( $r$ -band), which can be used to locate the corotation regions. [194] used the potential-density phase-shift method on deprojected  $H$ -band images to locate the corotation

Table 3.4: Available corotation radii of our LGD and SGD host galaxies.

Host name (1)	AC (2)	$N_{\text{Ia}}$ (3)	$N_{\text{CC}}$ (4)	$R_C/R_{25}$ (5)	$R_C/R_{25}$ (6)	References (7)
PGC043118	12	1	0	$0.33 \pm 0.05$	–	[195]
PGC040153	12	1	1	$0.30 \pm 0.05$	–	[195, 196]
PGC038068	12	0	3	$0.50 \pm 0.08$	–	[194, 197]
PGC030087	12	0	4	$0.54 \pm 0.13$	–	[198]
PGC024531	12	0	1	$0.87 \pm 0.11$	–	[193, 199]
PGC007525	12	0	2	$0.30 \pm 0.06$	–	[193]
PGC005974	12	0	3	$0.34 \pm 0.09$	–	[166, 186, 200]
PGC054018	9	0	1	$0.40 \pm 0.04$	–	[199]
PGC050063	9	1	3	$0.21 \pm 0.03$	$0.45 \pm 0.12$	[166, 186, 201]
PGC042833	9	0	2	$0.37 \pm 0.04$	$0.57 \pm 0.05$	[194, 199]
PGC039578	9	0	4	$0.34 \pm 0.06$	$0.57 \pm 0.07$	[186, 194, 202]
PGC038618	9	0	1	$0.30 \pm 0.01$	$0.54 \pm 0.06$	[194]
PGC037845	9	0	1	$0.21 \pm 0.06$	$0.40 \pm 0.06$	[194]
PGC037229	9	0	4	$0.46 \pm 0.08$	–	[186, 194]
PGC036789	9	0	1	$0.22 \pm 0.06$	–	[195]
PGC036243	9	0	2	$0.45 \pm 0.13$	–	[194, 203]
PGC034767	9	0	3	$0.28 \pm 0.03$	–	[204]
PGC032614	9	0	2	$0.69 \pm 0.02$	$0.83 \pm 0.04$	[199]
PGC031968	9	0	1	$0.26 \pm 0.02$	–	[199]
PGC027074	9	0	1	$0.30 \pm 0.06$	–	[195]
PGC024111	9	1	1	$0.65 \pm 0.06$	–	[195]
PGC022279	9	0	1	$0.16 \pm 0.06$	–	[193]
PGC002246	9	0	1	$0.14 \pm 0.06$	$0.57 \pm 0.06$	[193]
PGC002081	9	0	1	$0.38 \pm 0.05$	–	[186, 205]
PGC038031	6	1	0	$0.22 \pm 0.03$	$0.42 \pm 0.02$	[195, 199]
PGC027723	6	1	0	$0.17 \pm 0.06$	$0.44 \pm 0.06$	[195]
PGC012626	6	2	0	$0.48 \pm 0.03$	–	[194]
PGC035594	5	0	1	$0.32 \pm 0.06$	–	[199]
PGC034836	5	0	2	$0.12 \pm 0.06$	$0.58 \pm 0.06$	[194]
PGC030010	5	0	1	$0.17 \pm 0.06$	$0.41 \pm 0.06$	[195]

*Notes.* Column 1 is the host galaxy PGC name; Col. 2 is the galaxy AC (see Subsection 3.2.2); Cols. 3 and 4 are the numbers of Type Ia and CC SNe in the galaxy; Cols. 5 and 6 are the normalized corotation radii of the galaxy; Col. 7 is the references of corotation radii. The  $R_C/R_{25}$  values are calculated using the  $R_C$  in arcsec from the mentioned references and the galaxy  $R_{25}$  in the SDSS  $g$ -band (see Subsection 3.2.1). When more than one references are available for the same corotation region and the reported radii are matched within the errors, we list their mean values. Nuclear and circumnuclear corotation radii (coincided with star-forming rings/ovals), as well as those with uncertain (very weak/noisy) estimation are not selected from the references.

radii for a large number of spiral galaxies. [199] used the changes in direction of the radial component of the in-plane velocities, using the emission in  $H\alpha$ , at the resonance radii to find corotations in disc galaxies. For more details of these and other methods, the reader is referred to the original papers mentioned in Table 3.4. Farther in our study, we use these corotation radii normalized to the optical radii of host galaxies in the SDSS  $g$ -band, i.e.  $R_C/R_{25}$ .

In Table 3.4, it can be seen that for some individual galaxies more than one corotation radius is found. This is not unexpected because real spiral galaxies are more complex physical objects in comparison with the simple model presented in Fig. 3.3. In some galaxies, single pattern velocities and single corotation radii are observed, while in other systems multiple spiral patterns with different velocities and resonant coupling [206], and therefore multiple corotation radii are discovered [194, 199]. In particular, [194] found that GD galaxies have on average 2-3 corotation radii, except for exceptionally strong GD spirals ( $AC=12$ ), which mostly have a single corotation radius. This is in agreement with our ACs of SNe host galaxies and collected corotation radii in Table 3.4.

In Fig. 3.4, we present the galactocentric  $R_C/R_{25}$  positions for 30 host galaxies of Table 3.4, separated according to their ACs: 6 SGD ( $AC=5$  and  $6$ ), 17 LGD ( $AC=9$ ), and 7 LGD ( $AC=12$ ) galaxies. Here, we separate LGD host galaxies between two ACs in order to check possible differences between the distributions and the mean values of their corotation radii. A similar separation is impossible for SGD galaxies due to the small size of this subsample (see Table 3.4). In Fig. 3.4, we also show the galactocentric  $R_{SN}/R_{25}$  positions of SNe for each host galaxy.

The mean values of normalized corotation radii and the standard deviations are  $0.33 \pm 0.16$ ,  $0.41 \pm 0.18$ , and  $0.46 \pm 0.21$  for SGD, LGD with  $AC=9$  and  $AC=12$  galaxies, respectively. For the united LGD ( $AC=9$  and  $12$ ) subsample, the normalized corotation radius is  $0.42 \pm 0.18$ . Meanwhile, the two-sample KS and AD tests show that the difference between the distributions of  $R_C/R_{25}$  values in LGD ( $AC=9$  and  $12$ ) and SGD galaxies is statistically not significant ( $P_{KS} = 0.550$  and  $P_{AD} = 0.312$ ). The same is valid when comparing the  $R_C/R_{25}$  distributions in LGD ( $AC=12$ ) and SGD galaxies ( $P_{KS} = 0.433$  and  $P_{AD} = 0.268$ ). Therefore, further in our study we do not separate the LGD subsample. Fig. 3.5 shows the histograms and cumulative

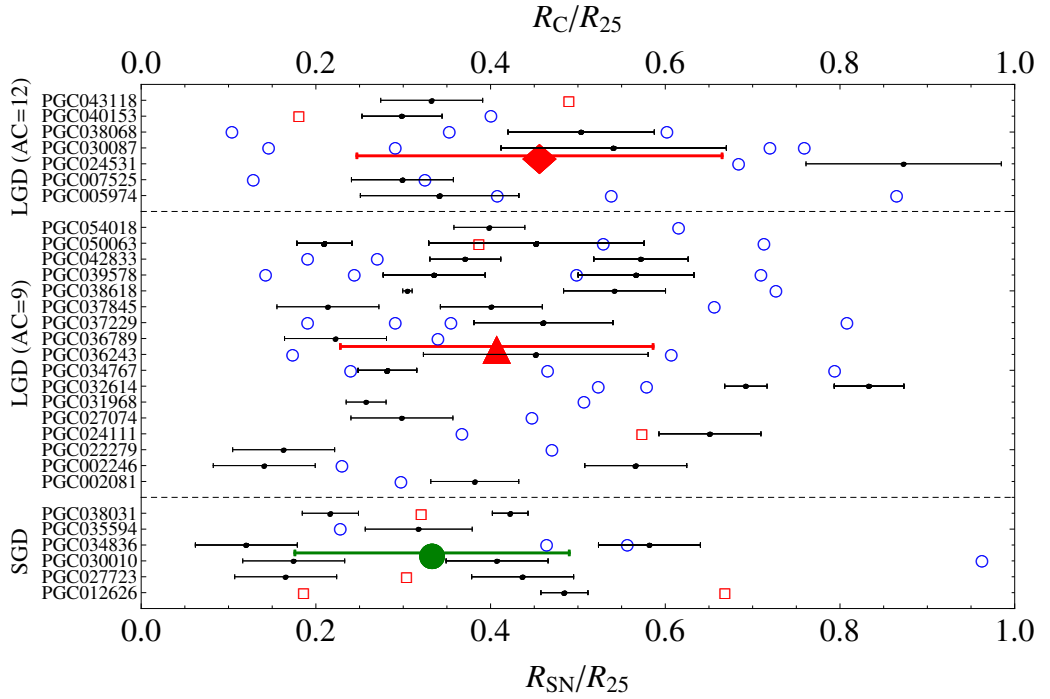


Figure 3.4: Galactocentric positions of normalized corotation radii (black points) and their errors for 30 host galaxies of Table 3.4. SGD (AC=5 and 6), LGD (AC=9), and LGD (AC=12) galaxies are separated by horizontal dashed lines. The filled diamond, triangle, and circle are the corresponding mean values of the corotation radii (with their standard deviations). For each host galaxy, galactocentric positions of Type Ia (red empty squares) and CC (blue empty circles) SNe are also presented. In PGC 050063, one of the CC SNe is located at  $R_{\text{SN}}/R_{25} = 1.59$  and not shown in the plot.

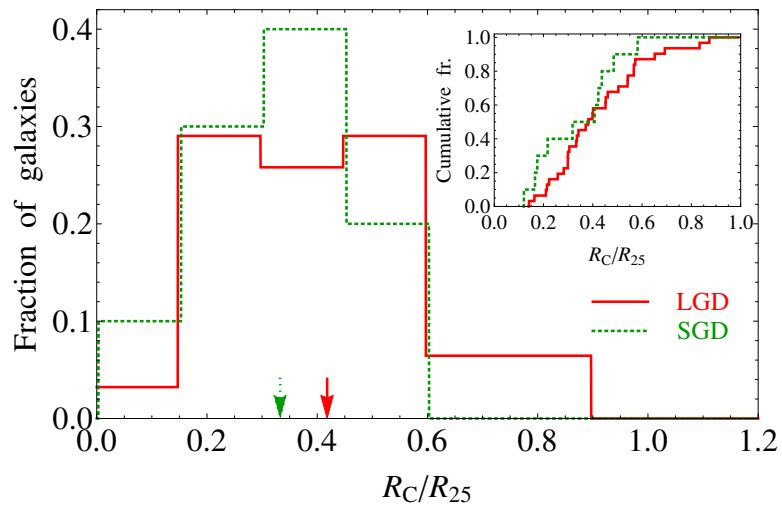


Figure 3.5: Histograms and cumulative distributions (inset) of  $R_C/R_{25}$  values of LGD (red solid) and SGD (green dotted) galaxies. The mean values are shown by arrows.

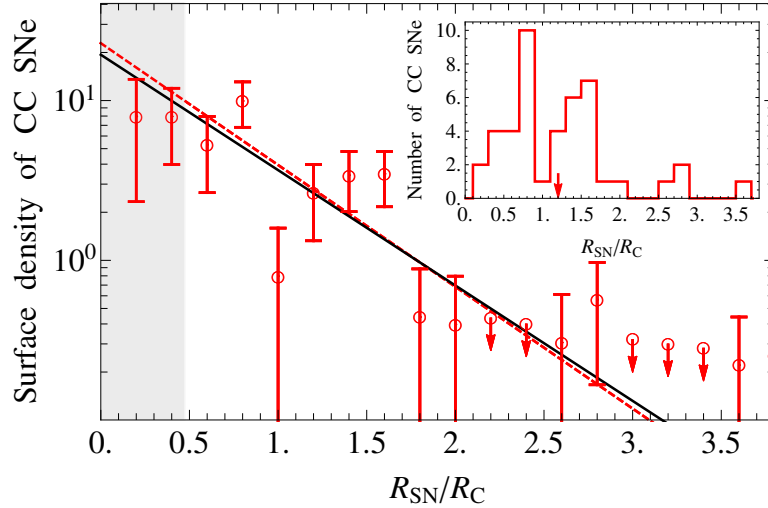


Figure 3.6: Surface density profile of CC SNe (with arbitrary normalization) in LGD host galaxies. The error bars assume a Poisson distribution. The upper-limits of surface density (with +1 SN if none is found) are represented by down arrows. The black solid and red dashed lines are the best maximum-likelihood fits of global and inner-truncated (from 0.48 corotation radii outwards to avoid the obscured inner region [grey shaded]) exponential surface density models, respectively. The inset presents the histogram of SN radii (the mean value is shown by arrow).

distributions of  $R_C/R_{25}$  values of LGD and SGD galaxies. Also, it is important to note, that the  $\langle R_C/R_{25} \rangle$  value for LGD galaxies is in good agreement with that ( $\approx 0.45$ ) adopted in [61].

To check the possible impact of DWs on the distribution of SNe (as schematically presented in Fig. 3.3), we now normalize the SN radii to the corresponding corotation radii of host galaxies. When a host galaxy has two corotation radii in Table 3.4, we use a proximity criterion, selecting only the value of  $R_C$  that is closest to the value of  $R_{SN}$ . For LGD host galaxies, Fig. 3.6 displays the histogram and surface density of 44 CC SNe positions in units of the corotation radii ( $R_{SN}/R_C$ ). The surface density of CC SNe is consistent with the best-fitting global ( $P_{KS} = 0.600$ ,  $P_{AD} = 0.463$ ) and inner-truncated ( $P_{KS} = 0.457$ ,  $P_{AD} = 0.526$ ) exponential profiles with the MLE scale lengths of  $(0.60 \pm 0.04) R_C$  and  $(0.57 \pm 0.05) R_C$ , respectively. However, the figure indicates a strong dip at the corotation radius, and excess surface densities of CC SNe at  $\simeq 0.8$  and  $1.5 R_C$ .

Since the lifetime of massive progenitors of CC SNe is significantly short, their explosion sites, on average, coincide with the birthplace. Therefore, the prominently high surface density

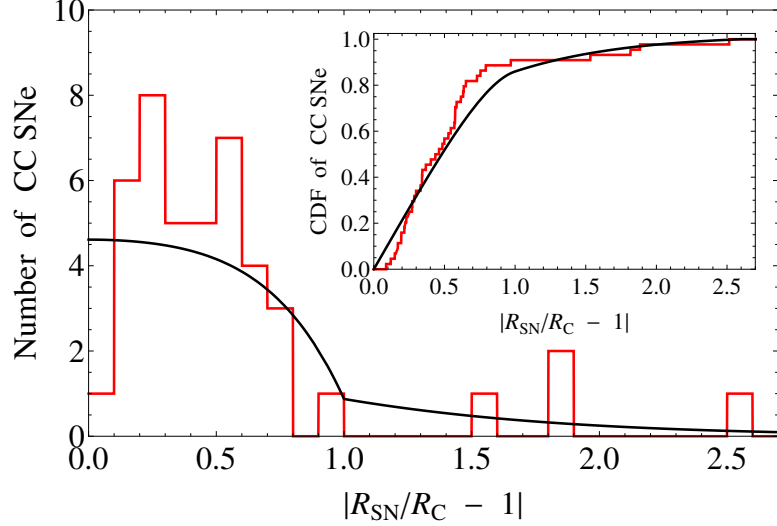


Figure 3.7: Differential distribution of the distances of CC SNe to nearest corotation radius in the global disc of LGD galaxies (normalized to the corotation radius). The inset presents the CDF of the distances. The black curves indicate the distribution of normalized distances to corotation expected for the best-fitting exponential surface density model (scale length of  $0.60 R_C$ ), using eqs. (3.1), (3.2), (3.3), and (3.4).

of CC SNe in comparison with the best-fitting exponential profile around the mentioned radii, inside and outside the corotation region, can be considered as a plausible indicator of triggered massive SF by the DWs in LGD host galaxies. These results are in agreement with those of [166], who found clear evidence of massive SF triggering in the sense of a high density of H II regions at the fixed radii, avoiding the corotation region, created after the passage of the arm material through the DW in some GD galaxies (see also [54, 56]).

Considering that the different LGD host galaxies have various corotation radii (see Table 3.4 and Fig. 3.4) distributed around the mean value of  $\langle R_C/R_{25} \rangle = 0.42 \pm 0.18$  (see Fig. 3.5), the radii of triggered SF by DWs should be blurred within a radial region including  $\sim 0.4$  to  $\sim 0.7$  range in units of  $R_{25}$ , preventing to observe a drop in the mean corotation region (middle panel of Fig. 3.2). Therefore, most probably, the impact of DWs (triggering effect) is responsible for a marginally higher surface density of CC SNe within the mentioned radial range, and for the inconsistency of the surface density distribution with the inner-truncated exponential profile in LGD hosts (middle panel of Fig. 3.2 and Table 3.3).

To check the significance of the drop of surface density at  $R_C$  and excess at  $\simeq 0.8$  and  $1.5 R_C$  (see Fig. 3.6), we study the distribution of CC SNe distances to the nearest corotation in units

of corotation radius,  $D = |R_{\text{SN}} - R_{\text{C}}|/R_{\text{C}}$ . Fig. 3.7 displays the differential and cumulative distances in the global disc of LGD galaxies. Since a given value of distance can occur either for position  $1 - D$  or for position  $1 + D$  (both in units of corotation radius), the probability distribution function (PDF) of distances follows

$$\text{PDF}(D) = \begin{cases} f(1 - D) + f(1 + D) & 0 < D \leq 1 \\ f(1 + D) & D > 1 \end{cases} \quad (3.1)$$

$$f(x) = \frac{x}{h^2} \exp\left(-\frac{x}{h}\right), \quad (3.2)$$

where  $h$  is the best-fitting scale length of the SNe (in units of the corotation radii). The CDF for  $D$  is then

$$\text{CDF}(D) = \begin{cases} g(1 - D) - g(1 + D) & 0 < D \leq 1 \\ 1 - g(1 + D) & D > 1 \end{cases} \quad (3.3)$$

$$g(x) = \left(1 + \frac{x}{h}\right) \exp\left(-\frac{x}{h}\right). \quad (3.4)$$

In Fig. 3.7, the black curves are the best-fitting (with MLE) expected distribution. Fig. 3.7 highlights the lack of CC SNe at corotation and excess outside/inside the  $R_{\text{C}}$  in the LGD hosts. However, a KS test indicates a  $P$ -value of 0.176, while an AD test indicates a  $P$ -value of 0.197. We check the significance of the drop/excess in the global disc, adding also four CC SNe from SGD sample. The result is:  $P_{\text{KS}} = 0.170$  and  $P_{\text{AD}} = 0.224$ . For the inner-truncated disc of LGD (LGD+SGD) galaxies, the  $P_{\text{KS}} = 0.353$  (0.445) and  $P_{\text{AD}} = 0.299$  (0.428). Thus, the lack of CC SNe at corotation and excess at  $\simeq 0.8$  and  $1.5 R_{\text{C}}$  do not appear statistically significant. Note that these tests ignore the uncertainties on the corotation radii. Including them would weaken even more the statistical significance of these features in the surface density profile of CC SNe.

It is important to note that, if one wants to test the SF activity at the corotation, the estimates of corotation radii based on kinematic or dynamic arguments [199] would be preferable as they would be more independent of the regions with lack of SF [186] or specific morphological

features in the discs [194]. Only 18 CC SNe (17 in LGD and one in SGD) have host galaxies with such preferable estimates of  $R_C$ . If we consider only these objects, the triggering evidence and the dip in the global disc remain not significant ( $P_{KS} = 0.514$  and  $P_{AD} = 0.425$ ), probably due to even smaller statistics.

Another importance is that galaxies with several spiral patterns with different angular velocities, i.e. more than one corotation, might have interactions between the patterns (e.g. at  $R_C$  of one with inner/outer Lindblad resonance of the other [199]) causing turbulence in the interface regions between the patterns and thereby increase SF activity at those regions (see reviews by [160, 161]). Therefore, the distribution of CC SNe (Figs. 3.6 and 3.7) might be contaminated by the objects at the  $R_C$ , weakening the observed dip. In Table 3.4, we see that 31 CC SNe (30 in LGD and one in SGD) have host galaxies with single  $R_C$ . If we consider only these objects, the triggering evidence and the dip in the global disc are again statistically not significant ( $P_{KS} = 0.457$  and  $P_{AD} = 0.354$ ).

Unfortunately, due to the insufficient number of CC SNe in SGD galaxies (only 4 objects, see Table 3.4), as well as Type Ia SNe in the LGD (4 cases) and SGD (4 objects) subsamples, a similar study of their distributions relative to  $R_C$  is ineffective. In the future, when more information is available on corotation radii of SN host galaxies, we will be able to extend our study including all SN types in LGD and SGD galaxies.

### 3.5 Chapter Conclusions

In this Chapter, using a well-defined and homogeneous sample of SN host galaxies from the coverage of SDSS DR13, we analyse the radial and surface density distributions of Type Ia and CC SNe in host galaxies with different ACs to find the possible impact of spiral DWs as triggers for SF. Our sample consists of 269 relatively nearby ( $\leq 150$  Mpc, the mean distance is 82 Mpc), low-inclination ( $i \leq 60^\circ$ ), morphologically non-disturbed and unbarred Sa–Sc galaxies, hosting 333 SNe in total. In addition, we perform an extensive literature search for corotation radii, collecting data for 30 host galaxies with 56 SNe.

The main results concerning the deprojected and inner-truncated ( $\tilde{r} \geq 0.2$ ) distributions of SNe in host galactic discs are the following:

1. We find no statistical differences between the pairs of the  $R_{25}$ -normalized radial distributions of Type Ia and CC SNe in discs of host galaxies with different spiral ACs, with only one significant exception: CC SNe in LGD and NGD galaxies have significantly different radius distributions (Table 3.2). The radial distribution of CC SNe in NGDs is concentrated to the centre of galaxies with relatively narrow peak and fast exponential decline at the outer region, while the distribution of CC SNe in LGD galaxies has a broader peak, shifted to the outer region of the discs (upper panel of Fig. 3.2).
2. The surface density distributions of Type Ia and CC SNe in most of the subsamples are consistent with the exponential profiles. Only the distribution of CC SNe in LGD galaxies appears to be inconsistent with an exponential profile (Table 3.3 for the AD statistic but only very marginally so for the KS statistic), being marginally higher at  $0.4 \lesssim R_{\text{SN}}/R_{25} \lesssim 0.7$ . The inconsistency becomes more evident when comparing the same distribution with the scaled exponential profile of CC SNe in NGD galaxies (middle panel of Fig. 3.2).
3. Using a smaller sample of LGD galaxies with estimated corotation radii, we show, for the first time, that the surface density distribution of CC SNe shows a dip at corotation, and enhancements at  ${}_{-0.2}^{+0.5}$  corotation radii around it (Fig. 3.6). However, these features are not statistically significant (Fig. 3.7). The CC SNe enhancements around corotation may, if confirmed with larger samples, indicate that massive SF is triggered by the DWs in LGD host galaxies. Considering that the different LGD host galaxies have various corotation radii (Table 3.4 and Fig. 3.4) distributed around the mean value of  $\langle R_{\text{C}}/R_{25} \rangle = 0.42 \pm 0.18$  (Fig. 3.5), the radii of triggered SF by DWs are most probably blurred within a radial region including  $\sim 0.4$  to  $\sim 0.7$  range in units of  $R_{25}$ , without a prominent drop in the mean corotation region (middle panel of Fig. 3.2).

These results for CC SNe in LGD galaxies may, if confirmed with larger samples and better

corotation estimates, support the large-scale shock scenario [59], originally proposed by [162], which predicts a higher SF efficiency, avoiding the corotation region [54, 56, 61, 166].

# Chapter 4

## Constraining Type Ia SNe via their distances from spiral arms

### 4.1 Introduction

From host galaxy studies, significant correlations are observed between SN Ia LC decline rate and the global ages of their hosts or local age at SN explosion sites [39, 52, 157, 158, 207]. On average, SNe Ia with larger  $\Delta m_{15}$  values are associated with older stellar environments. On the other hand, important relationships between host stellar population and properties of SNe Ia progenitors can be found by looking at the distribution of SNe Ia relative to spiral arms of galaxies [61, 66]. It is worth noting that, according to the spiral DW theory [53, 162], SF typically occurs at shock fronts near the edges of spiral arms. However, SN Ia LC decline rates have never been examined in SN studies based on where they are located on spiral arms or between, as well as  $\Delta m_{15}$  as a function of the mentioned distance. In this Chapter, we link the  $\Delta m_{15}$  and SN Ia distributions relative to spiral arms of nearby host galaxies and demonstrate, for the first time, how this could provide another interesting way to study the properties of SN Ia progenitors.

## 4.2 Sample selection and reduction

The database of this Chapter consists of SNe Ia from the sample of [52], after applying the restrictions described below. Note that [52] database is a compilation of 407 nearby SNe Ia ( $z \lesssim 0.036$ ) with known spectroscopic subclasses and  $B$ -band LC decline rates ( $\Delta m_{15}$ ). In addition, the database contains information on the distances of SNe Ia host galaxies, morphologies,  $ugriz$  magnitudes, and other parameters. For the current study, we selected only normal, 91T-, and 91bg-like SN Ia subclasses, which include a sufficient number of events from a statistical perspective.

For hosts, we restricted to Sab–Scd morphologies since we are interested in studying SNe Ia in galaxies with well-developed arms, where spiral DWs play an important role [167, 177, 208]. Following the approach of [73], we visually checked the levels of morphological disturbances of the host galaxies using their images from different surveys. The hosts with interacting and merging attributes were excluded from the sample since we are interested in studying SNe Ia in non-disturbed spiral galaxies. In addition, to avoid projection and absorption effects in the discs due to high inclinations, as well as to accurately investigate the immediate vicinity of SNe in terms of the existence of host spiral arms, the sample is limited to galaxies with  $i < 60^\circ$ . Only 142 SNe Ia in 137 host galaxies met the applied restrictions.

In spiral galaxies, the vast majority of SNe Ia belonging to normal, 91T-, and 91bg-like subclasses are discovered in disc of hosts [209]. Given this and using SN coordinates on the  $g$ -band images,<sup>1</sup> for each SNe Ia we visually inspected the area of a circular ring in a quadrant of host disc, where the SN is discovered, in terms of presence of well-pronounced spiral arms. This is important because we aimed to link SN progenitors to a population of stars born due to the SF after passing and compressing gas clouds through the DW [60, 61]. SNe Ia in the circumnuclear region or in the far outer disc (SN galactocentric distance  $< 0.1 R_{25}$  or  $> R_{25}$ ) were excluded from this study,<sup>2</sup> as well as those visually identified within the radius swept up by host galactic bar. As a result of this selection, we were finally left with 77 SNe Ia in 74 host

---

<sup>1</sup>We used the FITS images from the SDSS ([sdss.org](http://sdss.org)), the SkyMapper ([skymapper.anu.edu.au](http://skymapper.anu.edu.au)), and the Pan-STARRS ([outerspace.stsci.edu/display/PANSTARRS](http://outerspace.stsci.edu/display/PANSTARRS)) surveys.

<sup>2</sup> $R_{25}$  is the  $g$ -band 25<sup>th</sup> magnitude isophotal semi-major axis of the disc.

Table 4.1: Morphological distribution of the sampled SNe Ia host galaxies, split between different SN subclasses.

SN	Sab	Sb	Sbc	Sc	Scd	All
Normal	6	18	25	17	1	67
91T	2	0	4	2	0	8
91bg	2	0	0	0	0	2
ALL	10	18	29	19	1	77

Table 4.2: Numbers of *arm* and *interarm* SNe Ia within Sab–Scd galaxies, split between different SN subclasses.

SN	<i>arm</i>	<i>interarm</i>
Normal	37	30
91T	6	2
91bg	0	2
All	43	34

galaxies (see Table 4.1).

We determined the host spiral arm structures and the SNe positions with respect to the spiral arms according to the approaches detailed in [61]. In short, we defined *arm* and *interarm* SNe Ia that are discovered inside the host arm edges or in the interarm region, respectively. To accomplish this, we used the residual images of the host galaxies after subtraction of the fitted  $r^{1/4}$  bulge+exponential disc profiles from the smoothed  $g$ -band fits images. In the residual images, the values of the interarm pixels are negative, since the fitted profiles use fluxes from both the arm and interarm regions. Similar to [61], we fixed the edges of the spiral arms when the flux values change the sign. Fig. 4.1 shows examples of original and bulge+disc subtracted images of galaxies that host arm and interarm SNe Ia. Table 4.2 lists the numbers of SNe Ia in arm and interarm subsamples.

For each SNe Ia in the subtracted images, we measured the distance ( $d$ ) from the  $g$ -band surface brightness peak of the nearest spiral arm through the galactocentric direction (**bs** distance in Fig. 4.2). Only for two cases (SN1997cw and SN2002ck), the interarm SN association with the nearest spiral arm is somewhat ambiguous. Following [61], we normalized  $d$  to the corresponding semiwidth of the spiral arm, i.e.  $\tilde{d} = d/W_{\pm}$ , to compensate for the various linear

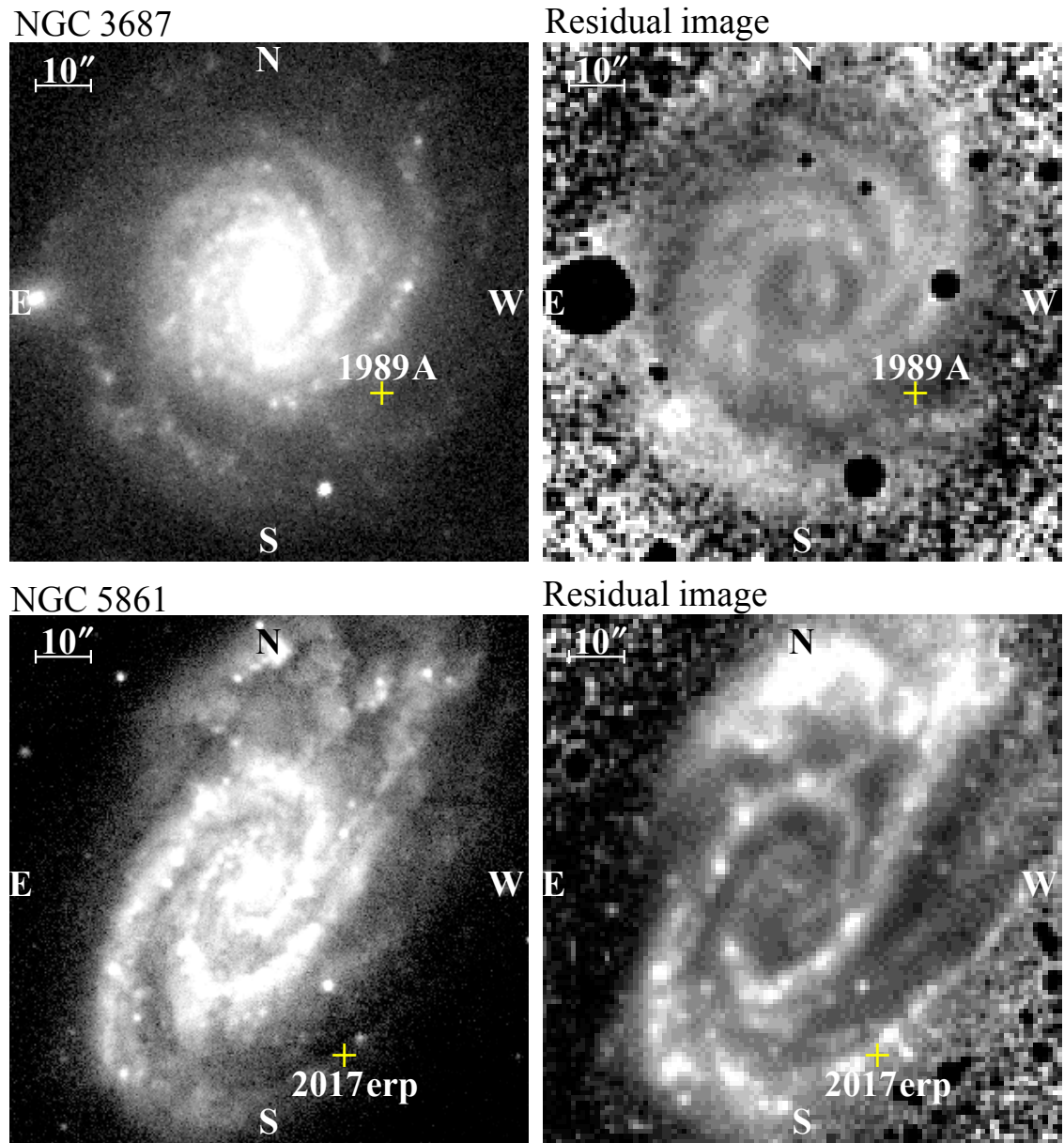


Figure 4.1: Upper panels: SDSS *g*-band image of *interarm* SN 1989A host galaxy (left) and its residual image (right), after subtracting bulge and disc components. Bottom panels: Pan-STARRS *g*-band image of *arm* SN 2017erp host (left) and its residual image (right). The locations of SNe are signed by crosses in all images (north is up and east to the left). Names of host galaxies are noted. In the residual images, bright projected stars are masked.

Table 4.3: The database of 77 SNe Ia of the study. The first ten entries are presented, while the entire table are available online [210].

SN	Arm/interarm definition	$\tilde{d}$	$\tilde{D}$	$\tilde{r}_{\text{SN}}$
1989A	interarm	1.442	0.272	0.524
1989B	arm	0.220	0.420	0.171
1990N	arm	0.830	0.117	0.859
1990O	interarm	1.753	0.541	0.764
1995al	arm	0.516	0.601	0.302
1995E	arm	0.478	0.398	0.411
1996ai	arm	0.584	0.163	0.151
1996bo	arm	0.445	0.537	0.122
1996Z	interarm	1.226	0.173	0.649
1997bp	interarm	2.326	0.837	0.459

sizes of the arm width. The semiwidth is the distance from the spiral arm peak to the inner/outer edge of the arm through the galactocentric direction. The  $W_-$  is the inner semiwidth (ba length in Fig. 4.2) with negative sign when SN is located between the nearest spiral arm peak and the host galaxy nucleus, and the  $W_+$  is the outer semiwidth (bc length in Fig. 4.2) with positive sign when the arm peak is between SN and the nucleus (see [61], for details).

It is worth noting that, according to the DW theory [53, 162], SF activities usually take place at a shock front around the inner edges of spiral arms inside the corotation radius ( $R_C$ ), and around the outer edges of arms outside the corotation (see Fig. 4.2). For each SNe Ia, we also measured the distance ( $D$ ) from the shock front of spiral arm through the galactocentric direction (as and cs distances in Fig. 4.2 inside and outside  $R_C$  radius, respectively). We normalized  $D$  to the width ( $W$ ) of the spiral arm (ac length in Fig. 4.2), i.e.  $\tilde{D} = D/W$ .

In addition, we estimated the deprojected galactocentric distances of SNe Ia ( $R_{\text{SN}}$ ), using well-known approach of correction for the host galactic disc inclination (see for details [138]). This requires the offsets of SNe from the nucleus of host galaxies ( $\Delta\alpha$  and  $\Delta\delta$ ), the PA and inclinations of the discs. Eventually, for each SNe Ia, the  $R_{\text{SN}}$  is normalized to the  $g$ -band  $R_{25}$ , i.e.  $\tilde{r}_{\text{SN}} = R_{\text{SN}}/R_{25}$ , to compensate for the various linear sizes of hosts. Note that the mentioned parameters are not listed in [52], however they were compiled and/or estimated at the time of that study and are now available online [210].

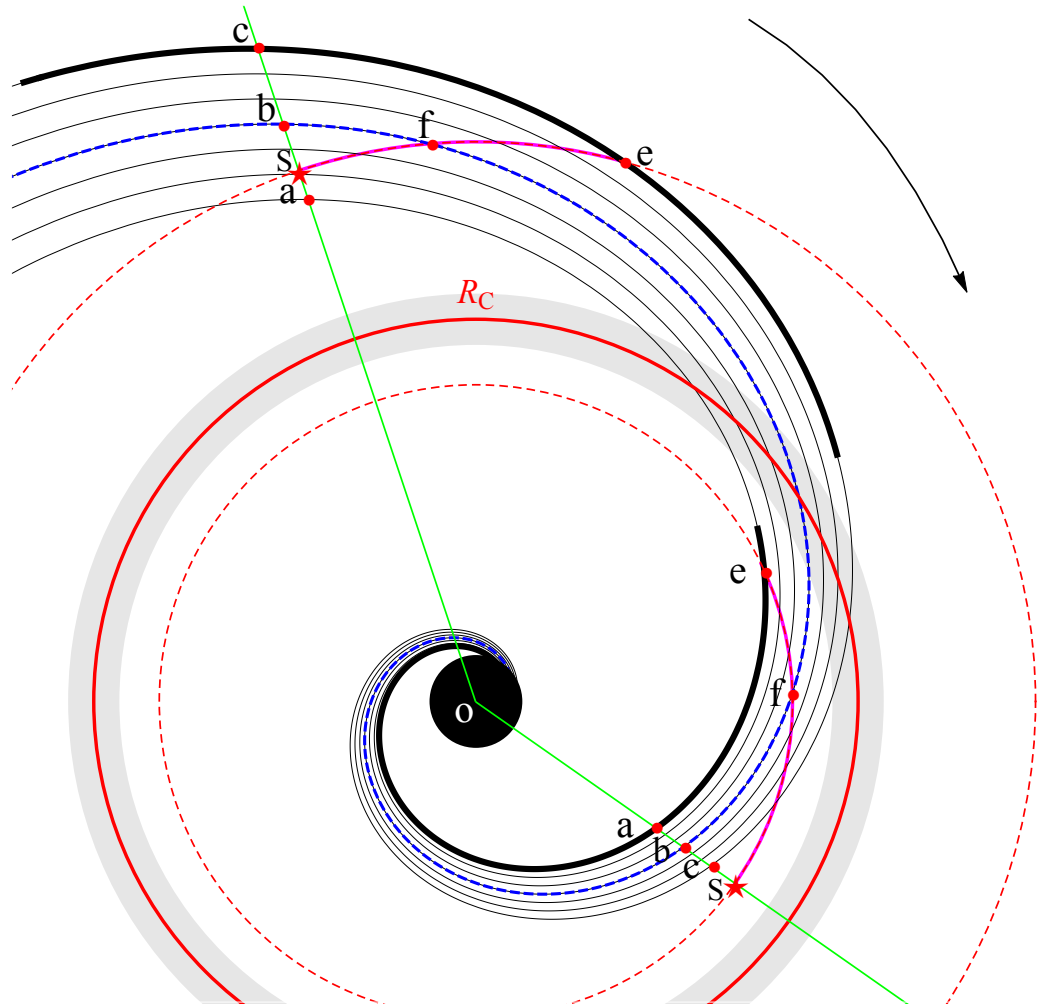


Figure 4.2: A scheme of GD galaxy with logarithmic arms (only one arm is shown), where additional SF is triggered by DWs. The arrow indicates the galaxy's rotational direction around nucleus (O). Thick black and blue dashed curves present shock fronts of spiral arm and arm's density (brightness) peak, respectively. A broad gray ring and a red solid circle indicate the corotation region and radius  $R_C$ , respectively. Two orbits of SN progenitors are represented by red dashed circles. The purple arc depicts traveled distance of an SN progenitor from birthplace (e) up to the explosion (s), through the arm peak (f) in the particular cases. The radial directions connecting SNe and nucleus are shown by green lines. The  $ac$ ,  $ba$ , and  $bc$  lengths are full, inner, and outer (semi)widths of the arm, respectively.

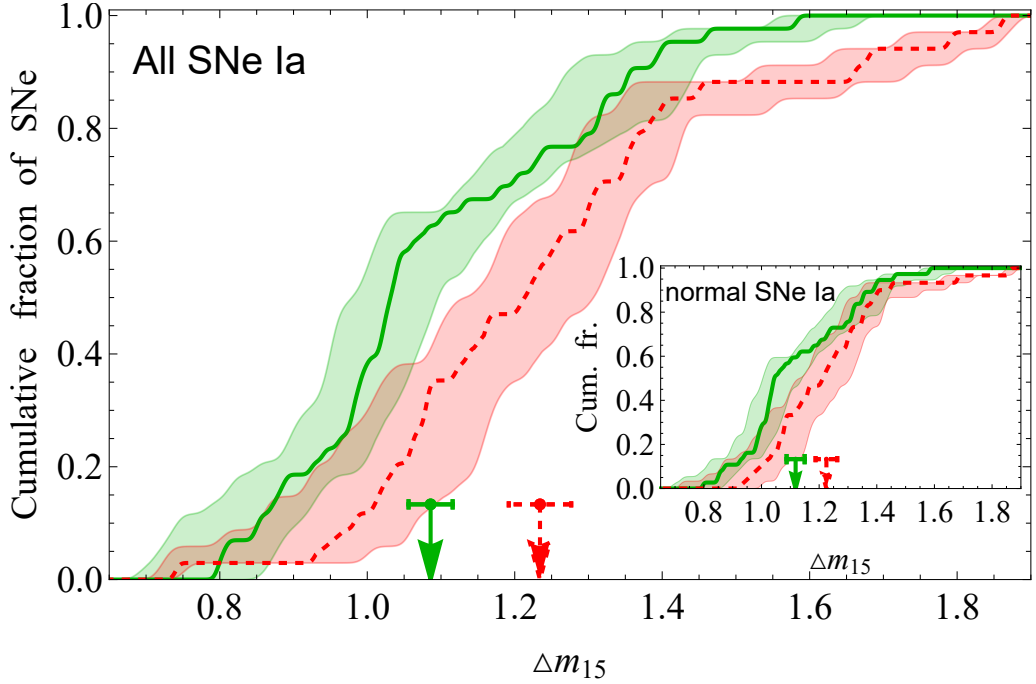


Figure 4.3: Cumulative  $\Delta m_{15}$  distributions of all *arm* (green solid) and *interarm* SNe Ia (red dashed). The associated spreads for each cumulative curve are shown by colored regions, taking into account the uncertainty in  $\Delta m_{15}$  values. Arrows show the mean values (with their standard errors) of the distributions. The inset is the same but only for normal SNe Ia.

Table 4.3 contains new database of this paper on all 77 individual SNe Ia (SN name, *arm* and *interarm* SN definition,  $\tilde{d}$ ,  $\tilde{D}$ ,  $\tilde{r}_{\text{SN}}$ ), while [52] contains data on the spectroscopic subclasses and *B*-band  $\Delta m_{15}$  of the events, as well as data on host galaxies.

## 4.3 Results and discussion

### 4.3.1 SNe Ia in *arm* and *interarm* regions of spiral galaxies

Fig. 4.3 presents the cumulative  $\Delta m_{15}$  distributions of all sampled SNe Ia in *arm* and *interarm* regions. The inset in Fig. 4.3 shows the same distributions, but only for normal SNe Ia. To statistically compare the distributions, we use nonparametric methods [93]: the two-sample KS and AD tests.<sup>3</sup> The *P*-values of the tests in Table 4.4 indicate that the two

<sup>3</sup>Due to the small number statistics, to get a better estimate of the *P*-value of the KS and AD tests, we employ MC simulation with  $10^5$  iteration, as explained in detail in [52]. The threshold for the tests has traditionally been set at a 5 per cent significance level.

Table 4.4: Comparison of the LC decline rate distributions of *arm* and *interarm* SNe Ia.

SN	$N_{\text{armSN}}$	$\langle \Delta m_{15} \rangle$	versus	$N_{\text{interarmSN}}$	$\langle \Delta m_{15} \rangle$	$P_{\text{KS}}^{\text{MC}}$	$P_{\text{AD}}^{\text{MC}}$
All	43	$1.09 \pm 0.03$	versus	34	$1.23 \pm 0.04$	<b>0.006</b>	<b>0.005</b>
Normal	37	$1.12 \pm 0.03$	versus	30	$1.21 \pm 0.04$	<b>0.037</b>	0.075

*Notes.* The  $\Delta m_{15}$  mean values and their standard errors for each sample are presented. MC simulation with  $10^5$  iteration is used to provide  $P_{\text{KS}}^{\text{MC}}$  and  $P_{\text{AD}}^{\text{MC}}$  probabilities for the KS and AD tests. Differences in the distributions that are statistically significant ( $P \leq 0.05$ ) are marked in bold.

$\Delta m_{15}$  distributions, being compared for all sampled SNe Ia, are significantly different. For each SN Ia subclass, we also try to perform the same comparison. However, this can only be done for normal SNe Ia, while the numbers are insufficient for 91T- and 91bg-like events (see Table 4.2). As for all SNe Ia, the tests' results show that the  $\Delta m_{15}$  distributions of normal SNe Ia in *arm* and *interarm* regions are inconsistent significantly (with only barely AD test significance): the  $\Delta m_{15}$  values of *arm* SNe Ia are, on average, smaller (slower declining LCs) in comparison with those of *interarm* SNe Ia (faster declining LCs).

The results presented above can be interpreted within the framework of DW theory [53, 162] and WD explosion models with a sub- $M_{\text{Ch}}$  [28, 29]. According to the DW theory, stars (or SN Ia progenitors) were born around shock fronts of spiral arms (birthplace  $\mathbf{e}$  in Fig. 4.2) and migrate in the same direction as the disc rotation relative to the spiral pattern (traveled distance  $\mathbf{eS}$ ). In comparison with arm SNe Ia, interarm SNe Ia should have, on average, longer lifetime of their progenitors to travel from the birthplace through the entire arm and explode in interarm regions. Therefore, it can be assumed that interarm SNe Ia originates from an older progenitors than those in arms. The arm/interarm separation thus provides an effective way to distinguish, on average, between younger and older SN Ia progenitors.

On the other hand, as mentioned in the Introduction, in sub- $M_{\text{Ch}}$  explosion models [26, 27] the  $\Delta m_{15}$  of SN Ia is correlated with the age of the progenitor system (larger  $\Delta m_{15}$  values - older progenitors; [28, 29]). The described link, together with what is indicated in the paragraph above, allows us to assume that interarm SNe Ia come, on average, from older stellar population with faster declining LCs in contrast to arm SNe Ia.

Table 4.5: Results of Spearman’s rank correlation tests for different continuous parameters of SNe Ia.

SN	$N_{\text{SN}}$	Par. 1 versus Par. 2	$r_s$	$P_s^{\text{MC}}$
All	77	$\Delta m_{15}$ versus $\tilde{r}_{\text{SN}}$	0.032	0.783
Normal	67	$\Delta m_{15}$ versus $\tilde{r}_{\text{SN}}$	-0.021	0.867
All	77	$\tilde{d}$ versus $\tilde{r}_{\text{SN}}$	0.330	<b>0.003</b>
Normal	67	$\tilde{d}$ versus $\tilde{r}_{\text{SN}}$	0.370	<b>0.002</b>
All	77	$\Delta m_{15}$ versus $\tilde{D}$	0.288	<b>0.011</b>
Normal	67	$\Delta m_{15}$ versus $\tilde{D}$	0.280	<b>0.022</b>
All	77	$\Delta m_{15}$ versus $ \tilde{d} $	0.183	0.111
Normal	67	$\Delta m_{15}$ versus $ \tilde{d} $	0.077	0.360

*Notes.* Spearman’s coefficient ( $-1 \leq r_s \leq 1$ ) is a measure of rank correlation. The test’s null hypothesis is that the variables are independent, whereas the alternate hypothesis is that they are not. The permutations with  $10^5$  MC iterations are used to generate the  $P_s^{\text{MC}}$  values. Statistically significant correlations are marked in bold ( $P \leq 0.05$ ).

### 4.3.2 The distribution of SNe Ia relative to spiral arms

To supplement and develop the results obtained in the previous section, it is preferable to analyse continuous parameter distributions, such as the galactocentric radii of SNe and their distances from the host spiral arm, and relate them with SN LC decline rates rather than utilizing the *arm* and *interarm* discrete binning of SNe Ia.

In this context, a negative radial gradient of stellar population age seen in spiral discs [151] prompts us to check the dependency between the  $\Delta m_{15}$  and  $\tilde{r}_{\text{SN}}$  of SNe Ia. This dependency has been studied extensively in the past, but no significant correlation has been found [36, 43, 155, 209]. For different subsamples of our study, the Spearman’s rank test in Table 4.5 also shows not significant trends between the mentioned parameters. In our recent study [209], we explained this negative result by the observed fact that in stacked spiral discs the azimuthally averaged stellar population age radially varies only from around 10 down to 8.5 Gyr from the center to the periphery [151]. While a significant correlation is observed between the LC decline rate and the global ages of hosts (the ages range approximately from 1 to 10 Gyr, [39, 52, 157, 158]). The relatively narrower radial age range is most likely the reason why the  $\Delta m_{15}$  versus  $\tilde{r}_{\text{SN}}$  correlation cannot be well-observed.

However, we can uncover an important relationship between host stellar population and

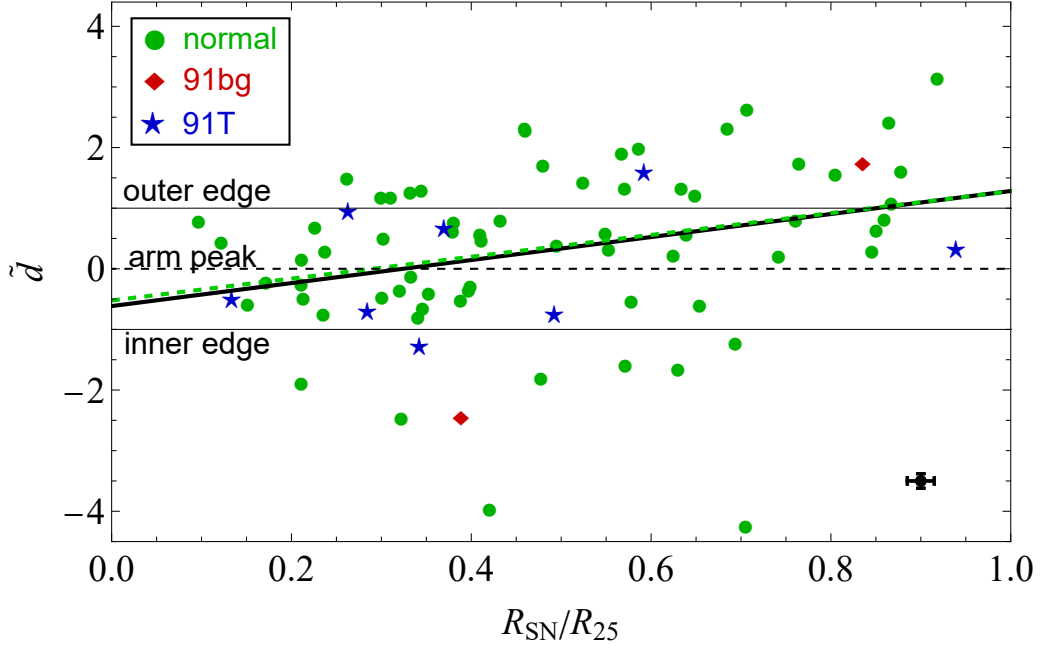


Figure 4.4: Distribution of the distances of SNe Ia relative to the peaks of spiral arms versus the deprojected and normalized galactocentric distance. The inner and outer edges (solid lines), as well the peak of spiral arm (dashed line) are shown by parallel lines. The best fits for all and normal SN subclass are presented by the solid- and dashed-thick lines, respectively. The error bars in the bottom-right corner display the typical measurement errors.

properties of SNe Ia progenitors by looking at the distribution of SNe Ia relative to spiral arms of galaxies [60, 61, 66]. The relation between the normalized distances  $\tilde{d}$  of SNe Ia from the arm peak and their deprojected and normalized galactocentric distances  $\tilde{r}_{\text{SN}}$  are shown in Fig 4.4. There is a positive trend between the parameters, as shown by the fit line to the data. The Spearman’s rank correlation test in Table 4.5 indicates that this trend is statistically significant for all and normal SNe Ia samples. In [61], the corresponding trend was not significant, probably because of approximately 3.5 times smaller sample of SNe Ia and their different selection criteria for hosts and SN Ia subclasses.

In Fig 4.4, the fit line to the distances of SNe Ia relative to the arm peak intersects with the arm roughly at a value of 0.35 in units of isophotal radii. Since direct measurements of the corotation radii of host galaxies are not available for the current sample, we examine the averaged value of  $R_C$  for seven host galaxies of SNe Ia from our previous paper [208]. These galaxies’ averaged morphological type, Sbc, agrees well with that of the host galaxy sample

used in the current study (Table 4.1). Moreover, the mean  $R_C \approx 0.38 \pm 0.05$  for the mentioned sample from [208] is in good agreement with the intersection point in Fig 4.4. Therefore, this intersection point 0.35 can be adopted as an average corotation radius for our hosts in units of isophotal radii.

The findings in Fig 4.4 can be interpreted in the context of the DW theory where the steady waves in GD galaxies have a strong influence on triggering SF processes close to the shock fronts of spiral arms ([53, 162], see also Fig. 4.2). This is supported by the mentioned quantitative agreement for the average corotation radius of hosts and the observational fact that the SNe Ia explosion sites are mainly distributed around the inner and outer edges of the arms (shock fronts) inside and outside the corotation radius, respectively. Such locations of SNe Ia may be due to a combination of the circular velocity of progenitors in the disc relative to the pattern speed of the spiral arms [61] and the ages of SN Ia progenitors [145]. Long lived progenitors could travel farther by their circular orbits from the birthplaces around the shock fronts to the explosion sites. Inside the corotation radius this circular direction is from the inner to outer edges, while outside the corotation the direction is from the outer to inner edges of arms (e.g. **es** arcs in Fig 4.2). Given that spiral galaxies are outnumbered by short-lived (prompt, i.e. 200-500 Myr) SN Ia progenitors [137, 145], we observe their distribution close to their birthplaces around the shock fronts.

From the above described DW scenario, we can assume that the traveled circular distance of SN progenitor is an indicator of their age. On the other hand, from the **esc** (**esa**) curvilinear triangle outside (inside) the corotation in Fig 4.2, it can be understood that the **sc** (**sa**) distance is proportional to the **es** distance. Here, the **sc** (or **sa**) is the distance of SN Ia from the shock front of spiral arm through the galactocentric direction, which we measured in Section 4.2 and normalized to the arm width (i.e.  $\tilde{D}$ ), while the **es** is the traveled circular distance of SN progenitor.

Considering that SNe Ia LC decline rate can also be an age indicator for the progenitors in sub- $M_{Ch}$  explosion models, in Table 4.5 and Fig 4.5 we study the correlations between  $\Delta m_{15}$  values and  $\tilde{D}$  distances from the shock fronts of host spiral arms. The corresponding  $P_s$  values

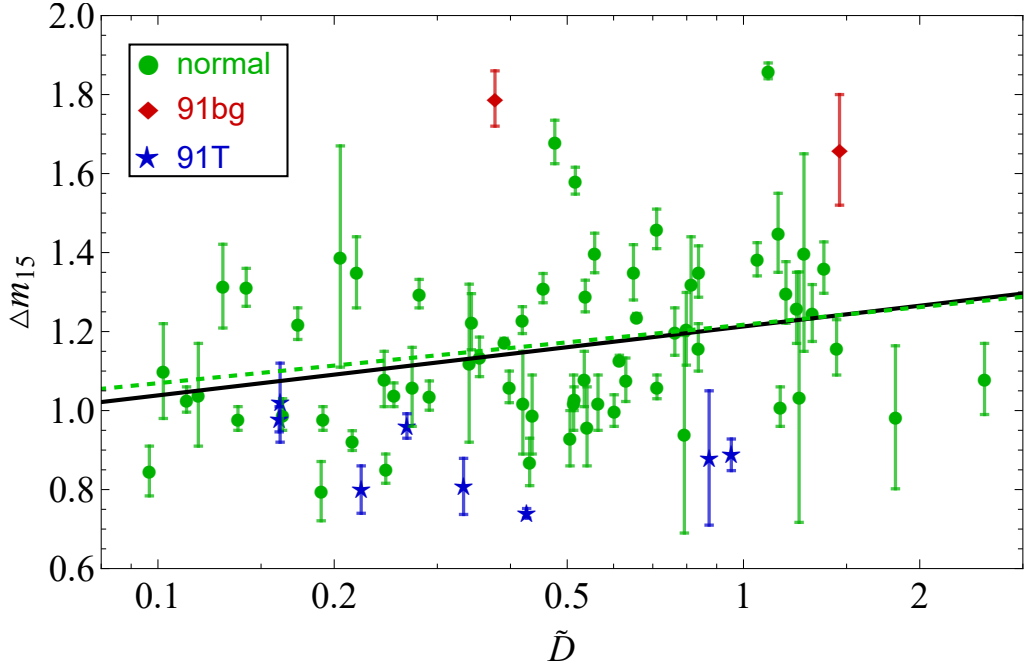


Figure 4.5: Distributions of  $\Delta m_{15}$  values of SNe Ia versus  $\tilde{D}$  distances from the shock fronts of host spiral arms. The best fits for all and normal SN subclass are presented by the solid- and dashed-thick lines, respectively.

in Table 4.5 show that there are significant correlations between these parameters. The result enables us to draw the conclusion that, on average, the progenitors of SNe Ia with smaller  $\Delta m_{15}$  values have shorter lifetimes and thus traveled shorter distances from the shock fronts, i.e. birthplace, in contrast to progenitors with larger  $\Delta m_{15}$  values, which have longer lifetimes and thus traveled farther away from the shock fronts.

The correlation tests in Table 4.5 show the positive trend between the  $\Delta m_{15}$  of SNe Ia and their measured distances from the arm peak, which might be assumed from the result of the  $\Delta m_{15}$  differences between SN Ia in arm/interarm regions. However, the  $P_s$  values of the test show that this trend is not statistically significant. This insignificance likely caused by the blurs in  $|\tilde{d}|$  as a lifetime indicator in the distribution of  $\Delta m_{15}$  versus  $|\tilde{d}|$ , because the SN distance from the arm peak does not represent the progenitors' traveled distance during entire lifetime (till to SN explosion): the spiral arm peak cannot be considered as a main birthplace of progenitors of SNe Ia.

It is worth noting that when conducting all statistical tests of our study without two SNe Ia

with ambiguous association with the nearest spiral arm (see Section 4.2), all the results of the study and their significance remain unchanged.

## 4.4 Chapter Conclusions

In this Chapter, using a sample of Sab–Scd galaxies hosting 77 SNe Ia and our measurements of the SN distances from the nearby spiral arms, we perform an analysis of the SNe distribution relative to host arms and study their LC decline rates ( $\Delta m_{15}$ ).

We demonstrate that the  $\Delta m_{15}$  values of *arm* SNe Ia are typically smaller (slower declining) than those of *interarm* SNe Ia (faster declining).

We show that the SN distances from the spiral arms and their galactocentric radii are correlated: before and after the average corotation radius, SNe Ia are located near the inner and outer edges (shock fronts) of spiral arms.

For the first time, we find a correlation between  $\Delta m_{15}$  values and the SN distances from the shock fronts of the arms.

The results can be interpreted within the frameworks of DW theory, where SN progenitors were born around shock fronts of spiral arms and migrate crossing the spiral pattern to the explosion sites, and WD explosion models with sub- $M_{\text{Ch}}$ , where SN LC decline rate is an indicator of progenitor age. On average, the progenitors of SNe Ia with smaller  $\Delta m_{15}$  values have shorter lifetimes and thus traveled shorter distances from the shock fronts, i.e. birthplace, in contrast to progenitors with larger  $\Delta m_{15}$  values, which have longer lifetimes and thus traveled farther away from the shock fronts.

# General Conclusions

This PhD thesis is concerned with the study of SNe and their host galaxy dynamical features. The most significant conclusions are follows:

1. In Sa–Sm galaxies, all CC and the vast majority of Type Ia SNe belong to the disc, rather than the bulge component. The result suggests that the rate of SNe Ia in spiral galaxies is dominated by a relatively young/intermediate progenitor population. This observational fact makes the deprojection of galactocentric radii of both types of SNe a key point in the statistical studies of their distributions.
2. The radial distribution of Type Ia SNe in S0–S0/a galaxies is inconsistent with that in Sa–Sm hosts. This inconsistency is mostly attributed to the contribution by SNe Ia in the outer bulges of S0–S0/a galaxies. In these hosts, the relative fraction of bulge to disc SNe Ia is probably changed in comparison with that in Sa–Sm hosts, because the progenitor population from the discs of S0–S0/a galaxies should be much lower due to the lower number of young/intermediate stellar populations.
3. The radial distribution of CC SNe in barred Sa–Sbc galaxies is not consistent with that of unbarred Sa–Sbc hosts, while for Type Ia SNe the distributions are not significantly different. At the same time, the radial distributions of both Type Ia and CC SNe in Sc–Sm galaxies are not affected by bars. These results are explained by a substantial suppression of massive SF in the radial range swept by strong bars of early-type barred galaxies.
4. The radial distribution of CC SNe in unbarred Sa–Sbc galaxies is more centrally peaked

and inconsistent with that in unbarred Sc–Sm hosts. On the other hand, the radial distribution of Type Ia SNe in unbarred galaxies is not affected by host morphology. These results can be well explained by the distinct distributions of massive stars in the discs of early- and late-type spirals. In unbarred Sa–Sbc galaxies, SF is more concentrated to the inner regions ( $H\alpha$  emission outside the nucleus) and should thus be responsible for the observed radial distribution of CC SNe.

5. The radial distribution of CC SNe, in contrast to Type Ia SNe, is inconsistent with the exponential surface density profile, because of the central ( $\tilde{r} \lesssim 0.2$ ) deficit of SNe. However, in the  $\tilde{r} \in [0.2; \infty)$  range, the inconsistency vanishes for CC SNe in most of the subsamples of spiral galaxies. In the inner-truncated disc, only the radial distribution of CC SNe in barred early-type spirals is inconsistent with an exponential surface density profile, which appears to be caused by the impact of bars on the radial distribution of CC SNe.
6. In the inner regions of non-disturbed spiral hosts, we do not detect a relative deficiency of Type Ia SNe with respect to CC, contrary to what was found by other authors, who had explained this by possibly stronger dust extinction for Type Ia than for CC SNe. Instead, the radial distributions of both types of SNe are similar in all the subsamples of Sa–Sbc and Sc–Sm galaxies, which supports the idea that the relative increase of CC SNe in the inner regions of spirals found by the other authors is most probably due to the central excess of CC SNe in disturbed galaxies.
7. As was found in earlier studies, the physical explanation for the more concentrated distribution of SNe Ibc with respect to SNe II in non-disturbed and unbarred spiral galaxies is that SNe Ibc arise from more metal-rich environments. The radial distributions of Types Ib and Ic SNe are sufficiently similar that the KS and AD tests fail to distinguish them with statistical significance.
8. As in earlier studies, we confirm that in the stacked spiral disc, the  $\Delta m_{15}$  of SNe Ia do not correlate with their galactocentric radii, and such disc is outnumbered by slower

declining/prompt events.

9. For the first time, we demonstrate that from the perspective of the dynamical timescale of the SFD, its old stellar population ( $\gtrsim 2$  Gyr) hosts mostly faster declining SNe Ia ( $\Delta m_{15} > 1.25$ ). By linking the LC decline rate and progenitor age, we show that the SFD phenomenon gives an excellent possibility to constrain the nature of SNe Ia.
10. We find no statistical differences between the pairs of the  $R_{25}$ -normalized radial distributions of Type Ia and CC SNe in discs of host galaxies with different spiral ACs, with only one significant exception: CC SNe in LGD and NGD galaxies have significantly different radius distributions. The radial distribution of CC SNe in NGDs is concentrated to the centre of galaxies with relatively narrow peak and fast exponential decline at the outer region, while the distribution of CC SNe in LGD galaxies has a broader peak, shifted to the outer region of the discs.
11. The surface density distributions of Type Ia and CC SNe in most of the subsamples are consistent with the exponential profiles. Only the distribution of CC SNe in LGD galaxies appears to be inconsistent with an exponential profile for the AD statistic but only very marginally so for the KS statistic), being marginally higher at  $0.4 \lesssim R_{\text{SN}}/R_{25} \lesssim 0.7$ . The inconsistency becomes more evident when comparing the same distribution with the scaled exponential profile of CC SNe in NGD galaxies.
12. Using a smaller sample of LGD galaxies with estimated corotation radii, we show, for the first time, that the surface density distribution of CC SNe shows a dip at corotation, and enhancements at  ${}_{-0.2}^{+0.5}$  corotation radii around it. However, these features are not statistically significant. The CC SNe enhancements around corotation may, if confirmed with larger samples, indicate that massive SF is triggered by the DWs in LGD host galaxies. Considering that the different LGD host galaxies have various corotation radii distributed around the mean value of  $\langle R_C/R_{25} \rangle = 0.42 \pm 0.18$ , the radii of triggered SF by DWs are most probably blurred within a radial region including  $\sim 0.4$  to  $\sim 0.7$  range in units of  $R_{25}$ , without a prominent drop in the mean corotation region.

13. In Sab–Scd galaxies, the  $\Delta m_{15}$  values of *arm* SNe Ia are typically smaller (slower declining) than those of *interarm* SNe Ia (faster declining).
14. The SN distances from the spiral arms and their galactocentric radii are correlated: before and after the average corotation radius, SNe Ia are located near the inner and outer edges (shock fronts) of spiral arms.
15. For the first time, we find a correlation between  $\Delta m_{15}$  values and the SN distances from the shock fronts of the arms. The results can be interpreted within the frameworks of DW theory, where SN progenitors were born around shock fronts of spiral arms and migrate crossing the spiral pattern to the explosion sites, and WD explosion models with sub- $M_{\text{Ch}}$ , where SN LC decline rate is an indicator of progenitor age. On average, the progenitors of SNe Ia with smaller  $\Delta m_{15}$  values have shorter lifetimes and thus traveled shorter distances from the shock fronts, i.e. birthplace, in contrast to progenitors with larger  $\Delta m_{15}$  values, which have longer lifetimes and thus traveled farther away from the shock fronts.

# Acknowledgement

I am profoundly grateful to Dr. Artur Hakobyan for his supervision, unwavering support, assistance, and patient mentorship. His guidance and encouragement were instrumental in the successful culmination of this research, and his substantial role significantly contributed to my professional development. My sincere thanks to all my coauthors, especially to Drs. Daniel Kunth, Gary Mamon, Massimo Turatto, and Vardan Adibekyan with whom I collaborated while working on some of my papers. Scientific visits I made at the Institut d'Astrophysique de Paris played a pivotal role in shaping both my research and professional path. I convey my appreciation to all my colleagues from the Center for Cosmology and Astrophysics at the Alikhanyan National Science Laboratory. Lastly, I extend my heartfelt gratitude to my family members and my close friends who have provided direct and indirect support throughout this challenging journey.

The work was supported by the Science Committee of RA, in the frames of the research project № 21T-1C236.

# Bibliography

- [1] Baade, W., *The Absolute Photographic Magnitude of Supernovae*, The Astrophysical Journal, 1938, **88**, 285-304.
- [2] Riess, A. G. and et al., *Observational Evidence from Supernovae for an Accelerating Universe and a Cosmological Constant*, The Astronomical Journal, 1998, **116**, 1009-1038.
- [3] Perlmutter, S. and et al., *Measurements of  $\Omega$  and  $\Lambda$  from 42 High-Redshift Supernovae*, The Astrophysical Journal, 1999, **517**, 565-586.
- [4] Minkowski, R., *Spectra of Supernovae*, Publications of the Astronomical Society of the Pacific, 1941, **53**, 224-225.
- [5] Filippenko, A. V., *Optical Spectra of Supernovae*, Annual Review of Astronomy and Astrophysics, 1997, **35**, 309-355.
- [6] Turatto, M., *Classification of Supernovae*, Supernovae and Gamma-Ray Bursters. Edited by K. Weiler., Lecture Notes in Physics, 2003, **598**, 21-36.
- [7] Anderson, J. P. and et al., *Progenitor mass constraints for core-collapse supernovae from correlations with host galaxy star formation*, Monthly Notices of the Royal Astronomical Society, 2012, **424**, 1372-1391.
- [8] Smartt, S. J., *Progenitors of Core-Collapse Supernovae*, Annual Review of Astronomy and Astrophysics, 2009, **47**, 63-106.
- [9] Lisakov, S., *Core-collapse supernovae and their progenitors*, Ph.D. thesis, Université Côte d'Azur, 2018.
- [10] Smith, N. and et al., *Observed fractions of core-collapse supernova types and initial masses of their single and binary progenitor stars*, Monthly Notices of the Royal Astronomical Society, 2011, **412**, 1522-1538.
- [11] Heger, A. and et al., *How Massive Single Stars End Their Life*, The Astrophysical Journal, 2003, **591**, 288-300.

- [12] Taubenberger, S., *The Extremes of Thermonuclear Supernovae*, Handbook of Supernovae, Springer International Publishing AG, 2017, 317-373.
- [13] Phillips, M. M. and et al., *The Reddening-Free Decline Rate Versus Luminosity Relationship for Type Ia Supernovae*, The Astronomical Journal, 1999, **118**, 1766-1776.
- [14] Kangas, T., *Observational studies of core-collapse supernova progenitors and their environments*, Ph.D. thesis, University of Turku, 2017.
- [15] Modjaz, M. and et al., *Optical Spectra of 73 Stripped-envelope Core-collapse Supernovae*, The Astronomical Journal, 2014, **147**, id.99/17.
- [16] Phillips, M. M., *The Absolute Magnitudes of Type Ia Supernovae*, The Astrophysical Journal, 1993, **413**, L105-L108.
- [17] Livio, M. and Mazzali, P., *On the progenitors of Type Ia supernovae*, Physics Reports, 2018, **736**, 1-23.
- [18] Ruiter, A. J., *Type Ia supernova sub-classes and progenitor origin*, IAU Symposium, 2020, **357**, 1-15.
- [19] Whelan, J. and Iben, I., *Binaries and Supernovae of Type I*, The Astrophysical Journal, 1973, **186**, 1007-1014.
- [20] Cappellaro, E. and et al., *SN Ia light curves and radioactive decay*, Astronomy and Astrophysics, 1997, **328**, 203-210.
- [21] Parrent, J., Friesen, B. and Parthasarathy, M., *A review of type Ia supernova spectra*, Astrophysics and Space Science, 2014, **351**, 1-52.
- [22] Liu, Z.-W., Röpke, F. K. and Han, Z., *Type Ia Supernova Explosions in Binary Systems: A Review*, Research in Astronomy and Astrophysics, 2023, **23**, id.082001/43.
- [23] Iben, I. and Tutukov, A. V., *Supernovae of type I as end products of the evolution of binaries with components of moderate initial mass*, The Astrophysical Journal Supplement Series, 1984, **54**, 335-372.
- [24] Iben, I. and Tutukov, A. V. *On the evolution of close binaries with components of initial mass between 3 Msun and 12 Msun*, The Astrophysical Journal Supplement Series, 1985, **58**, 661-710.
- [25] Maoz, D., Mannucci, F. and Nelemans, G., *Observational Clues to the Progenitors of Type Ia Supernovae*, Annual Review of Astronomy and Astrophysics, 2014, **52**, 107-170.
- [26] Sim, S. A. and et al., *Detonations in Sub-Chandrasekhar-mass C+O White Dwarfs*, The Astrophysical Journal, 2010, **714**, L52-L57.

- [27] Blondin, S. and et al., *Evidence for sub-Chandrasekhar-mass progenitors of Type Ia supernovae at the faint end of the width-luminosity relation*, Monthly Notices of the Royal Astronomical Society, 2017, **470**, 157-165.
- [28] Shen, K. J., Toonen, S. and Graur, O., *The Evolution of the Type Ia Supernova Luminosity Function*, The Astrophysical Journal, 2017, **851**, L50/5.
- [29] Shen, K. J. and et al., *Non-local Thermodynamic Equilibrium Radiative Transfer Simulations of Sub-Chandrasekhar-mass White Dwarf Detonations*, The Astrophysical Journal, 2021, **909**, L18/11.
- [30] van den Bergh, S. and Tammann, G. A., *Galactic and extragalactic supernova rates*, Annual Review of Astronomy and Astrophysics, 1991, **29**, 363-407.
- [31] Cappellaro, E., Evans, R. and Turatto, M., *A new determination of supernova rates and a comparison with indicators for galactic star formation*, Astronomy and Astrophysics, 1999, **351**, 459-466.
- [32] Förster, F. and Schawinski, K., *The radial distribution of Type Ia supernovae in early-type galaxies: implications for progenitor scenarios*, Monthly Notices of the Royal Astronomical Society, 2008, **388**, L74-L78.
- [33] Johnson, H. M. and MacLeod, J. M., *The Spatial Distribution of Supernovae in Galaxies*, Publications of the Astronomical Society of the Pacific, 1963, **75**, 123-132.
- [34] Bartunov, O. S., Tsvetkov, D. Y., Filimonova, I. V., *Distribution of Supernovae Relative to Spiral Arms and H II Regions*, Publications of the Astronomical Society of the Pacific, 1994, **106**, 1276-1284.
- [35] van Dyk, S. D., Hamuy, M. and Filippenko, A. V., *Supernovae and Massive Star Formation Regions*, The Astronomical Journal, 1996, **111**, 2017-2027.
- [36] Gallagher, J. S. and et al., *Chemistry and Star Formation in the Host Galaxies of Type Ia Supernovae*, The Astrophysical Journal, 2005, **634**, 210-226.
- [37] Hakobyan, A. A. and et al., *Study of the HII regions in the spiral galaxy NGC6384*, Astrophysics, 2007, **50**, 426-439.
- [38] Hakobyan, A. A., *The statistical investigation of supernovae and their host galaxies*, Ph.D. thesis, Byurakan Astrophysical Observatory, 2009.
- [39] Gupta, R. R. and et al., *Improved Constraints on Type Ia Supernova Host Galaxy Properties Using Multi-wavelength Photometry and Their Correlations with Supernova Properties*, The Astrophysical Journal, 2011, **740**, id.92/12.

- [40] Rigault, M. and et al., *Evidence of environmental dependencies of Type Ia supernovae from the Nearby Supernova Factory indicated by local  $H\alpha$* , Astronomy and Astrophysics, 2013, **560**, A66/17.
- [41] Aramyan, L. S. and et al., *On the Nature of Unconfirmed Supernovae*, Astrophysics, 2013, **56**, 153-164.
- [42] Anderson, J. P. and et al., *Statistical Studies of Supernova Environments*, Publications of the Astronomical Society of Australia, 2015, **32**, id.e019/30.
- [43] Uddin, S. A. and et al., *The Influence of Host Galaxies in Type Ia Supernova Cosmology*, The Astrophysical Journal, 2017, **848**, id.56/14.
- [44] Kang, Y. and et al., *Early-type Host Galaxies of Type Ia Supernovae. II. Evidence for Luminosity Evolution in Supernova Cosmology*, The Astrophysical Journal, 2020, **889**, id.8/23.
- [45] Barkhudaryan, L. V., *Constraining Type Ia supernovae through their heights in edge-on galaxies*, Monthly Notices of the Royal Astronomical Society, 2023, **520**, L21-L27.
- [46] James, P. A., Bretherton, C. F. and Knapen, J. H., *The  $H\alpha$  galaxy survey. VII. The spatial distribution of star formation within disks and bulges*, Astronomy and Astrophysics, 2009, **501**, 207-220.
- [47] James, P. A. and Percival, S. M., *Discovery of kpc-scale line emission in barred galaxies, not linked to AGN or star formation*, Monthly Notices of the Royal Astronomical Society, 2015, **450**, 3503-3513.
- [48] James, P. A. and Percival, S. M., *Star formation suppression and bar ages in nearby barred galaxies*, Monthly Notices of the Royal Astronomical Society, 2018, **474**, 3101-3109.
- [49] Donohoe-Keyes, C. E. and et al., *Redistribution of stars and gas in the star formation deserts of barred galaxies*, Monthly Notices of the Royal Astronomical Society, 2019, **489**, 4992-5003.
- [50] George, K. and et al., *More insights into bar quenching. Multi-wavelength analysis of four barred galaxies*, Astronomy and Astrophysics, 2020, **644**, A79/9.
- [51] Minchev, I. and et al., *Estimating stellar birth radii and the time evolution of Milky Way's ISM metallicity gradient*, Monthly Notices of the Royal Astronomical Society, 2018, **481**, 1645-1657.
- [52] Hakobyan, A. A. and et al., *Supernovae and their host galaxies - VII. The diversity of Type Ia supernova progenitors*, Monthly Notices of the Royal Astronomical Society, 2020, **499**, 1424-1440.

- [53] Lin, C. C. and Shu, F. H., *On the Spiral Structure of Disk Galaxies*, The Astrophysical Journal, 1964, **140**, 646-655.
- [54] Cepa, J. and Beckman, J. E., *Star Formation Triggering by Density Waves in the Grand Design Spirals NGC 3992 and NGC 628*, The Astrophysical Journal, 1990, **349**, 497-502.
- [55] Knapen, J. H., *Molecular gas observations and enhanced massive star formation efficiencies in M 100*, Astronomy and Astrophysics, 1996, **308**, 27-39.
- [56] Seigar, M. S. and James, P. A., *A test of arm-induced star formation in spiral galaxies from near-infrared and H $\alpha$  imaging*, Monthly Notices of the Royal Astronomical Society, 2002, **337**, 1113-1117.
- [57] Grosbøl, P. and Dottori, H., *Pattern speed of main spiral arms in NGC 2997. Estimate based on very young stellar complexes*, Astronomy and Astrophysics, 2009, **499**, L21-L24.
- [58] Martínez-García, E. E., González-Lópezlira, R. A. and Bruzual-A, G., *Spiral Density Wave Triggering of Star Formation in Sa and Sab Galaxies*, The Astrophysical Journal, 2009, **694**, 512-545.
- [59] Moore, E., *Predetonation Lifetime and Mass of Supernovae from Density-Wave Theory of Galaxies*, Publications of the Astronomical Society of the Pacific, 1973, **85**, 564-567.
- [60] Mikhailova, G. A., Bartunov, O. S. and Tsvetkov, D. Y., *Distribution of type Ib/c supernovae relative to galactic spiral arms*, Astronomy Letters, 2007, **33**, 715-719.
- [61] Aramyan, L. S. and et al., *Supernovae and their host galaxies - IV. The distribution of supernovae relative to spiral arms*, Monthly Notices of the Royal Astronomical Society, 2016, **459**, 3130-3143.
- [62] de Lapparent, V., Baillard, A. and Bertin, E., *The FIGI catalogue of 4458 nearby galaxies with morphology. II. Statistical properties along the Hubble sequence*, Astronomy and Astrophysics, 2011, **532**, A75/19.
- [63] Kormendy, J. and Kennicutt, R. C., *Secular Evolution and the Formation of Pseudobulges in Disk Galaxies*, Annual Review of Astronomy and Astrophysics, 2004, **42**, 603-683.
- [64] Gadotti, D. A., *Barred Galaxies: an Observer's Perspective*, Chaos in Astronomy, Astrophysics and Space Science Proceedings, Springer-Verlag Berlin Heidelberg, 2009, 159-172.
- [65] Hakobyan, A. A. and et al., *The radial distribution of core-collapse supernovae in spiral host galaxies*, Astronomy and Astrophysics, 2009, **508**, 1259-1268.
- [66] Petrosian, A. and et al., *Active and Star-forming Galaxies and Their Supernovae*, The Astronomical Journal, 2005, **129**, 1369-1380.

- [67] Hakobyan, A. A., *The statistical investigation of type Ib/c and II supernovae and their host galaxies*, *Astrophysics*, 2008, **51**, 69-76.
- [68] Nazaryan, T. A. and et al., *Paired galaxies with different activity levels and their supernovae*, *Astrophysics and Space Science*, 2013, **347**, 365-374.
- [69] Wang, L., Höflich, P. and Wheeler, J. C., *Supernovae and Their Host Galaxies*, *The Astrophysical Journal*, 1997, **483**, L29-L32.
- [70] Anderson, J. P. and et al., *On the environments of Type Ia supernovae within host galaxies*, *Monthly Notices of the Royal Astronomical Society*, 2015, **448**, 732-753.
- [71] Ahn, C. P. and et al., *The Tenth Data Release of the Sloan Digital Sky Survey: First Spectroscopic Data from the SDSS-III Apache Point Observatory Galactic Evolution Experiment*, *The Astrophysical Journal Supplement Series*, 2014, **211**, id.17/16.
- [72] Hakobyan, A. A. and et al., *Supernovae and their host galaxies. I. The SDSS DR8 database and statistics*, *Astronomy and Astrophysics*, 2012, **544**, 81-99.
- [73] Hakobyan, A. A. and et al., *Supernovae and their host galaxies - II. The relative frequencies of supernovae types in spirals*, *Monthly Notices of the Royal Astronomical Society*, 2014, **444**, 2428-2441.
- [74] Spergel, D. N. and et al., *Three-Year Wilkinson Microwave Anisotropy Probe (WMAP) Observations: Implications for Cosmology*, *The Astrophysical Journal Supplement Series*, 2007, **170**, 377-408.
- [75] Barbon, R. and et al., *The Asiago Supernova Catalogue - 10 years after*, *Astronomy and Astrophysics Supplement Series*, 1999, **139**, 531-536.
- [76] Habergham, S. M. and et al., *Environments of interacting transients: impostors and Type II<sub>n</sub> supernovae*, *Monthly Notices of the Royal Astronomical Society*, 2014, **441**, 2230-2252.
- [77] Baillard, A. and et al., *The EFIGI catalogue of 4458 nearby galaxies with detailed morphology*, *Astronomy and Astrophysics*, 2011, **532**, A74/27.
- [78] Hakobyan, A. A. and et al., *VizieR Online Data Catalog: Properties of 500 SNe and their 419 hosts (Hakobyan+, 2016)*, *VizieR Online Data Catalog*, 2016.
- [79] McCarthy, M. F., *Location of supernovae in parent galaxies*, *Ricerche Astronomiche*, 1973, **8**, 411-428.
- [80] Barbon, R., Capaccioli, M. and Ciatti, F., *Studies of supernovae*, *Astronomy and Astrophysics*, 1975, **44**, 267-271.

- [81] Iye, M. and Kodaira, K., *Distribution of supernovae in spiral galaxies of type Sb-Sd*, Publications of the Astronomical Society of Japan, 1975, **27**, 411-419.
- [82] Vettolani, G. and Zamorani, G., *Distribution of supernovae, supernova remnants and exponential disks*, Monthly Notices of the Royal Astronomical Society, 1977, **178**, 693-700.
- [83] Tsvetkov, D. Y., *The Space Distribution of Type-I and Type-II Supernovae in Spiral Galaxies*, Soviet Astronomy Letters, 1981, **7**, 254-256.
- [84] Tsvetkov, D. Y., *Frequency of Outbursts and Spatial Distribution of Type-I and Type-II Supernovae*, Soviet Astronomy, 1987, **31**, 39-44.
- [85] Kazarian, M. A., *Galaxies with a UV excess in which supernovae have been observed*, Astrophysics, 1997, **40**, 296-307.
- [86] Ivanov, V. D., Hamuy, M. and Pinto, P. A., *On the Relation between Peak Luminosity and Parent Population of Type Ia Supernovae: A New Tool for Probing the Ages of Distant Galaxies*, The Astrophysical Journal, 2000, **542**, 588-596.
- [87] Wang, X. and et al., *Evidence for Two Distinct Populations of Type Ia Supernovae*, Science, 2013, **340**, 170-173.
- [88] Onic, D., Arbutina, B. and Urosevic, D., *Radial Dependence of Extinction in Parent Galaxies of Supernovae*, Revista Mexicana de Astronomía y Astrofísica, 2008, **44**, 103-110.
- [89] Hatano, K., Branch, D. and Deaton, J., *Extinction and Radial Distribution of Supernova Properties in Their Parent Galaxies*, The Astrophysical Journal, 1998, **502**, 177-181.
- [90] Massey, F. J., *The Kolmogorov-Smirnov Test for Goodness of Fit*, Journal of the American Statistical Association, 1951, **46**, 68-78.
- [91] Pettitt, A. N., *A two-sample Anderson-Darling rank Statistic*, Biometrika, 1976, **63**, 161-168.
- [92] Hakobyan, A. A. and et al., *Early-type galaxies with core collapse supernovae*, Astronomy and Astrophysics, 2008, **488**, 523-531.
- [93] Engmann, S. and Cousineau, D., *Comparing distributions: The Two-Sample Anderson-Darling Test as an Alternative to the Kolmogorov-Smirnoff Test*, Journal of Applied Quantitative Methods, 2011, **6**, 1-17.
- [94] Mannucci, F. and et al., *The supernova rate per unit mass*, Astronomy and Astrophysics, 2005, **433**, 807-814.

- [95] Hakobyan, A. A. and et al., *Five supernova survey galaxies in the southern hemisphere. I. Optical and near-infrared database*, *Astrophysics*, 2009, **52**, 40-53.
- [96] Hakobyan, A. A. and et al., *Five supernova survey galaxies in the southern hemisphere. II. The supernova rates*, *Astrophysics*, 2011, **54**, 301-314.
- [97] Li, W. and et al., *Nearby supernova rates from the Lick Observatory Supernova Search - III. The rate-size relation, and the rates as a function of galaxy Hubble type and colour*, *Monthly Notices of the Royal Astronomical Society*, 2011, **412**, 1473-1507.
- [98] Hamuy, M. and Pinto, P. A., *Selection Effects, Biases, and Constraints in the CalÁn/Tololo Supernova Survey*, *The Astronomical Journal*, 1999, **117**, 1185-1205.
- [99] Navasardyan, H. and et al., *Supernovae in isolated galaxies, in pairs and in groups of galaxies*, *Monthly Notices of the Royal Astronomical Society*, 2001, **328**, 1181-1192.
- [100] Bartunov, O. S. and Tsvetkov, D. I., *A Comparative Study of Type-I and Type-II Supernovae*, *Astrophysics and Space Science*, 1986, **122**, 343-354.
- [101] Turatto, M., Cappellaro, E. and Petrosian, A. R., *Supernovae in Markarian galaxies*, *Astronomy and Astrophysics*, 1989, **217**, 79-86.
- [102] Petrosian, A. R. and Turatto, M., *Supernovae in the host galaxies of AGNs*, *Astronomy and Astrophysics*, 1990, **239**, 63-68.
- [103] Petrosian, A. R. and Turatto, M., *The spatial distribution of supernovae in paired and interacting galaxies*, *Astronomy and Astrophysics*, 1995, **297**, 49-55.
- [104] Li, W. and Li, Z., *Studies of multiple supernovae in spiral galaxies*, *Astronomy and Astrophysics*, 1995, **301**, 666-674.
- [105] Bressan, A., Della Valle, M. and Marziani, P., *On core-collapse supernovae in normal and in Seyfert galaxies*, *Monthly Notices of the Royal Astronomical Society*, 2002, **331**, L25-L29.
- [106] Wang, J., Deng, J. S. and Wei, J. Y., *Ongoing star formation in AGN host galaxy discs: a view from core-collapse supernovae*, *Monthly Notices of the Royal Astronomical Society*, 2010, **405**, 2529-2533.
- [107] Anderson, J. P. and James, P. A., *Comparisons of the radial distributions of core-collapse supernovae with those of young and old stellar populations*, *Monthly Notices of the Royal Astronomical Society*, 2009, **399**, 559-573.
- [108] Cappellaro, E. and et al., *The rate of supernovae from the combined sample of five searches*, *Astronomy and Astrophysics*, 1997, **322**, 431-441.

- [109] Shaw, R. L., *Supernovae: a new selection effect*, Astronomy and Astrophysics, 1979, **76**, 188-191.
- [110] Howell, D. A., Wang, L. and Wheeler, J. C., *The Distribution of High- and Low-Redshift Type Ia Supernovae*, The Astrophysical Journal, 2000, **530**, 166-171.
- [111] Leaman, J., and et al., *Nearby supernova rates from the Lick Observatory Supernova Search - I. The methods and data base*, Monthly Notices of the Royal Astronomical Society, 2011, **412**, 1419-1440.
- [112] Holwerda, B. W. and et al., *SN Ia host galaxy properties and the dust extinction distribution*, Monthly Notices of the Royal Astronomical Society, 2015, **446**, 3768-3775.
- [113] Oohama, N. and et al., *Properties of Disks and Bulges of Spiral and Lenticular Galaxies in the Sloan Digital Sky Survey*, The Astrophysical Journal, 2009, **705**, 245-254.
- [114] Yoshizawa, M. and Wakamatsu, K., *On the Relative Importance of the Bulge to the Disk of Spiral and S0 Galaxies*, Astronomy and Astrophysics, 1975, **44**, 363-370.
- [115] Simien, F. and de Vaucouleurs, G., *Systematics of Bulge-to-Disk Ratios*, The Astrophysical Journal, 1986, **302**, 564-578.
- [116] James, P. A. and Anderson, J. P., *The H $\alpha$  Galaxy Survey. III. Constraints on supernova progenitors from spatial correlations with H $\alpha$  emission*, Astronomy and Astrophysics, 2006, **453**, 57-65.
- [117] Cameron, E., *On the Estimation of Confidence Intervals for Binomial Population Proportions in Astronomy: The Simplicity and Superiority of the Bayesian Approach*, Publications of the Astronomical Society of Australia, 2011, **28**, 128-139.
- [118] Barnard, G. A., *A New Test for  $2 \times 2$  Tables*, Nature, 1945, **156**, 177-177.
- [119] Stanishev, V. and et al., *Type Ia supernova host galaxies as seen with IFU spectroscopy*, Astronomy and Astrophysics, 2012, **545**, A58/33.
- [120] Galbany, L. and et al., *Nearby supernova host galaxies from the CALIFA Survey. I. Sample, data analysis, and correlation to star-forming regions*, Astronomy and Astrophysics, 2014, **572**, A38/24.
- [121] Bartunov, O. S., Makarova, I. N. and Tsvetkov, D. I., *The radial distribution of supernovae in galaxies*, Astronomy and Astrophysics, 1992, **264**, 428-432.
- [122] Tsvetkov, D. Y., Pavlyuk, N. N. and Bartunov, O. S., *The SAI Catalog of Supernovae and Radial Distributions of Supernovae of Various Types in Galaxies*, Astronomy Letters, 2004, **30**, 729-736.

- [123] van den Bergh, *Distribution of Supernovae in Spiral Galaxies*, The Astronomical Journal, 1997, **113**, 197-200.
- [124] Haberman, S. M., James, P. A. and Anderson, J. P., *A central excess of stripped-envelope supernovae within disturbed galaxies*, Monthly Notices of the Royal Astronomical Society, 2012, **424**, 2841-2853.
- [125] Bernardi, M. and et al., *Systematic effects on the size-luminosity relations of early- and late-type galaxies: dependence on model fitting and morphology*, Monthly Notices of the Royal Astronomical Society, 2014, **443**, 874-897.
- [126] D'Agostino, R. B. and Stephens, M. A., *Goodness-of-fit techniques*, Statistics: Textbooks and Monographs, New York: Dekker, 1986.
- [127] van den Bergh, S. and McClure, R. D., *Supernova Rates and Galaxy Inclinations*, 1990, The Astrophysical Journal, 1990, **359**, 277-279.
- [128] McMillan, R. J. and Ciardullo, R., *Constraining the Ages of Supernova Progenitors. I. Supernovae and Spiral Arms*, The Astrophysical Journal, 1996, **473**, 707-712.
- [129] Prieto, J. L., Stanek, K. Z. and Beacom, J. F., *Characterizing Supernova Progenitors via the Metallicities of their Host Galaxies, from Poor Dwarfs to Rich Spirals*, The Astrophysical Journal, 2008, **673**, 999-1008.
- [130] Boissier, S. and Prantzos, N., *Relative frequencies of supernovae types: dependence on host galaxy magnitude, galactocentric radius, and local metallicity*, Astronomy and Astrophysics, 2009, **503**, 137-150.
- [131] Kangas, T. and et al., *Spatial distributions of core-collapse supernovae in infrared-bright galaxies*, Monthly Notices of the Royal Astronomical Society, 2013, **436**, 3464-3479.
- [132] Herrero-Illana, R., Pérez-Torres, M. Á. and Alberdi, A., *Evidence of nuclear disks in starburst galaxies from their radial distribution of supernovae*, Astronomy and Astrophysics, 2012, **540**, L5/7.
- [133] Panther, F. H. and et al., *SN1991bg-like supernovae are associated with old stellar populations*, Publications of the Astronomical Society of Australia, 2019, **36**, id.e031/9.
- [134] Rose, B. M., Garnavich, P. M. and Berg, M. A., *Think Global, Act Local: The Influence of Environment Age and Host Mass on Type Ia Supernova Light Curves*, The Astrophysical Journal, 2019, **874**, id.32/18.
- [135] Díaz-García, S. and et al., *Distribution of star formation in galactic bars as seen with H $\alpha$  and stacked GALEX UV imaging*, Astronomy and Astrophysics, 2020, **644**, A38/23.

- [136] Shen, J. and Sellwood, J. A., *The Destruction of Bars by Central Mass Concentrations*, The Astrophysical Journal, 2004, **604**, 614-631.
- [137] Raskin, C. and et al., *Prompt Ia Supernovae are Significantly Delayed*, The Astrophysical Journal, 2009, **707**, 74-78.
- [138] Hakobyan, A. A. and et al., *Supernovae and their host galaxies - III. The impact of bars and bulges on the radial distribution of supernovae in disc galaxies*, Monthly Notices of the Royal Astronomical Society, 2016, **456**, 2848-2860.
- [139] Martin, D. C. and et al., *The Galaxy Evolution Explorer: A Space Ultraviolet Survey Mission*, The Astrophysical Journal, 2005, **619**, L1-L6.
- [140] Roming, P. W. A. and et al., *The Swift Ultra-Violet/Optical Telescope*, Space Science Reviews, 2005, **120**, 95-142.
- [141] Sánchez-Menguiano, L. and et al., *The shape of oxygen abundance profiles explored with MUSE: evidence for widespread deviations from single gradients*, Astronomy and Astrophysics, 2018, **609**, A119/47.
- [142] Díaz-García, S., Salo, H., Laurikainen, E. and Herrera-Endoqui, M., *Characterization of galactic bars from 3.6  $\mu\text{m}$   $S^4G$  imaging*, Astronomy and Astrophysics, 2016, **587**, A160/40.
- [143] Hakobyan, A. A. and et al., *VizieR Online Data Catalog: Properties of 185 SNe Ia and their 180 hosts (Hakobyan+, 2021)*, VizieR Online Data Catalog, 2021.
- [144] Kennicutt, R. C., *Star Formation in Galaxies Along the Hubble Sequence*, Annual Review of Astronomy and Astrophysics, 1998, **36**, 189-232.
- [145] Childress, M. J., Wolf, C., Zahid, H. J., *Ages of Type Ia supernovae over cosmic time*, Monthly Notices of the Royal Astronomical Society, 2014, **445**, 1898-1911.
- [146] Crocker, R. M. and et al., *Diffuse Galactic antimatter from faint thermonuclear supernovae in old stellar populations*, Nature Astronomy, 2017, **1**, id.0135/6.
- [147] Barkhudaryan, L. V. and et al., *Supernovae and their host galaxies - VI. Normal Type Ia and 91bg-like supernovae in ellipticals*, Monthly Notices of the Royal Astronomical Society, 2019, **490**, 718-732.
- [148] Han, Z. and Podsiadlowski, P., *The single-degenerate channel for the progenitors of Type Ia supernovae*, Monthly Notices of the Royal Astronomical Society, 2004, **350**, 1301-1309.
- [149] Fisher, R. and Jumper, K., *Single-degenerate Type Ia Supernovae Are Preferentially Overluminous*, The Astrophysical Journal, 2015, **805**, id.150/10.

- [150] Ruiter, A. J. and et al., *On the brightness distribution of Type Ia supernovae from violent white dwarf mergers*, Monthly Notices of the Royal Astronomical Society, 2013, **429**, 1425-1436.
- [151] González Delgado, R. M. and et al., *The CALIFA survey across the Hubble sequence. Spatially resolved stellar population properties in galaxies*, Astronomy and Astrophysics, 2015, **581**, A103/44.
- [152] Di Matteo, P. and et al., *Signatures of radial migration in barred galaxies: Azimuthal variations in the metallicity distribution of old stars*, Astronomy and Astrophysics, 2013, **553**, A102/8.
- [153] Timmes, F. X., Brown, E. F. and Truran, J. W., *On Variations in the Peak Luminosity of Type Ia Supernovae*, The Astrophysical Journal, 2003, **590**, L83-L86.
- [154] Kasen, D., Röpke, F. K. and Woosley, S. E., *The diversity of type Ia supernovae from broken symmetries*, Nature, 2009, **460**, 869-872.
- [155] Galbany, L. and et al., *Type Ia Supernova Properties as a Function of the Distance to the Host Galaxy in the SDSS-II SN Survey*, The Astrophysical Journal, 2012, **755**, id.125/14.
- [156] Pavlyuk, N. N. and Tsvetkov, D. Y., *Distributions of supernovae of different types along the radius and in z coordinate of galaxies*, Astronomy Letters, 2016, **42**, 495-505.
- [157] Pan, Y.-C. and et al., *The host galaxies of Type Ia supernovae discovered by the Palomar Transient Factory*, Monthly Notices of the Royal Astronomical Society, 2014, **438**, 1391-1416.
- [158] Campbell, H., Fraser, M. and Gilmore, G., *How SN Ia host-galaxy properties affect cosmological parameters*, Monthly Notices of the Royal Astronomical Society, 2016, **457**, 3470-3491.
- [159] della Valle, M. and Livio, M., *On the Progenitors of Type Ia Supernovae in Early-Type and Late-Type Galaxies*, The Astrophysical Journal, 1994, **423**, L31-L33.
- [160] Dobbs, C. and Baba, J., *Dawes Review 4: Spiral Structures in Disc Galaxies*, Publications of the Astronomical Society of Australia, 2014, **31**, id.e035/40.
- [161] Shu, F. H., *Six Decades of Spiral Density Wave Theory*, Annual Review of Astronomy and Astrophysics, 2016, **54**, 667-724.
- [162] Roberts, W. W., *Large-Scale Shock Formation in Spiral Galaxies and its Implications on Star Formation*, The Astrophysical Journal, 1969, **158**, 123-143.
- [163] Sellwood, J. A., *The lifetimes of spiral patterns in disc galaxies*, Monthly Notices of the Royal Astronomical Society, 2011, **410**, 1637-1646.

- [164] Foyle, K., Rix, H.-W. and Walter, F., *Arm and Interarm Star Formation in Spiral Galaxies*, The Astrophysical Journal, 2010, **725**, 534-541.
- [165] Grosbøl, P. and Dottori, H., *Star formation in grand-design, spiral galaxies. Young, massive clusters in the near-infrared*, Astronomy and Astrophysics, 2012, **542**, A39/22.
- [166] Cedrés, B., Cepa, J. and et al., *Density waves and star formation in grand-design spirals*, Astronomy and Astrophysics, 2013, **560**, A59/10.
- [167] Pour-Imani, H. and et al., *Strong Evidence for the Density-wave Theory of Spiral Structure in Disk Galaxies*, The Astrophysical Journal, 2016, **827**, L2/6.
- [168] Shabani, F. and et al., *Search for star cluster age gradients across spiral arms of three LEGUS disc galaxies*, Monthly Notices of the Royal Astronomical Society, 2018, **478**, 3590-3604.
- [169] Mueller, M. W. and Arnett, W. D., *Propagating star formation and irregular structure in spiral galaxies*, The Astrophysical Journal, 1976, **210**, 670-678.
- [170] Gerola, H. and Seiden, P. E., *Stochastic star formation and spiral structure of galaxies*, The Astrophysical Journal, 1978, **223**, 129-139.
- [171] Maoz, D. and Mannucci, F., *Type-Ia Supernova Rates and the Progenitor Problem: A Review*, Publications of the Astronomical Society of Australia, 2012, **29**, 447-465.
- [172] Williams, B. F. and et al., *Constraints for the Progenitor Masses of Historic Core-collapse Supernovae*, The Astrophysical Journal, 2018, **860**, id.39/10.
- [173] Maund, J. R., *The very young resolved stellar populations around stripped-envelope supernovae*, Monthly Notices of the Royal Astronomical Society, 2018, **476**, 2629-2663.
- [174] Xiao, L. and et al., *Core-collapse supernovae ages and metallicities from emission-line diagnostics of nearby stellar populations*, Monthly Notices of the Royal Astronomical Society, 2019, **482**, 384-401.
- [175] McCall, M. L. and Schmidt, F. H., *Supernovae in Flocculent and Grand Design Spirals*, The Astrophysical Journal, 1986, **311**, 548-553.
- [176] Maza, J. and van den Bergh, S., *Statistics of extragalactic supernovae*, The Astrophysical Journal, 1976, **204**, 519-529.
- [177] Elmegreen, D. M. and Elmegreen, B. G., *Arm Classifications for Spiral Galaxies*, The Astrophysical Journal, 1987, **314**, 3-9.

- [178] Albareti, F. D. and et al., *The 13th Data Release of the Sloan Digital Sky Survey: First Spectroscopic Data from the SDSS-IV Survey Mapping Nearby Galaxies at Apache Point Observatory*, The Astrophysical Journal Supplement Series, 2017, **233**, id.25/25.
- [179] Ann, H. B. and Lee, H.-R., *Spiral Arm Morphology of Nearby Galaxies*, Journal of Korean Astronomical Society, 2013, **46**, 141-149.
- [180] Bittner, A. and et al., *How do spiral arm contrasts relate to bars, disc breaks and other fundamental galaxy properties?*, Monthly Notices of the Royal Astronomical Society, 2017, **471**, 1070-1087.
- [181] Schlegel, D. J., Finkbeiner, D. P. and Davis, M., *Maps of Dust Infrared Emission for Use in Estimation of Reddening and Cosmic Microwave Background Radiation Foregrounds*, The Astrophysical Journal, 1998, **500**, 525-553.
- [182] Bottinelli, L. and et al., *Extragalactic database. VI. Inclination corrections for spiral galaxies and disk opaqueness in the B-band*, Astronomy and Astrophysics, 1995, **296**, 64-72.
- [183] Paturel, G. and et al., *Extragalactic database. VII. Reduction of astrophysical parameters*, Astronomy and Astrophysics Supplement Series, 1997, **124**, 109-122.
- [184] Cappellaro, E. and Turatto, M., *The rate of supernovae: biases and uncertainties*, Thermonuclear Supernovae, NATO Advanced Study Institute (ASI) Series C, 1997, **486**, 77-86.
- [185] Buta, R. J., *Galaxy Morphology*, Planets, Stars and Stellar Systems, by Oswalt, Terry D.; Keel, William C., Springer Science+Business Media Dordrecht, 2013, **6**, 1-89.
- [186] Elmegreen, B. G., Elmegreen, D. M. and Montenegro, L., *Optical Tracers of Spiral Wave Resonances in Galaxies. II. Hidden Three-Arm Spirals in a Sample of 18 Galaxies*, The Astrophysical Journal Supplement Series, 1992, **79**, 37-48.
- [187] Silverman, J. M. and et al., *Type Ia Supernovae Strongly Interacting with Their Circumstellar Medium*, The Astrophysical Journal Supplement Series, 2013, **207**, id.3/15.
- [188] Pastorello, A. and et al., *Supernovae 2016bdu and 2005gl, and their link with SN 2009ip-like transients: another piece of the puzzle*, Monthly Notices of the Royal Astronomical Society, 2018, **474**, 197-218.
- [189] Karapetyan, A. G. and et al., *VizieR Online Data Catalog: Properties of 333 SNe and their 269 hosts (Karapetyan+, 2018)*, VizieR Online Data Catalog, 2018.
- [190] Hakobyan, A. A. and et al., *Supernovae and their host galaxies - V. The vertical distribution of supernovae in disc galaxies*, Monthly Notices of the Royal Astronomical Society, 2017, **471**, 1390-1400.

- [191] Buta, R. J. and et al., *A Classical Morphological Analysis of Galaxies in the Spitzer Survey of Stellar Structure in Galaxies (S4G)*, The Astrophysical Journal Supplement Series, 2015, **217**, id.32/46.
- [192] Richardson, D. and et al., *A Comparative Study of the Absolute Magnitude Distributions of Supernovae*, The Astronomical Journal, 2002, **123**, 745-752.
- [193] Verley, S. and et al., *Star formation in isolated AMIGA galaxies: dynamical influence of bars*, Astronomy and Astrophysics, 2007, **474**, 43-53.
- [194] Buta, R. J., Zhang, X., *Pattern Corotation Radii from Potential-Density Phase-Shifts for 153 OSUBGS Sample Galaxies*, The Astrophysical Journal Supplement Series, 2009, **182**, 559-583.
- [195] Comerón, S. and et al., *ARRAKIS: atlas of resonance rings as known in the S<sup>4</sup>G*, Astronomy and Astrophysics, 2014, **562**, A121/160.
- [196] Canzian, B. and Allen, R. J., *Spiral Density Wave Theory, Corotation Resonance, and the Velocity Field of NGC 4321*, The Astrophysical Journal, 1997, **479**, 723-739.
- [197] Rautiainen, P., Salo, H. and Laurikainen, E., *Model-based pattern speed estimates for 38 barred galaxies*, Monthly Notices of the Royal Astronomical Society, 2008, **388**, 1803-1818.
- [198] Tamburro, D. and et al., *Geometrically Derived Timescales for Star Formation in Spiral Galaxies*, The Astronomical Journal, 2008, **136**, 2872-2885.
- [199] Font, J. and et al., *Interlocking Resonance Patterns in Galaxy Disks*, The Astrophysical Journal Supplement Series, 2014, **210**, id.2/30.
- [200] Egusa, F. and et al., *Determining Star Formation Timescale and Pattern Speed in Nearby Spiral Galaxies*, The Astrophysical Journal, 2009, **697**, 1870-1891.
- [201] Waller, W. H. and et al., *Ultraviolet Signatures of Tidal Interaction in the Giant Spiral Galaxy M101*, The Astrophysical Journal, 1997, **481**, 169-173.
- [202] Gonzalez, R. A. and Graham, J. R., *Tracing the Dynamics of Disk Galaxies with Optical and Infrared Surface Photometry: Color Gradients in M99*, The Astrophysical Journal, 1996, **460**, 651-664.
- [203] Kranz, T., Slyz, A. and Rix, H.-W., *Dark Matter within High Surface Brightness Spiral Galaxies*, The Astrophysical Journal, 2003, **586**, 143-151.
- [204] Fridman, A. M. and et al., *Gas motions in the plane of the spiral galaxy NGC 3631*, Monthly Notices of the Royal Astronomical Society, 2001, **323**, 651-662.

- [205] Sempere, M. J. and Rozas, M., *Dynamical model of the grand-design spiral galaxy NGC 157*, Astronomy and Astrophysics, 1997, **317**, 405-415.
- [206] Meidt, S. E., Rand, R. J. and Merrifield, M. R., *Uncovering the Origins of Spiral Structure by Measuring Radial Variation in Pattern Speeds*, The Astrophysical Journal, 2009, **702**, 277-290.
- [207] Rigault, M. and et al., *Strong dependence of Type Ia supernova standardization on the local specific star formation rate*, Astronomy and Astrophysics, 2011, **644**, A176/20.
- [208] Karapetyan, A. G. and et al., *The impact of spiral density waves on the distribution of supernovae*, Monthly Notices of the Royal Astronomical Society, 2018, **481**, 566-577.
- [209] Hakobyan, A. A. and et al., *Type Ia supernovae in the star formation deserts of spiral host galaxies*, Monthly Notices of the Royal Astronomical Society, 2021, **505**, L52-L57.
- [210] Karapetyan, A. G., *VizieR Online Data Catalog: Properties of 77 SNe Ia (Karapetyan, 2022)*, VizieR Online Data Catalog, 2022.